CHAPTER 6: ASSESSMENT OF A COMPREHENSIVE METHOD FOR PREDICTING PERFORMANCE

6.1 Overview

The analytical results presented in Chapter 5 demonstrate the difficulty of predicting the performance of an improved ground zone supporting a structure in liquefiable soil using a simplified method consisting of a series of uncoupled analyses. One way of potentially improving the ability to predict the performance of a treated ground and supported structure system is by using a more comprehensive analytical approach consisting of a coupled analysis.

A coupled analysis allows many of the important mechanisms and phenomena affecting improved ground performance to be modeled simultaneously. As discussed in Chapter 3, Section 3.3, this type of analysis typically includes some aspect of pore water pressure development, stress-strain softening, and strength reduction in the soil under dynamic loading conditions. Groundwater flow may also be incorporated. The dynamic loading is generally included in the numerical model by applying an acceleration record representative of the design earthquake.

One key advantage of the coupled analytical approach is the ability to account for the interdependent effects of various mechanisms and phenomena on each other as the numerical computations proceed. For instance, when an effective stress formulation is used, the inclusion of pore water pressure generation in the simulation can impact the strength and stress-strain behavior of the soil during shaking in the same manner as in the field. Another common advantage is the ability to input an acceleration time history for the design earthquake, as opposed to the seismic coefficient used in pseudostatic analyses, resulting in a more realistic representation of loading on the system.

Given the advantages of using a coupled solution for predicting the behavior of an improved ground and supported structure system, such an approach was evaluated for this purpose. In particular, a partially-coupled solution implemented in the computer program FLAC (Itasca Consulting Group, 1999) was assessed for reliability in predicting pore water pressure

generation, accelerations, and permanent deformations for improved and unimproved ground supporting structures within liquefiable soil deposits. A discussion is presented below of the program along with the soil and pore water pressure generation models considered and used. Calibration and verification of the selected soil model is also presented, along with a final assessment of the method for predicting the performance of improved ground supporting bridge components.

6.2 Selection of Numerical Modeling Tools

6.2.1 Computer Code

As discussed in Chapter 3, Section 3.3, there are many different numerical modeling codes for predicting the behavior of saturated, cohesionless soils under dynamic loading. The degree of coupling in these codes varies. Different degrees of "success" are generally reported regarding the use of these codes in predicting liquefaction and associated ground and structure movements under simulated seismic conditions. Several researchers have reported the successful prediction of this phenomena using codes that employ fully-coupled solutions, such as DYSAC2 (Arulanandan, 1996, and Arulanandan et al., 1997), DYNAFLOW (Arulanandan, 1996), and SWANDYNE (Madabhushi and Zeng, 1998). Likewise, the successful use of partially-coupled solutions in the programs FLAC (Puebla et al., 1997; Dickenson and Yang, 1998; McCullough and Dickenson, 1998) and TARA-3 (Finn, 1988 and 1991) for predicting this type of behavior has also been reported.

Given the number of computer codes available for modeling liquefaction and predicting associated ground deformations, selection of a suitable code for this research was based primarily on:

- some reported success in predicting this type of behavior,
- ability to incorporate a number of key factors and phenomena influencing the performance of unimproved and improved ground and a supported structure subjected to dynamic loading,

- flexibility for adding new formulations for alternative soil models or other phenomena, and
- some acceptance by the geotechnical engineering profession.

The computer code FLAC (for Fast Lagrangian Analysis of Continua) was selected as meeting the above criteria. This program uses an explicit, finite difference formulation for solving geomechanics problems. Material inertia terms are included in the solution formulation for both static and dynamic problems, requiring that a timestepping procedure be used in both cases. The version of the code used in this research (FLAC Version 3.4) allows plane strain, plane stress, or axisymmetric analyses to be performed. For this study 2-dimensional (2-D) plane strain analyses were used. More details regarding the program can be found in the User's Manuals (Itasca Consulting Group, 1999).

Modeling the behavior of saturated soil under dynamic loading is handled in FLAC using a partially-coupled analytical solution. In addition to allowing input of an earthquake acceleration or dynamic loading record and providing a pore pressure generation scheme, FLAC has a number of additional features important for modeling the liquefaction and ground performance problem, including:

- a stable, large strain formulation;
- ability to perform flow calculations during dynamic loading simulations;
- variety of structural elements including beams and piles;
- interface elements for use between structural elements and soil zones;
- special boundary for modeling the behavior of the free-field beyond the limits of the mesh; and
- ability to incorporate user-written code, including formulations for constitutive soil models.

6.2.2 Soil Models

The soil model provided with FLAC for simulating liquefaction uses a Mohr-Coulomb failure criteria along with an assumed linear elastic-perfectly plastic stress-strain behavior. The

linear elastic behavior is governed by the input elastic shear and bulk moduli, which are held constant throughout the analysis. Typically, the bulk modulus of the soil in a drained state is input along with the bulk modulus of water. Pore water pressure generation is introduced by first computing the volumetric strain induced by the cyclic shear strain using a formulation by Martin et al. (1975). In this formulation the volumetric strain that occurs in any cycle of loading is dependent on the shear strain that occurs during that cycle as well as the previously accumulated volumetric strain. It is computed using

$$\Delta\varepsilon_v = C_1 (\gamma - C_2\varepsilon_v) + C_3 \varepsilon_v^2/(\gamma + C_4 \varepsilon_v) \qquad (6.1)$$

where:

$\Delta\varepsilon_v$ is the volumetric strain increment that occurs over the current cycle,

ε_v is the volumetric strain that occurred over the previous cycles,

γ is the amplitude of the shear strain for the current cycle, and

C_1 to C_4 are constants dependent on the volumetric strain behavior of the sand.

The volumetric strain increments are computed during each half cycle of loading and applied as changes in normal strains to each saturated element, where the normal strains in the vertical and horizontal directions are taken as one-third of the computed volumetric strain. The application of the normal strains results in an adjustment of effective stresses and accounts for the development of pore water pressure. Although equation 6.1 was developed for simple shear cases, the FLAC formulation uses it for cases where both normal and/or shear strains occur by substituting the corresponding maximum shear strain into the formula in place of the simple shear strain.

Although two-dimensional, plane strain analyses were performed with FLAC in this research, the volumetric strain was divided by three and applied as normal strains to the system in three mutually perpendicular directions (x, y, and z) as originally formulated in the code. Dividing the volumetric strain by two and applying it in the vertical (y) and in-plane horizontal (x) directions, or applying it as a normal strain in the vertical direction only, results in an incorrect effective stress state. Therefore, the original formulation was used in the analyses performed.

Two different modifications to the FLAC soil model for liquefaction were implemented as part of this research to assess their potential for predicting liquefaction and associated deformations. In addition, an elastic-plastic soil model called UBCSAND (Byrne et al., 1995; Puebla et al., 1997) was also evaluated.

6.2.2.1 First Code Modification

In the first modification to the FLAC soil model, the shear and bulk moduli used in the linear elastic-perfectly plastic stress-strain formulation were computed on an individual element basis as a function of the mean effective confining stress. The maximum shear modulus, G_{max} , was computed using the formulation by Seed and Idriss

$$G_{max} = 1000\ K_{2max}\ (\sigma_m')^{0.5} \qquad (6.2)$$

where:

G_{max} is the maximum (small strain) shear modulus in pounds per square foot, psf (it was later converted to kPa to be consistent with metric units being used),

K_{2max} is the shear modulus number (Seed and Idriss, 1970), and

σ_m' is the mean effective confining stress in psf.

The shear modulus used in an element was assumed to be 75 percent of the maximum shear modulus for the given effective confining stress.

The bulk modulus, B, used for an element was computed using the formula:

$$B = K_b\ P_a\ (\sigma_m'/P_a)^{0.5} \qquad (6.3)$$

where:

K_b = bulk modulus coefficient,

P_a = atmospheric pressure, and

σ_m' is the mean effective confining stress.

The bulk modulus was constrained to be no greater than 49.7 times and no less than 0.6667 times the shear modulus to keep the Poisson's ratio between 0.0 and 0.49.

Both the shear and bulk moduli in the elements were updated as effective stresses changed due to seismic loading and associated pore water pressure generation.

6.2.2.2 Second Code Modification

In the second modification of the FLAC liquefaction code, the maximum shear modulus was once again computed for each individual element using the formula proposed by Seed and Idriss (1970), as given in equation 6.2. Code was then introduced to calculate a reduced tangent shear modulus for an element based on the magnitude of shear strain that had already occurred. This reduced shear modulus was evaluated using a hyperbolic type stress-strain formulation applied to the simple shear case by Pyke (1979) where the shear stress, τ, is related to the shear strain, γ, by

$$\tau = \tau_c + G_{max} (\gamma - \gamma_c) [1 / (1 + abs(\gamma - \gamma_c)/(\eta \gamma_y))] \qquad (6.4)$$

where:

G_{max} is the maximum shear modulus,

γ_y is the yield strain computed as the yield stress, τ_y, divided by G_{max},

γ_c is the shear strain at the last reversal of the shear stress-strain curve, and

$\eta = abs(\pm 1 - \tau_c / \tau_y)$ with τ_c being the shear stress at the last reversal and the first term being +1 or –1 depending on the direction of loading.

The bulk modulus, B, was computed from the maximum shear modulus using:

$$B = (2 G_{max} (1 + \nu)) / (3 (1 - 2 \nu)) \qquad (6.5)$$

where:

G_{max} is the maximum shear modulus, and

ν is the Poisson's ratio of the soil.

A Poisson's ratio of 0.05 was used in computing the bulk modulus because such a low value is common at the very small strain levels typical in the early stages of earthquake loading. During an analysis the bulk modulus, B, was constrained to be no greater than 49.7 times and no less than 0.6667 times the tangent shear modulus to keep Poisson's ratio between 0.0 and 0.49. The bulk modulus, B, computed as just described is representative of the soil in a drained state. To model undrained behavior in saturated soil, the water bulk modulus, B_w, was input to be used along with the shear modulus and drained bulk modulus for the soil.

In addition to including non-linear, shear stress-strain behavior, the second modification to the code also incorporated an update proposed by Byrne (1991) to the volumetric strain formulation by Martin et al. (1975) given in equation 6.1. Byrne's formula is

$$\Delta\varepsilon_v = C_1 \exp(-C_2 \varepsilon_v / \gamma) \qquad (6.6)$$

where:

$\Delta\varepsilon_v$ is the increment in volumetric strain that occurs over the current cycle,

ε_v is the accumulated volumetric strain for previous cycles,

γ is the shear strain amplitude for the current cycle, and

C_1 and C_2 are constants dependent on the volumetric strain behavior of the sand.

The volumetric strain estimated using this equation was applied as increments in normal strain to saturated elements, as previously described above, resulting in pore water pressure increments.

According to Byrne (1991) the constant C_1 in equation 6.6 controls the amount of volumetric strain increment and C_2 controls the shape of the volumetric strain curve. These constants are estimated from volumetric strain data obtained from cyclic simple shear tests on the particular sand of interest. When such data is not available Byrne (1991) indicates that the constants can be estimated using

$$C_1 = 7600 (D_r)^{-2.5} \qquad (6.7)$$

$$C_2 = 0.4 / C_1 \qquad (6.8)$$

where D_r is the relative density of the soil in percent.

Equations 6.6, 6.7, and 6.8 were shown by Byrne to provide volumetric strains in good agreement with those reported by Tokimatsu and Seed (1987) for dry sands tested in cyclic simple shear tests (Silver and Seed, 1971) at relative densities of 45, 60, and 80 percent.

6.2.2.3 UBCSAND

A third soil model called UBCSAND was also tested in FLAC. This model was developed by Professor Peter M. Byrne and his colleagues at the University of British Columbia, Vancouver, Canada. The model simulates the stress-strain behavior of soil under static or cyclic loading for drained or undrained conditions by using an elastic-plastic formulation, where the shear modulus has elastic and plastic components. The elastic shear and bulk moduli, G_e and B_e, are computed using the formulae

$$G_e = k_{Ge} P_a (p'/ P_a)^{ne} \quad (6.9)$$

$$B_e = k_{Be} P_a (p'/ P_a)^{me} \quad (6.10)$$

where:

k_{Ge} and k_{Be} are the elastic shear and bulk moduli numbers,

P_a is the atmospheric pressure,

ne and me are the elastic shear and bulk moduli exponents, and

p' is the mean effective confining stress defined as $(\sigma_1' + \sigma_3')/2$.

The tangent plastic shear modulus, G_p, is evaluated using a hyperbolic relationship formulated as

$$G_p = k_{Gp} P_a (p'/ P_a)^{np} (1 - R_f \eta/\eta_f)^2 \quad (6.11)$$

where:

k_{Gp} is the plastic shear modulus number,

np is the plastic shear modulus exponent,

η and η_f are the stress ratios on the plane of maximum shear stress and at failure, respectively, and

R_f is equal to the stress ratio at failure, η_f, divided by the ultimate stress ratio for the best fit hyperbola to the soil stress-strain data.

The plastic shear strain increments are computed from the plastic shear modulus and the increments in shear and effective confining stresses that occur. Plastic volumetric strain increments are then computed using the plastic shear strain increments and the dilation angle, ψ, where:

$$\sin \psi = (\sin \phi_{cv} - \sin \phi_d) \qquad (6.12)$$

where:
ϕ_{cv} is the constant volume friction angle, and
ϕ_d is the developed friction angle.

Additional details regarding the theory and formulation of the UBCSAND model, as well as typical values for the modulus numbers and exponents, are presented in Byrne et al. (1995) and Pueblo et al. (1997). The coded formulation of UBCSAND for FLAC was provided for use in this research by Professor Byrne.

6.2.2.4 Selected Model

The three soil models described above were implemented in FLAC and evaluated for potential use in this research by performing some preliminary simulations of centrifuge tests involving dynamic loading of liquefiable soils with and without supported structures and improved ground zones. These simulations indicated that predicted displacements, pore pressures, and accelerations obtained using the second modification of the FLAC soil model, which incorporated the shear stress-strain and volumetric strain formulations by Pyke and Byrne (hereinafter referred to as the Pyke-Byrne model), generally compared better with the measured behavior than those obtained with the other soil models. This performance was obtained despite the fact that the UBCSAND model was extensively calibrated to static and cyclic triaxial and simple shear tests performed under drained and undrained conditions on the sand used in the centrifuge tests. On the other hand, the Pyke-Byrne soil model was only calibrated to resonant

column and undrained, cyclic simple shear tests. On this basis the Pyke-Byrne model was selected for further calibration, verification, and assessment.

6.2.3 Simplifications and Adjustments

Despite the fact the Pyke-Byrne soil model gave the best overall predicted results for the centrifuge tests simulated, it includes a number of simplifications compared to more theoretically rigorous models. These simplifications include:

- Volumetric strain increments for pore water pressure generation are calculated and applied every half cycle of stress-strain loading using a volumetric strain formulation that was developed for every full cycle of loading;
- Effect of initial static shear stress on the pore water pressure generation and liquefaction resistance of the soil is not incorporated;
- Variation of liquefaction resistance or friction angle of the soil with changes in effective confining stresses is not included;
- Strength of cohesionless soil is based solely on the friction angle and effective stresses and does not consider the development of residual strengths at large strains, even for fully-liquefied soil; and
- Degradation of the shear modulus is formulated in terms of the simple shear strain and not in terms of the maximum shear strain resulting from a combination of normal and shear strains.

A number of adjustments were made in the modeling approach to provide predicted results that agreed better with observed behavior. These adjustments are listed below.

- K_o of 1.0 was assumed for level ground conditions existing prior to the placement of any surface structure, regardless of the soil density, to prevent premature liquefaction during the simulated earthquake loading.
- Strength properties input for cohesionless soils for dynamic loading were the peak friction angle and a reduced dilation angle, rather than the constant volume friction angle and full dilation angle.

- Dilation angles were only used for soils in zones where shear stresses were induced in the horizontal plane by the presence of surface structures.

In order to keep FLAC execution times at reasonable levels, the bulk modulus of water used in analyses involving multiple elements was reduced from 2.0e6 kPa to 2.0e5 kPa. A comparative analysis performed using the full and reduced bulk moduli indicated similar analytical results were obtained using the two values. In a FLAC simulation of soil liquefaction in a centrifuge test performed in a model box having rigid walls, the predicted pore water pressures obtained using the reduced bulk modulus of water were actually closer to the measured results than those obtained when the full bulk modulus was used.

Future improvements in the FLAC modeling of liquefaction and improved ground behavior should include reducing the number of simplifications and modeling adjustments associated with the Pyke-Byrne model formulation and use, while at the same time improving the model performance.

6.3 Calibration of Model

Prior to verifying the performance of the Pyke-Byrne soil model in FLAC by performing numerical simulations of centrifuge tests and field case histories, determination of soil parameter values for use in the simulations was necessary. The values were obtained by calibrating the model to laboratory test data performed on the particular soil used in the centrifuge test or present in the field, when available. For cases where laboratory test data was not available parameter values for "typical" sands were used, as obtained from the literature. A few centrifuge tests were also simulated with FLAC, as part of the calibration process, to see if any adjustment of the parameter values obtained from the laboratory tests were necessary when modeling a physical system comprised of many elements. The calibration analyses, as well as the verification analyses, were performed using FLAC Version 3.4.

The centrifuge tests used for the soil model calibration work, as well as the verification simulations discussed in the next section, were conducted in the early 1990's as part of research at Rennsaelaer Polytechnic Institute in Troy, New York, and the VELACS (Arulanandan and Scott, 1993/1994) project. In both cases Nevada Sand was used in the tests. Extensive

laboratory testing was performed on this sand for the VELACS project. The data from these tests was used to obtain the soil parameter values needed for the numerical simulations conducted as part of the verification work.

In addition to the centrifuge tests, one field case history from the 1987 Superstition Hills Earthquake in southern California was also used for verification of the Pyke-Byrne model. Since laboratory strength and cyclic loading test data for the sands at the site were not readily available, "typical" values were used. As part of the calibration process, the ability to predict liquefaction with the Pyke-Byrne model and these typical values was checked.

In the remainder of this section, laboratory test data for the Nevada Sand is discussed along with a summary of soil model parameter values obtained from this data in the calibration process. Parameter values for "typical" sand are also discussed.

6.3.1 Nevada Sand

As previously mentioned, extensive laboratory testing of Nevada Sand was performed as part of the VELACS project. This testing was primarily performed by the Earth Technology Corporation (TETC) and the results presented in a soils data report (Arumoli et. al, 1992). The testing program consisted of both general and more advanced laboratory tests. General testing included grain size, specific gravity, maximum and minimum density, and constant-head permeability tests. More advanced testing included monotonic and cyclic triaxial tests under drained and undrained conditions, monotonic and cyclic direct simple shear tests under undrained conditions, resonant column tests, and 1-D consolidation/rebound tests. The advanced tests were performed on samples prepared to relative densities of 40 and 60 percent. TETC also performed tests on a silt used in the VELACS Project, but the results are not presented here because none of the centrifuge tests that were numerically modeled involved it.

6.3.1.1 General Properties

The grain size distribution curve of Nevada Sand from sieve analyses performed by TETC is presented in Figure 6.1. As seen from the curve, the sand has a fine gradation.

Hydraulic conductivities (from constant head permeability tests), void ratios, and dry unit weights for the sand at three different relative densities are presented in Table 6.1, as reported by TETC. The maximum and minimum dry unit weights given for the sand were 17.33 kN/m^3 and 13.87 kN/m^3. The specific gravity was reported to be 2.67.

6.3.1.2 Strength Properties

Strength properties for the Nevada sand at relative densities of 40 and 60 percent were obtained from both monotonic triaxial compression and direct simple shear tests conducted by TETC. Peak effective friction angles for the Nevada Sand based on the results of these tests are summarized in Table 6.2. Triaxial extension tests were also performed, but there was significant scatter in the data.

The monotonic triaxial compression tests were performed on the sand under drained and undrained conditions. Effective confining stresses for both isotropically and anisotropically consolidated specimens were 40, 80, and 160 kPa. The results from these tests were used to determine the strength properties based on a maximum principal stress ratio (σ'_1/σ'_3) failure criteria.

Two of the three monotonic direct simple shear tests performed were undrained and the third was a drained, constant height test. Effective confining pressures used in the tests were 80 and 160 kPa.

6.3.1.3 Maximum Shear Modulus

Maximum shear moduli (i.e. - modulus at a strain level of approximately 0.0001%) for Nevada Sand at 40 and 60 percent relative densities and confining pressures of 40, 80, 160, and 320 kPa were determined from resonant column tests conducted by TETC. The moduli for the sand at a given relative density were used to back-calculate a shear modulus number for use in the maximum shear modulus formula developed by Seed and Idriss (1970), given in equation 6.2. The back-calculated shear modulus numbers for the sand at the 40 and 60 percent relative densities are presented in Table 6.2.

6.3.1.4 Volumetric Strain Constants

Values for the constants C_1 and C_2 used in the volumetric strain equation (equation 6.6) by Byrne (1991) were determined for the Nevada sand at relative densities of 40 and 60 percent from undrained cyclic simple shear tests performed by TETC at effective confining stresses of 80 and 160 kPa. Determination of the constants was accomplished by using a single element simulation in FLAC to model each test, as shown in Figure 6.2. The single element was assigned a friction angle and a maximum shear modulus number in accordance with the values presented in Table 6.2. C_1 and C_2 were initially estimated from equations 6.7 and 6.8 developed by Byrne.

The element was then subjected to the stress-controlled, cyclic loading used in the test and the number of cycles required to liquefy it in the simulation determined. Based on a comparison of the predicted number of cycles to liquefaction and the measured number in the laboratory test, the values of C_1 and C_2 were adjusted if necessary, with C_2 computed from C_1 using equation 6.8, and the simulation repeated until the predicted and measured number of cycles were approximately the same. The C_1 and C_2 values obtained in this manner for the 40 and 60 percent relative density sands are presented in Table 6.3. Shear stress-strain and excess pore water pressure curves obtained from simulations for the sand at 40 percent relative density and an effective consolidation pressure of 80 kPa are given in Figure 6.3. It should be noted that no attempt was made to adjust the shear modulus numbers used in these simulations, despite the fact the predicted shear strains close to liquefaction were lower than the measured values of 1 to 3 percent.

In addition to performing the above simulations with a single element, a limited number of cases were also repeated using a 2 element by 2 element grid and a 3 by 3 grid. These analyses gave approximately the same results as the single element analysis.

The volumetric strain constants obtained from the direct simple shear simulations were further checked by using them in simulations of a limited number of centrifuge tests involving liquefaction of Nevada sand. These tests included (all quantities given in prototype scale):

- a medium dense sand layer (relative density of 59%) subjected to 10 cycles of a 2-Hz sinusoidal acceleration record of varying amplitude (with a maximum amplitude of 0.2g);
- a medium dense sand layer (relative density of 53%) supporting a model footing and subjected to 10 cycles of a 2-Hz sinusoidal acceleration record having a uniform amplitude of approximately 0.35g; and
- adjacent, vertical zones of loose (relative density of 40%) and dense (relative density of 90%) sands subjected to 10 cycles of a 2-Hz sinusoidal acceleration record having a uniform amplitude of approximately 0.19g.

Values of C_1 and C_2 giving fairly reasonable agreement between the predicted and measured pore water pressures for these cases, as well as reasonable predicted movements for the model

footing and dense zone, are given in Table 6.3. More details regarding these centrifuge tests and the predicted results are given in the next section on verification.

The values in Table 6.3 indicate that the C_1 and C_2 constants for the 40 and 60 percent relative density sands obtained from calibration to the centrifuge tests were somewhat different from those obtained from calibration to the cyclic simple shear tests. The values obtained from the simple shear test simulations follow the same trend as those obtained using Byrne's formulae for the constants (equations 6.7 and 6.8), with C_1 decreasing (and C_2 increasing) as the relative density increases. On the other hand, for the centrifuge tests the same value of C_1 (and also C_2) gave reasonable predicted results for both the 40 percent relative density and 60 percent relative density cases. In some respects it seems unrealistic that the values of C_1 and C_2 providing a reasonable prediction of the centrifuge response for the Nevada Sand at 40 percent relative density are the same values giving a reasonable prediction of the response for the 60 percent relative density sand. However, the shear modulus numbers (K_{2max}) given in Table 6.2, which were backcalculated from resonant column tests on the Nevada Sand at these two relative densities, indicate the small strain shear stiffness of the sand at 60 percent relative density is not much larger than at 40 percent relative density. The difference in these shear moduli numbers is smaller than seen in modulus number values reported by Kramer (1996), based on the work of Seed and Idriss (1970), for clean sand at relative densities of 40 and 60 percent. So on this basis, it does not seem unreasonable to have similar volumetric strain constants for Nevada Sand at these two relative densities.

Both the constants obtained from the cyclic simple shear and centrifuge tests indicate the Nevada sand experiences larger volumetric strain, and therefore produces more induced pore water pressure for a given shear strain increment, than predicted using the values obtained from Byrne's formulae (equations 6.7 and 6.8). This trend is also supported by the C_1 and C_2 values obtained from centrifuge tests for Nevada sand at 90 percent relative density.

The C_1 and C_2 values obtained from calibration to the three centrifuge tests were adopted for the Nevada Sand for use in the verification analyses described in the next section.

6.3.2 "Typical" Sand

A set of soil parameters and properties was developed in the calibration phase for a "typical" clean sand based on values commonly used in geotechnical engineering and geotechnical earthquake engineering, as found in the literature. The ultimate goal was to

eventually use these properties in a parametric study, as opposed to those for the Nevada sand. The property values selected for the "typical" sand are presented below, along with a demonstration of their suitability for predicting liquefaction.

6.3.2.1 Strength

The peak effective friction angles obtained for Nevada Sand at 40 and 60 percent relative density, which are presented in Table 6.2, appear to be consistent with peak friction angles reported elsewhere for similar density sands (i.e. – Lambe and Whitman, 1969). Therefore, these friction angles were adopted for use as "typical" values.

6.3.2.2 Maximum Shear Modulus

The maximum shear modulus formula (equation 6.2) and associated K_{2max} values developed by Seed and Idriss (1970) for clean sands has generally found widespread acceptance within geotechnical earthquake engineering practice. Therefore, they were adopted and used for "typical" sands in the parametric studies described in Chapters 7 and 8. The K_{2max} values for different relative density sands are presented in Table 6.4 based on values tabulated by Kramer (1996) from Seed and Idriss (1970).

6.3.2.3 Volumetric Strain Constants

Byrne (1991) has shown that the volumetric strain formula given in equation 6.6, along with equations 6.7 and 6.8 for the constants C_1 and C_2, predict volumetric strains consistent with those reported by Tokimatsu and Seed (1987) for dry sands subjected to cyclic simple shear. He also shows that the volumetric strain predicted with equation 6.6 agrees more closely with the Tokimatsu and Seed data than the original formulation proposed by Martin et al. (1975), which has been widely used in pore water pressure generation schemes. Byrne's formulae for C_1 and C_2 given in equations 6.7 and 6.8 were therefore adopted for estimating volumetric strains of "typical" sands, in conjunction with equation 6.6, as part of a pore water pressure generation scheme in the Pyke-Byrne model.

The Pyke-Byrne model was tested for its ability to predict liquefaction of a "typical" clean sand using the liquefaction potential curve proposed in a 1997 NCEER report on liquefaction (shown in Figure 6.4) as the basis for performance. The test was conducted by using FLAC and the Pyke-Byrne model to simulate undrained, cyclic simple shear of a "typical" clean sand using a single element and applying boundary conditions consistent with the liquefaction

potential curve. Starting with initial C_1 and C_2 values for clean sand at a given relative density, calculated using equations 6.7 and 6.8, the element in the FLAC simulation was subjected to uniform, stress-controlled cyclic simple shear loading that should have resulted in liquefaction in 15 cycles. The cyclic shear stress applied was based on the cyclic resistance ratio obtained from the liquefaction potential curve in Figure 6.4 for a sand having an $(N_1)_{60}$ equivalent to the relative density of interest. If the predicted number of cycles causing liquefaction of the element in the FLAC analysis was not approximately 15, C_1 and C_2 were adjusted until liquefaction occurred in about 15 cycles.

Table 6.5 shows a comparison of the C_1 and C_2 values obtained from the Byrne equation for relative densities of 40, 60, and 75 percent, and the values that produced liquefaction in about 15 cycles in the FLAC simulations. As seen from the table, for the 40 percent relative density case there is good agreement between the C_1 and C_2 values proposed by Byrne and the values appropriate for the single element simulation. For the 60 percent relative density case, the C_1 value which worked well in the FLAC simulation was about 30 percent lower than the value obtained from Byrne's equation. Likewise the single element simulation for 75 percent relative density gave a C_1 value that was lower than obtained from Byrne's formula.

The difference between the C_1 value in the single element simulation at 60 percent relative density and Byrne's value is similar to the difference shown in Table 6.3 for the C_1 values that worked well for the simple shear and centrifuge test simulations using Nevada Sand at 60 percent relative density. The analysis results for the Nevada Sand at 60 percent relative density indicated the need to use a higher C_1 value (and lower C_2 value) when analyzing the larger scale centrifuge test as opposed to the smaller scale simple shear test. These results seem to support using the higher C_1 value obtained from Byrne's equation for a "typical" sand when modeling a large scale field problem in FLAC, rather than the smaller value obtained from the simple shear simulation.

Based on the above results Byrne's formulae (equations 6.7 and 6.8) were selected for calculating C_1 and C_2 values to be used when numerically modeling problems involving deposits of "typical" sand using the Pyke-Byrne model in FLAC.

6.4 Verification Analyses

After calibrating the Pyke-Byrne soil model to establish appropriate strength properties, stress-strain parameters, and volumetric strain constants to be used for different sands, numerical simulations were performed of centrifuge tests that involved the behavior of liquefiable soil under dynamic loading with and without structures and ground improvement. In addition one field case history involving liquefaction and lateral spreading during an actual earthquake was modeled.

When selecting centrifuge and field case histories from the literature to use in the verification process of the Pyke-Byrne model in FLAC, the emphasis was placed on cases having some application to liquefaction and the performance of a bridge on liquefiable soils with and without ground improvement. Relevant details of the centrifuge tests and field case history selected are presented in Table 6.6, including the applicability of the test or case history to the problem of liquefaction at a bridge.

Additional details are given below regarding the centrifuge tests and field case history, and the analysis approach used in FLAC. This is followed by a comparison of the predicted and measured responses.

6.4.1 Centrifuge Tests

As noted in Table 6.6, the centrifuge tests performed by other researchers that were analyzed using FLAC and involved dynamic loading of saturated soils included:

- a uniform, medium dense sand layer;
- model footing on a medium dense sand layer;
- dense embankment on a loose sand deposit;
- gravity retaining wall on a medium dense sand deposit;
- adjacent, vertical zones of loose and dense sand; and
- clayey sand embankment on a loose sand layer with and without ground improvement;

The soil used in all of the tests was Nevada Sand, whose properties were discussed above and presented in Tables 6.2 and 6.3.

When selecting centrifuge tests to model, those performed in rigid wall centrifuge boxes were chosen over those performed in laminar boxes (constructed of stacked rings that can translate laterally relative to each other) because the rigid wall type boundary could be modeled more accurately with FLAC. Modeling the laminar box would likely require use of the free-field boundary condition option in FLAC, which is a relatively new option and has not been rigorously tested.

In all of the centrifuge tests, instrumentation was used to collect data on the pore water pressures in the soil, along with the displacements and accelerations of the ground and any supported structures. This data was obtained using pore pressure transducers, accelerometers, and linear variable displacement transducers at the locations shown in schematics of the tests presented in Figures 6.5 to 6.10. Additional ground deformation information was obtained in some models by embedding dry, straight noodles vertically in the foundation soil prior to saturation. The position of these noodles before and after testing was carefully measured to provide estimates of the lateral ground movement.

Analyses of the centrifuge tests were performed using the Pyke-Byrne soil model along with the appropriate strength properties, stress-strain parameters, and pore water pressure generation parameters for the sands at their respective relative densities. The properties and parameters were selected from the values given in Table 6.7, which was developed from the properties and parameters for Nevada Sand presented in Tables 6.2 and 6.3 based on the VELACS laboratory test data.

The finite difference meshes used for the centrifuge test simulations in FLAC are shown in Figures 6.11 to 6.16. Noted on each mesh are the specific elements where pore pressures were monitored and nodes where accelerations and displacements were monitored during the simulated shaking for comparison with the measured values in the tests.

Prior to performing the dynamic simulation for a particular centrifuge test, the initial stress state in the system needed to be established. For level ground cases this was accomplished using a gravity turn on routine in FLAC, where the vertical and horizontal stresses and pore water pressures are calculated by the program based on the specified soil density, porosity, groundwater table level, and K_o values for the x (in-plane direction) and z (out-of-plane direction which is perpendicular to the in-plane direction) horizontal directions. The soil model used

during this phase was linear elastic with a constant shear and bulk modulus assigned to the deposit.

The initial stress state for cases involving a structure on top of a level ground deposit was established by first determining the stresses for the level ground using the method described above. The soil model for the foundation soil was then switched to the Duncan and Chang (1970) hyperbolic model and the load from the structure or embankment applied in stages until it was completely in place and equilibrium reached. The Duncan and Chang model was used during this load application, instead of the Pyke-Byrne model, because the latter was primarily developed for the small strains associated with dynamic loading. The initial stress state obtained with the Duncan and Chang model was more reasonable than that obtained using the Pyke-Byrne model.

Once the initial stress state was established in the grid representing a particular centrifuge test, the soil model was changed to the Pyke-Byrne model. The acceleration record used in the centrifuge test was then applied to the nodes along the bottom and side boundaries of the grid.

In each analysis some material damping was included for the soil elements in addition to the damping already incorporated in the nonlinear stress-strain model. The additional damping specified was 2 percent Rayleigh damping. It was applied at the natural frequency of the level ground supporting the structure or embankment rather than at the natural frequency of the entire system (i.e. – including both the foundation soil and the structure or embankment). Using the natural frequency of the level ground generally gave better predicted results than using the natural frequency of the entire system.

6.4.2 Field Case History

One field case history involving liquefaction and permanent ground deformations during an earthquake was simulated as part of the verification of the Pyke-Byrne model used in FLAC. The case history is from the Wildlife Site in the Imperial Valley of southern California during the 1987 Superstition Hills Earthquake, which had a magnitude of M=6.7. One purpose of analyzing this case history was to demonstrate that the numerical modeling procedure being used could adequately predict the performance of a real site subjected to a real earthquake motion, and thereby was not biased towards centrifuge tests.

Information concerning site and soil conditions at the Wildlife Site, as well as the earthquake, was obtained from a report by Baziar et al. (1992). A plan view of the site is shown

in Figure 6.17. Figure 6.18 shows the soil profile based on information available in the report. The profile generally consists of about 2.5 meters of very loose silt underlain by 1 meter of very loose sandy silt (also referred to as silty sand in Baziar et al.) and about 3.3 meters of loose silty sand to very fine sand. Beneath the silts and sands are about 0.7 meters of loose clayey silt and 4.5 meters of stiff silty clay underlain by other granular and fine-grained deposits. The site is bordered by a river whose bottom is approximately 4.9 meters below the adjacent ground surface. The groundwater and river levels are approximately 1.2 meters below grade.

As shown in Figures 6.17 and 6.18, the Wildlife site was instrumented with an array of pore water pressure transducers and accelerometers. These instruments recorded the ground response when the site was subjected to the earthquake motion, which was predominantly in the north-south direction and produced a peak ground surface acceleration of about 0.18g. In addition, lateral spreading displacements that occurred towards the river were measured after the earthquake at the ground surface and using an inclinometer installed near the array to 8.5-m depth.

The lateral displacements measured at the ground surface of the Wildlife Site after the Superstition Hills earthquake ranged from 11 to 23 cm toward the river, as shown in Figure 6.17. The inclinometer installed near the array indicated most of the lateral movement occurred in the upper part of the sandy silt layer from 2.5 to 3.5-m depth. Based on the pore pressure and ground movement data, as well as a series of analyses, Dobry et al. (1989) and Vucetic and Dobry (1988) concluded most of the liquefaction and ground deformation occurred in the silts and sands between the ground surface and 3.5-m depth.

The Wildlife Site case was analyzed using the finite difference grid shown in Figure 6.19. The large grid width was selected to eliminate boundary effects, and was determined by performing a series of analyses with different widths. Pore water pressures and accelerations were monitored in zones and at nodes close to the locations and depths where the instruments were located in the field.

The soil properties and stress-strain parameters assigned to the various soil layers modeled in the analysis are given in Table 6.8. The strength parameters were developed based on the blow count information available for the soil. Shear wave velocity data obtained at the site was used to compute the maximum shear moduli of the various layers, from which shear modulus numbers were backcalculated for use in the maximum shear modulus formula

developed by Seed and Idriss (1970). The volumetric strain constants C_1 and C_2 for the sand and sandy silt layers were estimated using equations 6.7 and 6.8 by Byrne. Permeabilities for the various layers were estimated based on the soil gradation.

Initial stress state conditions in the finite difference grid were obtained by initially using an elastic model and computing the stresses assuming the river channel was not present, as described above for the centrifuge tests. The zones in the river channel were then removed and replaced with a boundary pressure exerted by water in the river. Finally, the soil model was changed to the Pyke-Byrne model. It should be noted, that due to the steep angle of the river bank, the first two columns of mesh elements at the bank were assigned a cohesion of 24 kPa to prevent collapse of that slope prior to shaking.

Once equilibrium conditions were established in the mesh, it was subjected to the ground acceleration recorded at 7.5 meters depth in the field. Since the major component of the earthquake motion was in the North-South horizontal direction, this component of horizontal motion was used in the analysis along with the vertical component. Frequencies above 12 hertz were removed from the record prior to use since they represented only a minor component of the energy associated with the motion. Leaving these higher frequencies in the record would have required the use of smaller elements based on the recommendations of Kulhemeyer and Lysmer (1973) for minimum element sizes in dynamic analyses.

6.4.3 Results

Predicted and measured time histories of the ground accelerations, excess pore water pressures, and movements for select locations in the centrifuge tests and the field case history are presented in Figures 6.20 to 6.62 (refer to Table 6.9 for information regarding the figures that pertain to a particular test). For tests where digital files of the measured responses were available, the measured time histories are plotted. In other cases where digital files were not available, the upper and lower limits of the measured responses are indicated.

The results shown in Figures 6.20 to 6.62 allow a comparison of the predicted responses obtained using FLAC with the Pyke-Byrne model and the measured responses. Some observations regarding the predicted responses in comparison to the measured responses for the cases evaluated are presented in Table 6.9. Based on these observations the conclusions below are drawn regarding the ability to predict the behavior of shallow foundations and embankments

on liquefiable soil deposits with or without ground improvement during and after shaking using the Pyke-Byrne model in FLAC.

- Ground and structure accelerations may not be adequately predicted in all cases. In particular, there is a tendency in some cases to underpredict the acceleration at the top of a densified zone, embankment, or structure by up to a factor of approximately three.
- The development of excess pore water pressures beneath and immediately adjacent to structures during shaking is sometimes poorly predicted. In some cases it is overpredicted and in others it is underpredicted by a factor of three or more. In many cases, with or without structures present, the excess pore water pressures that develop during shaking in the foundation soil are predicted to dissipate faster than measured. On the other hand, the trends of excess pore water pressures that develop in the free-field and within densified zones during shaking appear to be predicted reasonably well.
- The trends and magnitude of vertical and horizontal displacements of structures and the supporting ground appear to be predicted reasonably well. As discussed later the horizontal and vertical displacements of a structure or embankment supported on liquefiable soil, with or without an improved ground zone, can be predicted within a factor of approximately two. The overall tendency is to overpredict the movement. In some cases, the maximum horizontal movement in the foundation soil is predicted to occur at a greater depth than actually measured. Free-field ground settlements are generally underpredicted.

In the process of developing the Pyke-Byrne model code, successful efforts were made in reducing the predicted rate of excess pore water pressure dissipation in the foundation soils after shaking stopped to agree better with the measured dissipation. This improvement was made by incorporating the re-solidification phenomena for liquefied soils observed and formulated by Florin and Ivanov (1961). In this phenomena the re-solidification of suspended sand is controlled by a solidification front that moves from the bottom to top of the liquefied soil at a velocity, v_s, given by:

$$v_s = (k \gamma' (1 - n))/ (\gamma_w(n_o - n)) \quad (6.13)$$

where:

k is the soil permeability,

n_o is the initial soil porosity,

n is the porosity after solidification occurs,

γ' is the buoyant unit weight of the soil,

γ_w is the unit weight of water.

In the Pyke-Byrne code the shear and bulk moduli of the soil elements that fully-liquefied were fixed at 20 kPa until the solidication front passed the element. After the solidification front passed, the shear and bulk moduli were allowed to increase in accordance with the effective confining stress, but not above a specified maximum value. The improvement in the excess pore water pressure behavior is shown in Figures 6.63 and 6.64 for one pore pressure record in the centrifuge test on a uniform, medium dense sand layer (Liu, 1992) and another record for the adjacent loose-dense sand zones (Adalier, 1996). Although implementation of this concept was relatively straightforward for these two cases, it is more complicated for cases involving a structure or a layered soil deposit. For this reason, the solidification routine was not used in the verification analyses just presented or for the parametric studies described in Chapters 7 and 8, with the understanding that pore water pressure dissipation may be predicted to occur more rapidly than might actually occur.

As noted above, densification settlements of soils that liquefied in the free-field in centrifuge tests were generally underpredicted in the FLAC simulations performed. This indicates that densification settlements of soils under structures and embankments could be potentially underpredicted. However, the final settlements predicted for structures supported on improved or unimproved soils appear to agree with the measured settlements reasonably well, as discussed in the next section. This suggests that the predicted densification settlements under the structures or embankments are either adequately modeled or compensated for in some other manner by the analyses.

Some of the discrepancies between the predicted and measured behaviors of the centrifuge tests and field case history can be attributed to some limitations of the code formulation for the Pyke-Byrne soil model. For example, in a few simulations it was observed that increments of volumetric strain due to cyclic shear strain increments were not computed at every shear strain reversal in some elements, particularly when the reversal was small. This indicates that further refinement of the soil model code for different loading conditions is still needed. However, despite these limitations it appears that the Pyke-Byrne model was still able to predict the overall performance of the systems, particularly the final displacements.

6.4.4 Assessment of Model

Based on the above information, it was concluded that accelerations and pore water pressures predicted with the Pyke-Byrne model in FLAC are not reliable enough by themselves for making judgements regarding the performance of structures supported on liquefiable soils with or without ground improvement. However, the predicted accelerations and pore water pressures may be useful for observing if there are any overall changes in these responses with different ground improvement schemes. The trend in those changes may be useful for understanding the general effect of ground improvement.

On the other hand the predicted ground and structure movements appeared to be more reliable than the predicted accelerations and excess pore water pressures. Therefore, a more rigorous comparison of the predicted and measured ground and structure movements was performed for the centrifuge tests and field case history. The results of this comparison is presented in Table 6.10, where the ratio of the predicted to measured ground and structure displacements are given for each test. As seen from the table, the predicted horizontal movements were on average 1.5 times the measured value with a range of approximately 0.6 to 2.3. The predicted settlements were on average 1.1 times the measured values, with a range of 0.6 to 1.5. Based on this information it appears the predicted horizontal and vertical movements are roughly anywhere from 0.5 to 2 times the actual values. This type of difference between predicted and measured movements is similar to what is reported in the literature for other numerical modeling methods.

In order to realistically evaluate the performance of different ground improvement schemes for liquefaction mitigation at a bridge as part of a parametric study, it is necessary to check that the numerical modeling method being used can adequately predict the difference in

performance between different improvement methods. This check was accomplished using the ground and structure movement data from the centrifuge tests performed by Adalier (1996) consisting of a clayey sand embankment on a loose, liquefiable sand layer with different improvements. The cases tested by Adalier, as shown in Figure 3.5, included:

- no improvement,
- densified zones under the embankment toes,
- cemented zones under the embankment toes,
- gravel berms placed against the embankment sides, and
- steel sheeting installed at the toes and connected with tie rods.

For the purposes of this assessment only the no improvement, densified zones, and gravel berm cases were considered. In the cemented zone and steel sheeting tests, there was some sliding of the cement blocks and steel sheets relative to the bottom of the centrifuge box. Accurately simulating this sliding phenomena in the FLAC analysis would be difficult and therefore these cases were not considered.

Figure 6.65 presents a comparison of the predicted and measured embankment crest settlements (average obtained from settlement points L3 and L4) for the three different improvement types for shaking events 1, 2 and 3. As seen from this figure the predicted and measured values indicate the same general trend in settlement reduction using the densification and gravel berms compared to the no improvement cases. The plots also indicate that the predicted settlements tend to be larger than the measured settlements for these three different improvement schemes. It can also be seen that the FLAC analyses indicate the gravel berm to be slightly more effective in reducing the embankment settlements for the second and third shakes, whereas the measured results indicate that the densified zones are slightly more effective than the gravel berms. The same type of trends between the predicted and measured crest settlements were observed when plotting the total crest settlements that accumulated over the three successive shakes, as shown in Figure 6.66.

A comparison of the predicted and measured maximum horizontal displacement under the embankment toe after three shakes for the different improvement cases is presented in Figure 6.67. Again, the predicted results indicate the same trend in the horizontal displacements at the

toe that the measured results show, with the two improvements reducing the horizontal displacement. The horizontal displacements tend to be overpredicted by the FLAC analyses by a factor of approximately 1.7 to 2.7 times the measured displacement.

It should be noted that the overprediction of settlements and horizontal displacements for the embankment on the loose sand with different improvements indicated in Figures 6.65 to 6.67 and in Table 6.10 can likely be attributed, in part, to the manner that the three successive shaking events on the same centrifuge model was handled in the FLAC analyses. In the analyses for shaking events 2 and 3, the finite element grid for the embankment prior to any shaking was used along with soil properties that were adjusted to account for any densification physically measured in the centrifuge model that occurred in prior shakes. The fact that the stress state and grid used in the FLAC analyses for shaking events 2 and 3 did not account for the changes in geometry and stress distribution that occurred during prior shakes probably caused more conservative deformations to be predicted.

Overall, the results in Figures 6.65, 6.66, and 6.67 show that analyses performed with the Pyke-Byrne model in FLAC can predict the relative reduction in movements of a structure on liquefiable soils, such as an embankment, using different types of ground improvement. Therefore, this numerical modeling approach will be useful for judging the effectiveness of different ground improvement schemes in reducing seismically-induced movements of bridge piers and abutments on liquefiable soils .

6.5 Implications for Model Use

The calibration and verification analyses performed with FLAC and the Pyke-Byrne model indicate that this numerical modeling approach can be used to:

- Capture the basic soil shear stress-strain and pore water pressure response associated with the development of liquefaction and
- Predict the overall behavior of a system consisting of a structure on a shallow foundation or embankment supported on liquefiable soil with or without ground improvement and subjected to shaking.

When used with the maximum shear modulus formula and K_{2max} values proposed by Seed and Idriss (1970) along with the volumetric strain formulae and constants proposed by Byrne (1991) for clean sand, the Pyke-Byrne soil model appears to adequately capture the liquefaction resistance of "typical" clean sand as given by the liquefaction potential curve in the 1997 NCEER liquefaction report. For a specific sand type, property and parameter values for the model can be developed from laboratory test data on that specific soil, as demonstrated by the calibration and verification work done using the laboratory and centrifuge tests performed with Nevada sand.

Based on the results of the verification analyses performed, the permanent deformations/displacements of a structure or embankment supported in liquefiable soil with or without improved ground zones can be predicted within a factor of about two, with the predicted values likely being anywhere from 0.5 to 2 times the actual values. The predicted pore water pressures and accelerations are not as reliable as the predicted deformations, and can likely only be used to get a sense of general trends in these responses rather than detailed insight.

Since one of the key factors in the performance of a bridge or other structure on an improved ground zone within a liquefiable soil deposit is the permanent deformations that occur, the inability to predict time histories of pore water pressure and acceleration consistently in all cases was not viewed as an impediment for using the Pyke-Byrne model in FLAC to assess the effects of ground improvement. Therefore, having a knowledge of the numerical analysis limitations, the Pyke-Byrne soil model with "typical" sand parameters was used with FLAC to perform parametric studies of ground improvement for mitigation of liquefaction effects at bridge piers and stub abutments on shallow foundations. The approach to these studies, results obtained, and lessons learned are presented in the next two chapters.

TABLE 6.1: Properties of Nevada Sand (after Arumoli et al., 1992)

Relative Density, Dr (%)	Dry Unit Weight (kN/m3)	Void Ratio	Hydraulic Conductivity (cm/sec)
40.2	15.08	0.736	6.6×10^{-3}
60.1	15.76	0.661	5.6×10^{-3}
91	16.95	0.546	2.3×10^{-3}

TABLE 6.2: Peak Friction Angles and Shear Modulus Numbers Used for Nevada Sand Based on VELACS Test Data (after Arumoli et al., 1992)

Relative Density, Dr (%)	Shear Modulus Number, K_{2max} [1]	Peak Effective Friction Angle, ϕ' (degrees)		
		Triaxial Compression		Undrained Simple Shear [2]
		Drained	Undrained	
40	35	35	34	33
60	42	37	36	35 [3]

Notes:
1. K_{2max} used to calculate maximum shear modulus, G_{max}, based on formula by Seed and Idriss (1970): $G_{max} = 1000\ K_{2max}\ (\sigma_m')^{0.5}$ where σ_m' is the mean effective confining stress in psf and G_{max} is in psf.
2. Test referred to as direct simple shear test in laboratory report by Arumoli et al. (1992).
3. Measured value of 30^o was slightly inconsistent with measured values from other strength tests. Therefore, value increased to 35^o for consistency.

TABLE 6.3: Volumetric Strain Constants for Nevada Sand Obtained from Simple Shear and Centrifuge Simulations

Relative Density, Dr (%)	From Simple Shear Simulations [1]		From Centrifuge Test Simulations [2]		From Byrne (1991) Formula [3]	
	C_1	C_2	C_1	C_2	C_1	C_2
40	1.15	0.35	0.8	0.5	0.75	0.53
60	0.6	0.67	0.8	0.5	0.27	1.46
90	-	-	0.13	3.08	0.099	4.04

Notes:
1. Conducted using single element. Bulk modulus of water of 2.0×10^6 kPa used in simulation.
2. Conducted using grid having multiple elements. Bulk modulus of water of 2.0×10^5 kPa used in simulation.
3. Values for C_1 and C_2 calculated from formula for sands given in equation 6.7 and 6.8.

TABLE 6.4: Shear Modulus Number, K_{2max}, for Clean Sand (after Kramer, 1996)

Relative Density, Dr (%)	K_{2max}[1]
30	34
40	40
45	43
60	52
75	59
90	70

Note:
1. K_{2max} values are based on work of Seed and Idriss (1970).

TABLE 6.5: Volumetric Strain Constants for "Typical" Sand

Relative Density, Dr (%)	From Byrne (1991) Formula		From Simple Shear Simulation[1, 2]	
	C_1	C_2	C_1	C_2
40	0.75	0.53	0.75	0.53
60	0.27	1.46	0.20	2.0
75	0.156	2.56	0.058	6.84

Notes:
1. C_1 and C_2 selected to give liquefaction of element in approximately 15 cycles using cyclic stress ratio determined from liquefaction potential curve presented in report by NCEER (1997).
2. Conducted using a single element. Bulk modulus of water of 2.0×10^6 kPa used in simulation.

TABLE 6.6: Summary of Centrifuge Tests and Field Case Histories Used for Verification

Case	Applicability to Bridge	Source of Data	Type of Data	Conditions	Applied Motion	Schematic of Conditions
Uniform Sand Deposit	Free-field conditions	Liu (1992)	Centrifuge test	Saturated, medium dense (Dr = 60%) sand	10-cycle, 2-Hz sinusoidal wave; amplitude of 0.05 to 0.24g.	Fig. 6.5
Limited Size Surface Load	Pier on footing	Liu (1992)	Centrifuge test	Circular model footing (steel disk) on saturated, medium dense (Dr = 53%) sand	10-cycle, 2-Hz sinusoidal wave; uniform amplitude of 0.35g	Fig. 6.6
Grade Change	Approach embankment at abutment	Adalier (1996)	Centrifuge test	Dense (Dr = 80%) sand embankment on saturated, loose (Dr = 40%) sand [1]	20-cycle, 2-Hz "noisy" wave; uniform amplitude of 0.31g [1]	Fig. 6.7
		Zeng (1993)	Centrifuge test	Submerged, metal block gravity retaining wall with surface load in medium dense (Dr = 60%) sand	12-cycle, 2-Hz, sinusoidal wave; amplitude of 0.1 to 0.25g	Fig. 6.8
		Baziar et al. (1992)	Field case history – Wildlife Site	4.9-m-deep river channel incised in layered soil deposit consisting of silts and sands	20-second strong motion: 0.17g peak amplitude, 3-Hz predominant frequency	Fig. 6.17 and 6.18
Ground Improvement	Improvement performance	Adalier (1996)	Centrifuge test	Adjacent, vertical zones of saturated [2] loose (Dr = 40%) and dense (Dr = 90%) sands	10-cycle, 2-Hz, sinusoidal wave; uniform amplitude of 0.19g	Fig. 6.9
		Adalier (1996)	Centrifuge test	Clayey sand embankment on saturated [2], loose (Dr = 40%) sand with and without improvements	3 successive shakes with 10-cycle, 1.6-Hz, sinusoidal waves having uniform amplitudes of 0.09, 0.16, and 0.25g, respectively	Fig. 6.10 for densified zones; Fig. 3.5 for all cases

Notes:

1. This case only analyzed for first of two shaking events. "Noisy" wave motion had predominant frequency of 2 Hz. Input motion was approximated in FLAC with a "saw-tooth" type wave having a predominant frequency of 2 Hz.
2. Soil was saturated with a fluid consisting of 60 percent glycerin and 40 percent water having a viscosity about 10 times that of water to counterbalance effect of high g's on soil hydraulic conductivity. Unless noted, other centrifuge test cases listed used water as the pore fluid.

TABLE 6.7: Parameter Values Used in Simulation of Centrifuge Tests

Relative Density, Dr (%)	Peak Effective Friction Angle, ϕ' (degrees)		Dilation Angle (degrees)		Shear Modulus Number	Hydraulic Conductivity (cm/sec)[1,2]	Volumetric Strain Constants	
	Drained	Undrained	Drained	Undrained			C1	C2
30	33	32	0	0	-	-	-	-
40	34	33	0.4	0.2	35	6.6×10^{-3}	0.8	0.5
50	35	34	0.4	0.2	40	6.1×10^{-3}	0.8	0.5
60	36	35	0.4	0.2	42	5.6×10^{-3}	0.8	0.5
70	37	36	0.6	0.4	-	-	-	-
80	38	37	0.8	0.6	63	3.4×10^{-3}	0.13	3.08
90	39	38	1.0	0.8	70	2.3×10^{-3}	0.13	3.08

Notes:

1. Hydraulic conductivity values presented are for a 1g gravitational field.
2. Hydraulic conductivity values shown were based on data reported by Arumoli et al. (1992) in report for VELACS project. Liu (1992) reports $k = 2.1 \times 10^{-3}$ cm/sec for Nevada sand; this value was used in simulation of his centrifuge tests of a uniform, medium dense sand layer and a model footing on a medium dense sand layer.

TABLE 6.8: Parameter Values Used in FLAC Simulation of Wildlife Site

Soil Type	Depth (m)	Average Blow Count, N (blows/ft)	Peak Friction Angle (degrees)	Dilation Angle (degrees)	Cohesion (kPa)	Shear Modulus Number, K_{2max} [2]	Hydraulic Conductivity (cm/sec)	Volumetric Strain Constants	
								C_1	C_2
Sandy Silt	0 – 2.5	2.3	28	0.2	0	23	5×10^{-5}	1.13	0.15
Sandy Silt [1]	2.5 – 3.5	3	28	0.2	0	23	5×10^{-5}	1.22	0.33
Silty Sand to Fine Sand	3.5 – 6.8	8.4	33	0.2	0	23	2.1×10^{-4}	0.44	0.91
Clayey Silt to Silty Clay	6.8 – 7.5	10.3	28	0	48	-	1×10^{-6}	0	0

Notes:

1. Sandy silt layer also described as silty sand layer in Baziar et al. (1992).
2. K_{2max} used to calculate maximum shear modulus, G_{max}, based on formula by Seed and Idriss (1970): $G_{max} = 1000\ K_{2max}\ (\sigma_m')^{0.5}$ where σ_m' is the mean effective confining stress in psf and G_{max} is in psf. For clayey silt/silty clay G_{max} computed using formula: $G_{max} = 2300\ s_u$ where s_u is the undrained shear strength of the soil.

TABLE 6.9: Comments on Predicted Results from FLAC Simulations in Comparison to Measured Response

Case	Source of Data	Model Setup and FLAC Grid [1]	Plot of Predicted and Measured Response	General Observations on Predicted Response
Uniform Sand Deposit	Liu (1992) – Uniform medium dense sand	Figs. 6.5 and 6.11	Figs. 6.20 to 6.25	Magnitude of acceleration peaks generally predicted within factor of 1 to 2. Peak pore water pressures predicted are about 0.7 to 1 times measured. Pore pressures dissipate too rapidly after shaking stops. Ground surface settlement is underpredicted.
Limited Size Surface Load	Liu (1992) – Footing on medium dense sand	Figs. 6.6 and 6.12	Figs. 6.26 to 6.31	Predicted peaks in footing acceleration are approximately 1 to 2 times measured. Development of negative excess pore water pressure below footing predicted, but subsequent increase in pore pressure to positive values due to migration is not. Predicted settlement of footing is about 0.8 times measured
Grade Change	Adalier (1996) – Dense embankment on loose sand	Figs. 6.7 and 6.13	Figs. 6.32 to 6.37	Predicted peaks in acceleration records can be as small as one-third of measured values. Peak pore water pressures underpredicted by a factor ranging from 1 to 3 or more. Predicted settlements are approximately 1 to 1.5 times greater than measured and predicted horizontal displacements are approximately within a factor of 2 of the measured values.
	Zeng (1993) – Gravity retaining wall in medium dense sand	Figs. 6.8 and 6.14	Figs. 6.38 to 6.43	
	Bazier et al. (1992) – Wildlife Site	Figs. 6.18 and 6.19	Figs. 6.44 to 6.50	
Ground Improvement	Adalier (1996) – Adjacent loose and dense sand zones	Figs. 6.9 and 6.15	Figs. 6.51 to 6.56	Acceleration peaks of dense zone underpredicted at some locations by a factor of up to 3. Predicted peak pore water pressures in dense zone are about 0.6 to 1.0 times measured. Predicted dense zone surface settlements and maximum horizontal movement of loose-dense boundary are approximately 0.6 times measured.
	Adalier (1996) – Embankment on loose sand with different improvements	Figs. 6.10 and 6.16 (dense zone improve-ment)	Figs. 6.57 to 6.62	Peaks in embankment acceleration generally underpredicted, by up to a factor of 3. Predictions of pore water pressures in ground beneath and adjacent to embankment vary from good to bad, with pressures generally dissipating too rapidly after shaking stops. General tendency to overpredict settlement and horizontal movement of embankment and underlying ground by factor up to about 1.5 to 2 times.

Note: 1. These figures show locations where predicted and measured responses were obtained.

TABLE 6.10: Comparison of Predicted and Measured Movements for Verification Cases

Case	Source of Data	Predicted to Measured Settlements		Predicted to Measured Horizontal Movements	
		Instruments Used	**Ratio**	**Instruments Used**	**Ratio**
Limited Size Surface Load	Liu (1992) – Footing on medium dense sand	LVDT1	0.77	-	-
Grade Change	Adalier (1996) – Dense embankment on loose sand [1]	L1, L2	1.22	-	-
	Zeng (1993) – Gravity retaining wall in medium dense sand	Measurement immediately behind wall	1.53	LVDT1	2.36
	Baziar et al. (1992) – Wildlife Site	-	-	Field Measurements	0.61
Ground Improvement	Adalier (1996) – Adjacent loose and dense sand zones	L4, L5, L6	0.60	Vertical noodles at boundary	0.62 [5]
	Adalier (1996) – Embankment on loose sand with different improvement [2]: (a) No improvement (b) Densified zones at toes (c) Gravel berms against sides	 (a) L3, L4 (b) L3, L4 (c) L3, L4	Average of all: 1.37 (a) 1.22 [3] (b) 1.52 [3] (c) 1.38 [3]	Vertical noodles under embankment: (a) toe and crest (b) toe and crest (c) toe	Average of all: 2.25 (a) 1.68 [4] (b) 2.37 [4] (c) 2.69 [4]
Average Predicted to Measured Ratios for All Cases:			**1.10**		**1.46**

Notes:
1. This case only analyzed for the first of two successive shaking events.
2. Cases involving cemented zones at embankment toes and steel sheetpiles at toes with tie rod not presented because of sliding that occurred between the bottom of the improvements and centrifuge box.
3. Value presented is average of three ratios computed using settlements for three separate shaking events performed in succession on the same model. Ratio for each shaking event was computed using only the settlement that occurred in that particular event.
4. Value presented is ratio based on total accumulated horizontal displacements measured after all three shaking events were performed. Maximum horizontal movements under toe and/or crest were used.
5. Maximum horizontal movement along vertical boundary between dense and loose zones used to compute ratio.

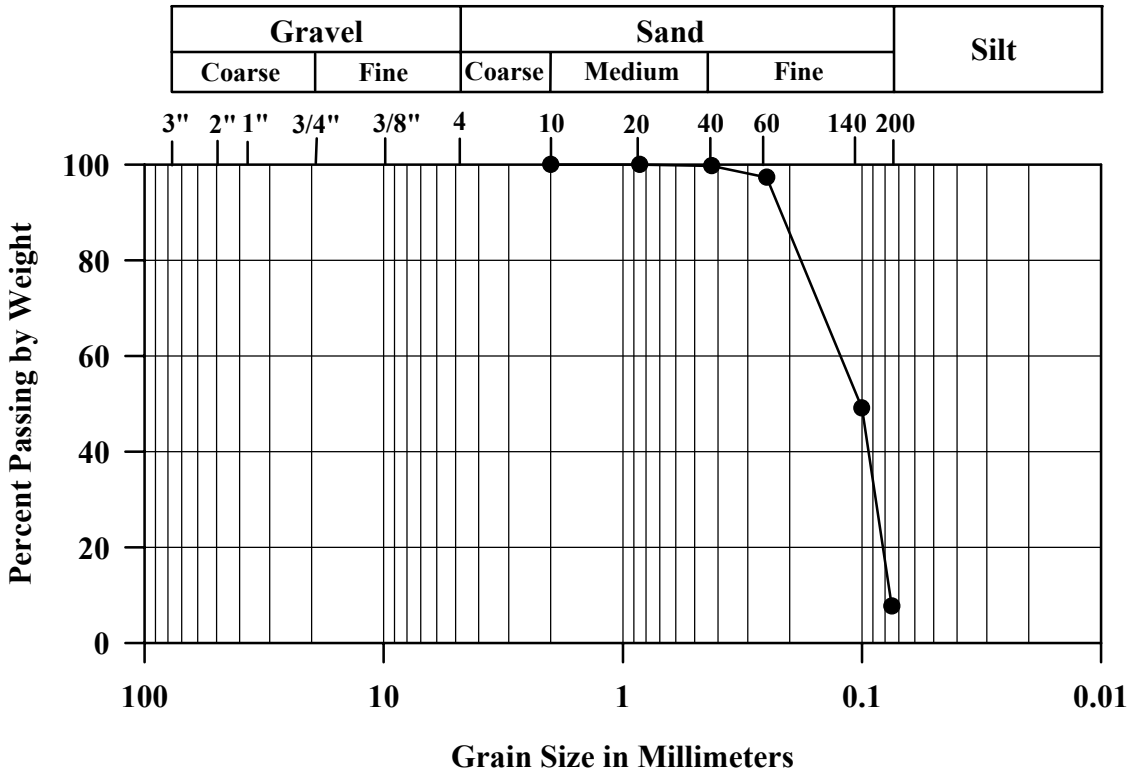

FIGURE 6.1: Grain Size Distribution Curve for Nevada Sand

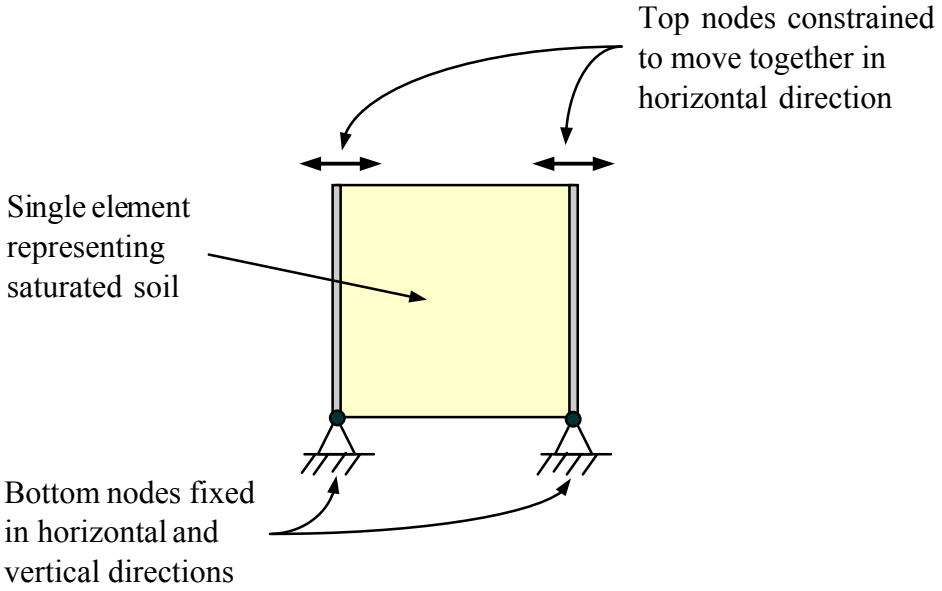

FIGURE 6.2: Single Element Model in FLAC for Simulating Cyclic Simple Shear Test

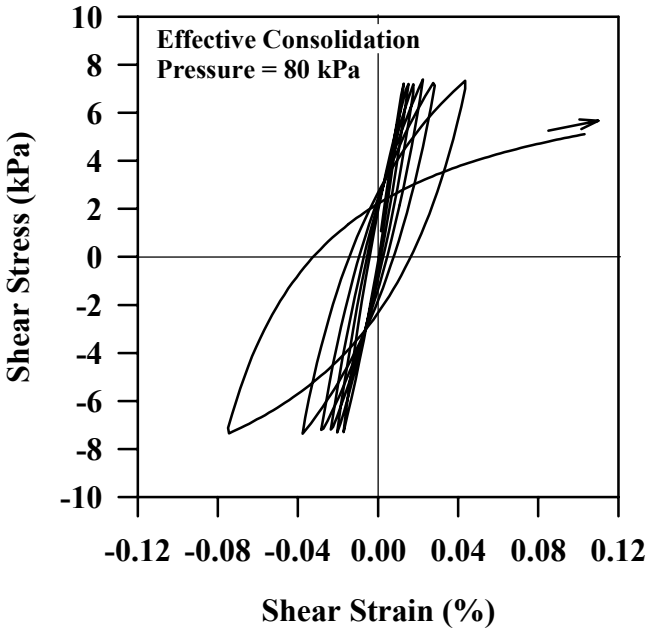

Note: Shear stress-strain curve shown is for 1/4 cycle less than pore water pressure plot due to large strain that develops.

(a) Shear Stress vs. Shear Strain

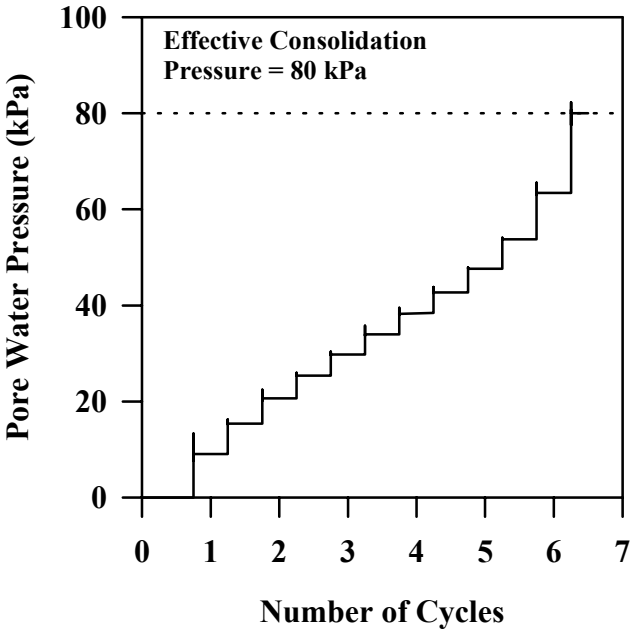

(b) Pore Water Pressure vs. Number of Loading Cycles

FIGURE 6.3: Predicted Response from FLAC for Cyclic Simple Shear Test on Nevada Sand at Dr = 40%, VELACS Test No. CSS 40-09

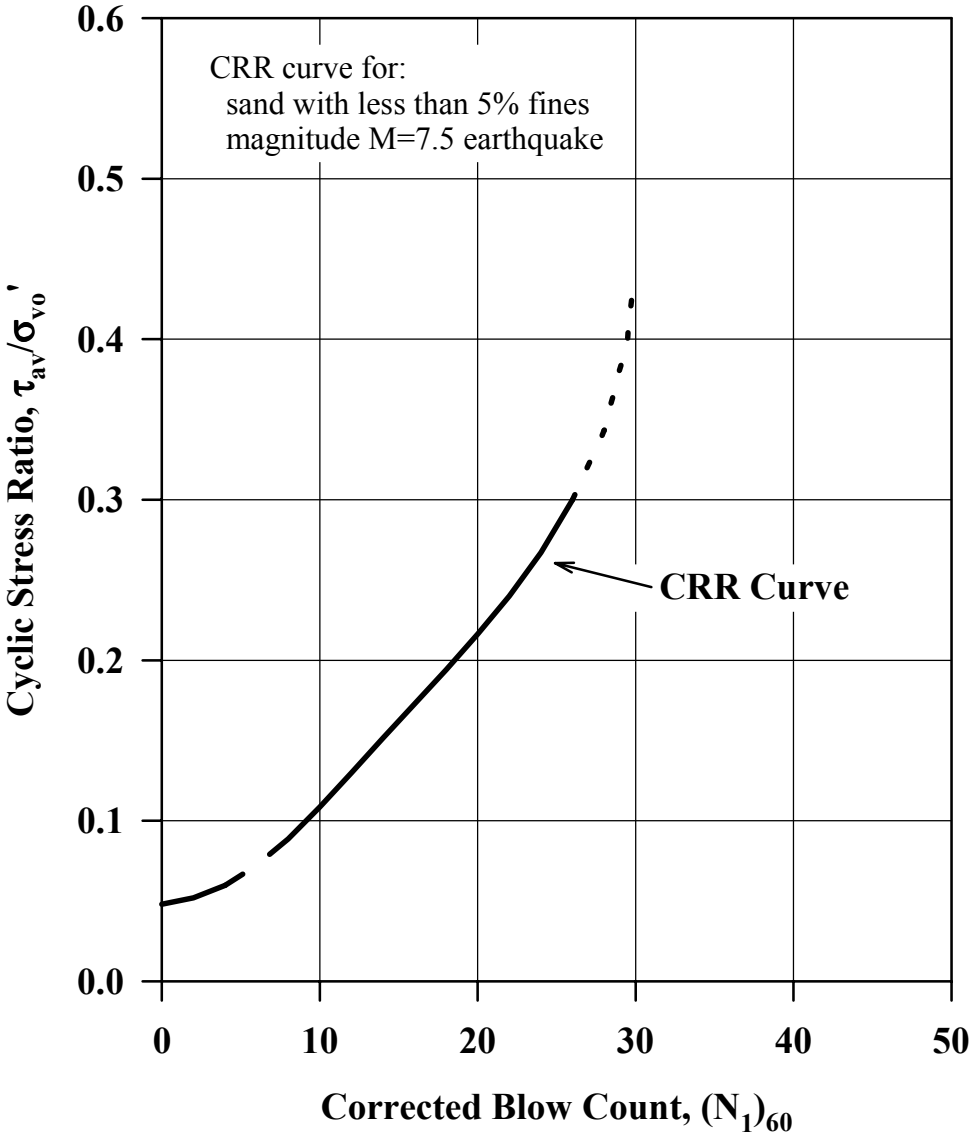

Note: Curve shown developed using equation by Blake for approximation of simplified base curve per NCEER (1997).

FIGURE 6.4: Simplified Base Curve Recommended for Calculation of Cyclic Resistance Ratio (CRR) from SPT Data (after NCEER, 1997)

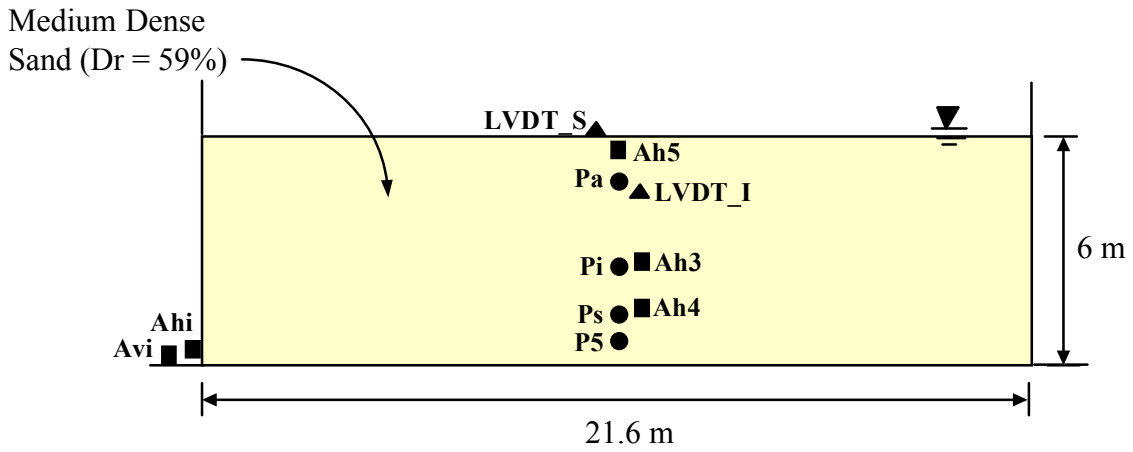

P5 ● Pore Pressure Transducer
Ah3 ■ Accelerometer (horizontal)
LVDT_I ▲ Settlement Point

Notes:
1. Dimensions shown are in prototype scale.
2. All accelerometers recorded horizontal acceleration, with exception of Avi which recorded vertical.

FIGURE 6.5: Uniform Medium Dense Sand Layer in CentrifugeTest by Liu (after Liu, 1992)

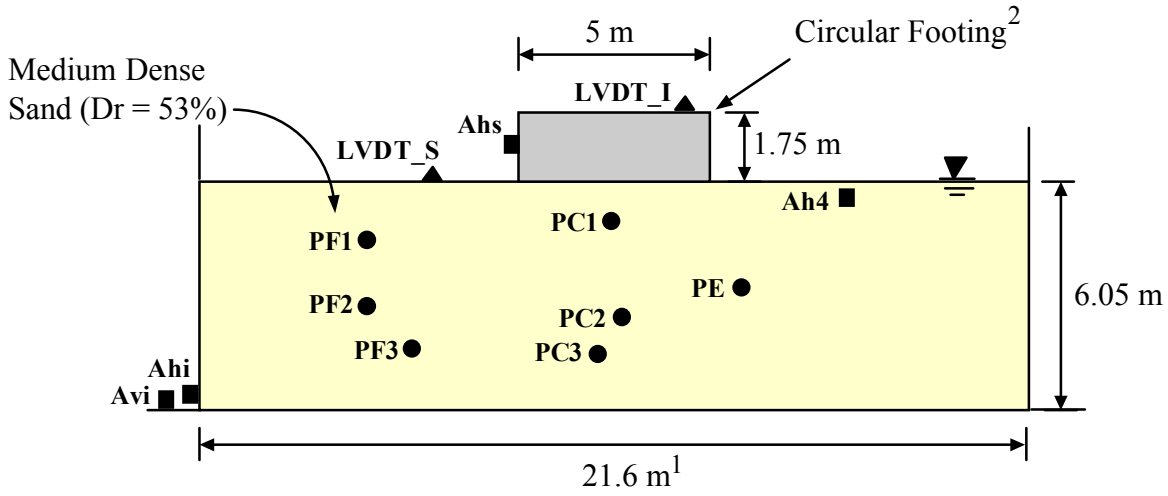

PF2 ● Pore Pressure Transducer
Ah4 ■ Accelerometer (horizontal)[3]
LVDT_I ▲ Settlement Point

Notes:
1. All dimensions given in prototype scale.
2. Footing has diameter of 5 m and exerts bearing pressure of 125 kPa. It is centered in box having width of 9.65 m.
3. All accelerometers recorded horizontal acceleration, with exception of Avi which recorded vertical.

FIGURE 6.6: Footing on Medium Dense Sand Layer in CentrifugeTest by Liu (after Liu, 1992)

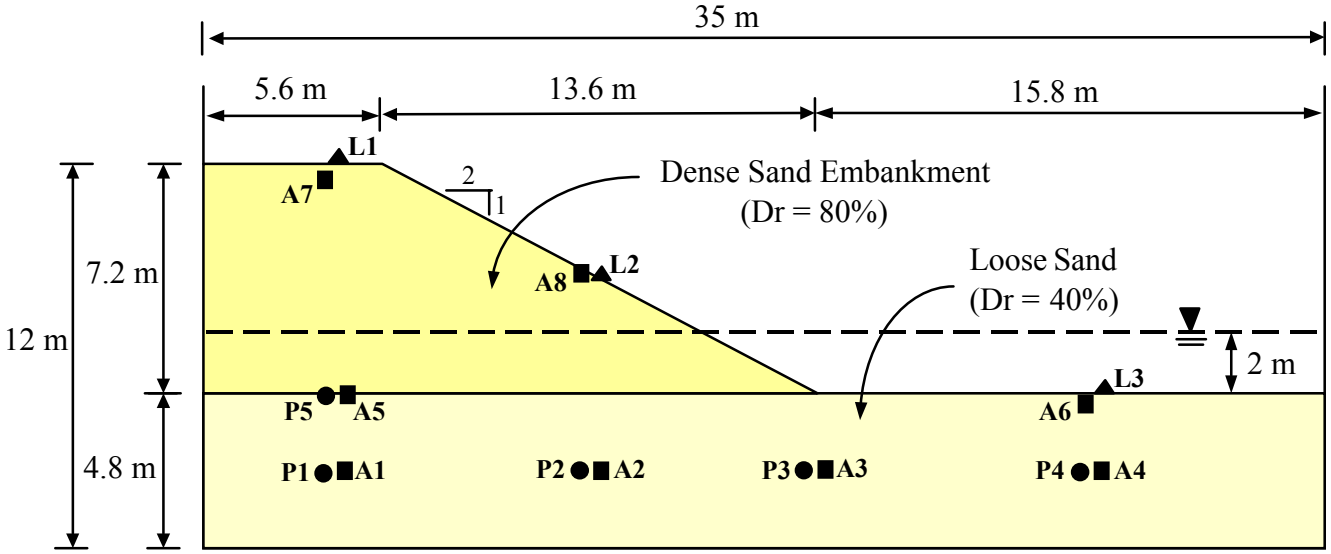

● Pore Pressure Transducer
■ Accelerometer (horizontal)
▲ Settlement Point

Notes:
1. Dimensions shown are in prototype scale.
2. Straight noodles were embedded vertically in loose sand and embankment to provide horizontal deformation information.

FIGURE 6.7: Dense Sand Embankment on Loose Sand Foundation in Centrifuge Test by Adalier (after Adalier, 1996)

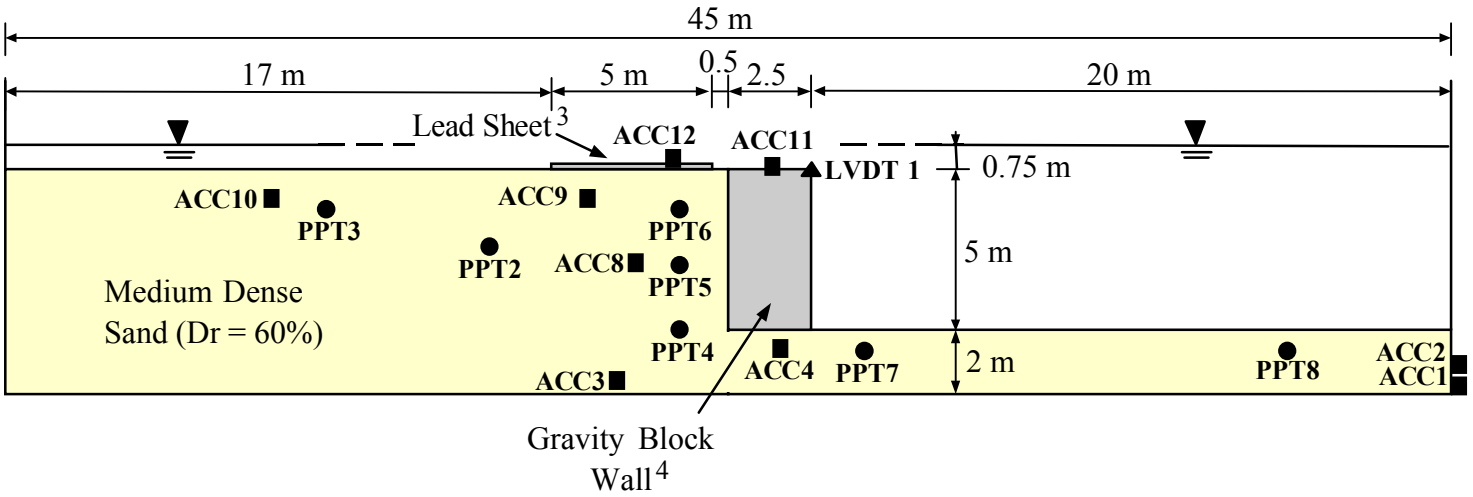

PPT7 ● Pore Pressure Transducer
ACC3 ■ Accelerometer [2]
LVDT 1 ▲ Horizontal Displacement Gauge

Notes:
1. Dimensions shown are in prototype scale.
2. All accelerometers record horizontal accelerations with exceptions of ACC2, ACC11, and ACC12, which record vertical accelerations
3. Lead sheet is 0.1 meter thick (prototype scale).
4. Gravity block wall is aluminum alloy.

FIGURE 6.8: Submerged Gravity Block Wall with Surface Load on Medium Dense Sand Layer in Centrifuge Test by Zeng (after Zeng, 1993)

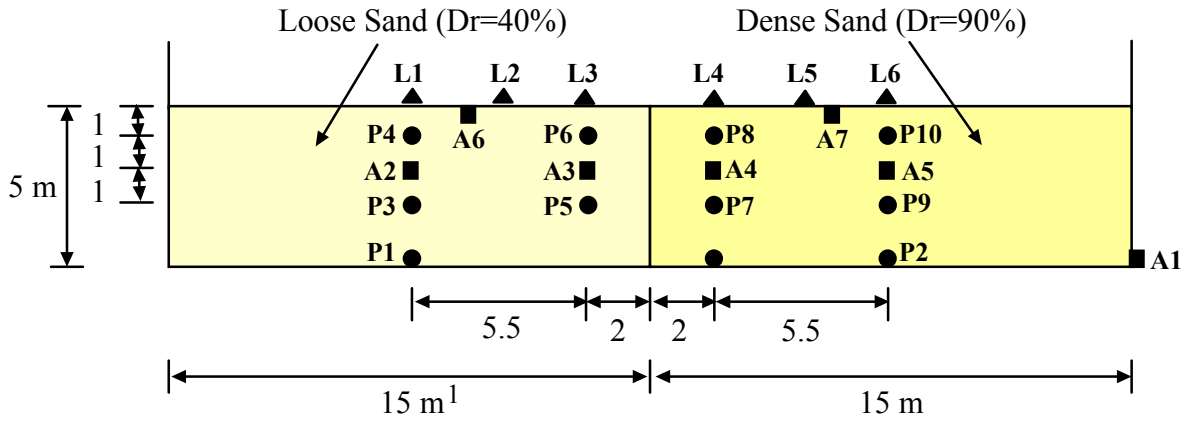

P7 ● Pore Pressure Transducer
A3 ■ Accelerometer (horizontal)
L1 ▲ Settlement Point

Notes:
1. Dimensions are shown in prototype scale.
2. Straight noodles were embedded vertically in soil at loose-dense boundary, and 0.5 m on each side of it, to provide horizontal movement information.

FIGURE 6.9: Adjacent Loose/Dense Sand Zones in Centrifuge Test by Adalier (after Adalier, 1996)

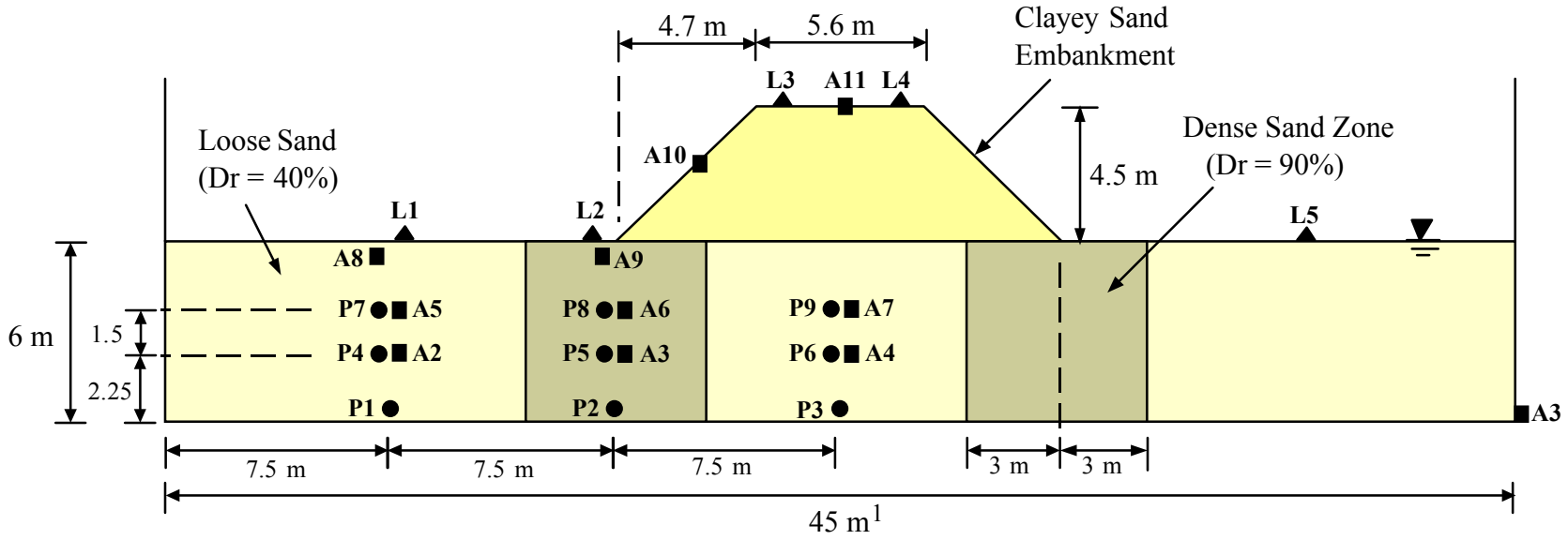

P7 ● Pore Pressure Transducer
A3 ■ Accelerometer (horizontal)
L1 ▲ Settlement Point

Notes:
1. All dimensions are shown in prototype scale.
2. Model shown is for densified zone improvement. Other models tested by Adalier (1996) included no improvement, cemented zone, gravel berm, and sheet piles with tie rod. Refer to Figure 3.5 for schematics of those cases. Instrument locations for these other cases was similar to shown here.
3. Straight noodles were embedded vertically in foundation soil at select locations for horizontal movement information.

FIGURE 6.10: Embankment on Loose Sand Layer with Densification Improvement in Centrifuge Test by Adalier (after Adalier, 1996)

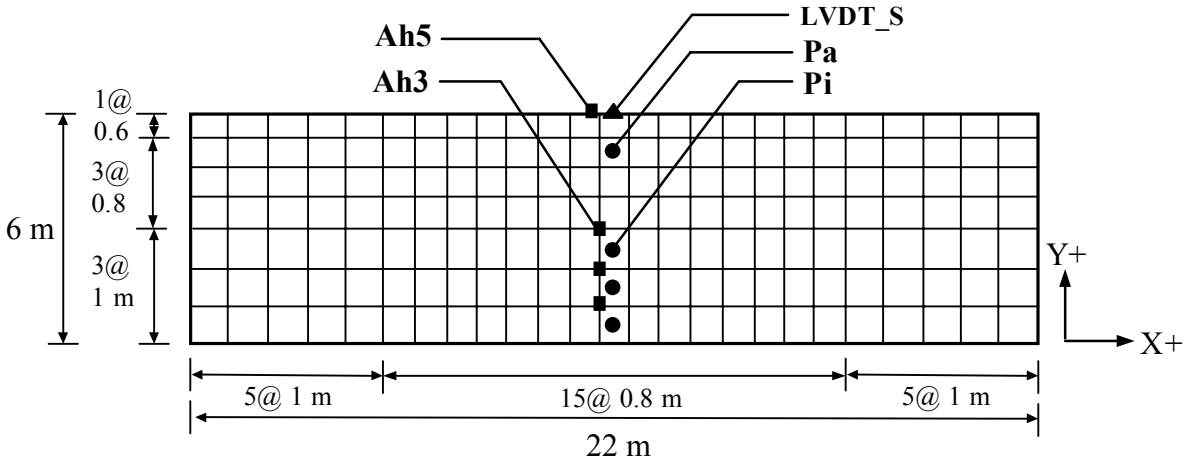

Time Histories Obtained:
- ● Pore pressure in element
- ■ X-acceleration at node
- ▲ Y-displacement at node

Notes:
1. Horizontal (x) acceleration record applied to nodes along bottom and sides of grid. Bottom of grid is fixed in vertical (y) direction.
2. Label indicates predicted time history for a particular element or node is provided as a figure, along with measured response. Label is same as instrument identification used in centrifuge test. Location of node or element is approximately same as corresponding instrument.

FIGURE 6.11: Mesh Used in FLAC Analysis of Centrifuge Test on Uniform, Medium Dense Sand Layer

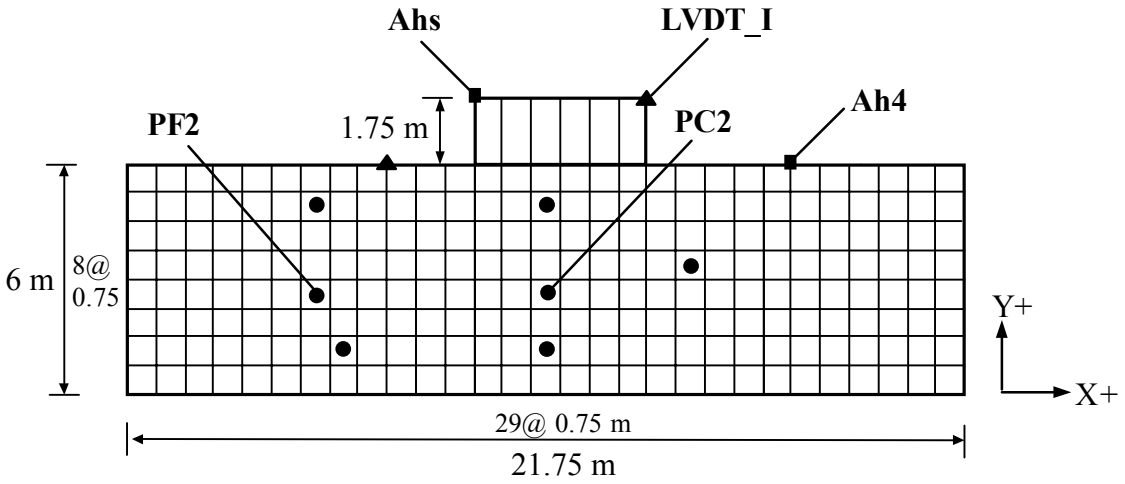

Time Histories Obtained:
- ● Pore pressure in element
- ■ X-acceleration at node
- ▲ Y-displacement at node

Notes:
1. Refer to Figure 6.11 for notes regarding side and bottom boundary conditions, location of time histories, and element and node labels.

FIGURE 6.12: Mesh Used in FLAC Analysis of Centrifuge Test of Footing on Medium Dense Sand Layer

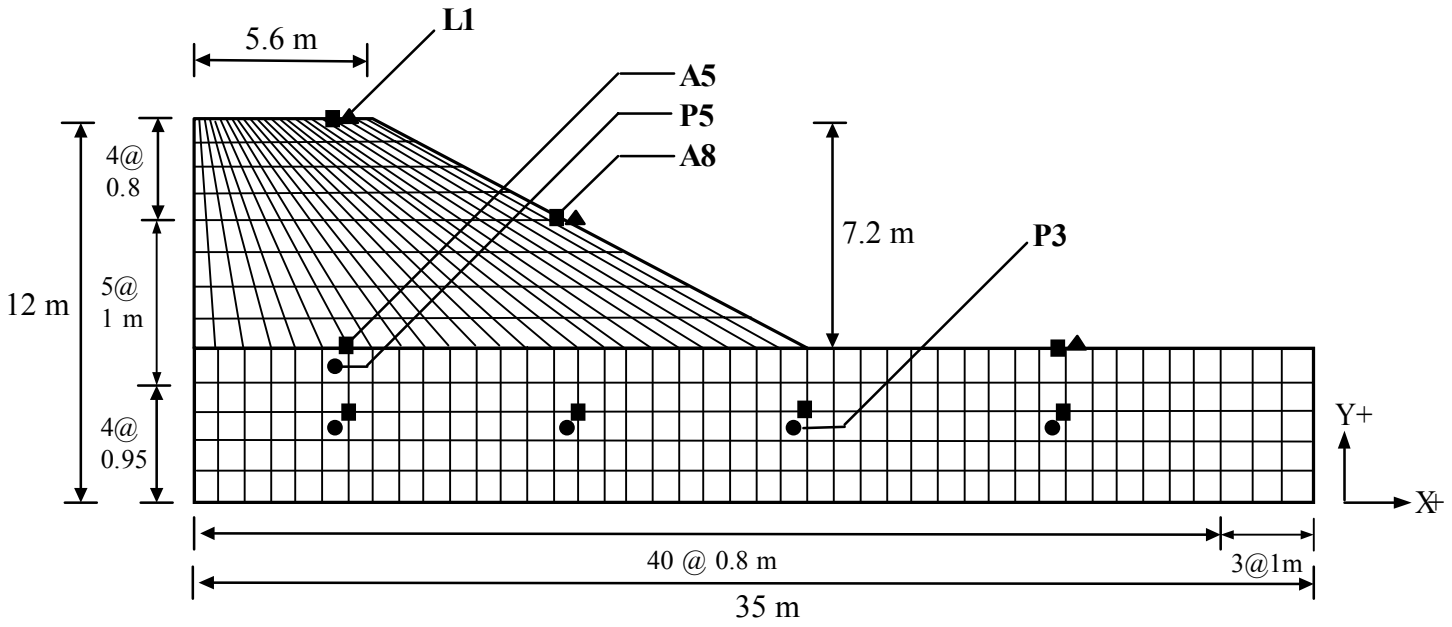

Time Histories Obtained:
- ● Pore pressure in element
- ■ X-acceleration at node
- ▲ Y-displacement at node

Notes:
1. Refer to figure 6.11 for notes regarding side and bottom boundary conditions, location of time histories, and element and node labels.

FIGURE 6.13: Mesh Used in FLAC Analysis of Centrifuge Test of Dense Sand Embankment on Loose Sand Foundation

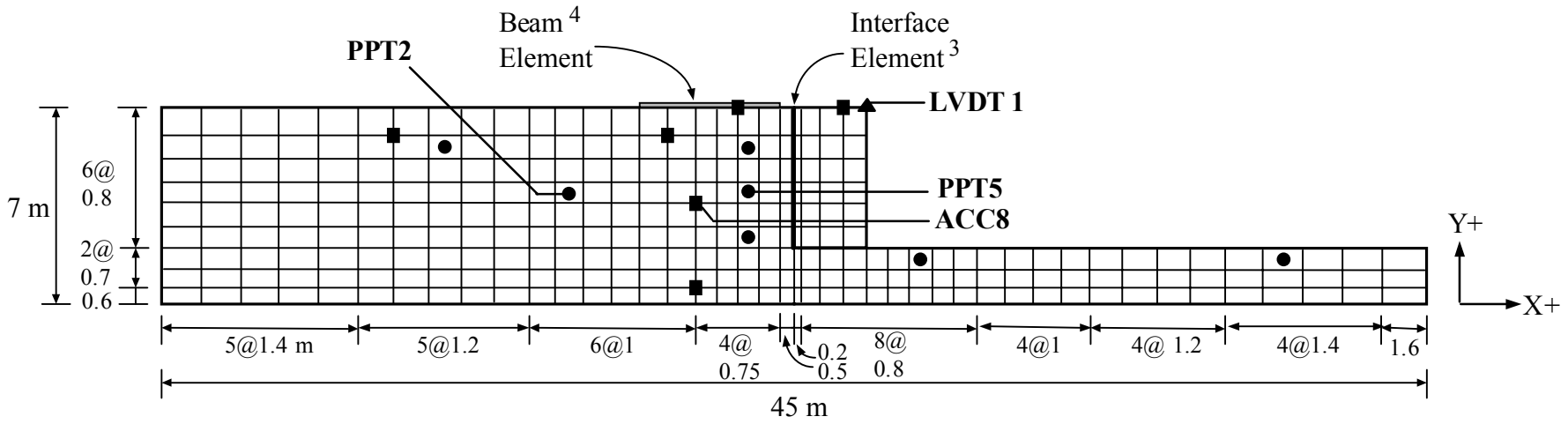

Time Histories Obtained:

- ● Pore pressure in element
- ■ X-acceleration at node
- ▲ X-displacement at node

Notes:

1. Horizontal (x) and vertical (y) acceleration records applied to nodes along bottom and sides of grid.
2. Refer to Fig. 6.11 for notes regarding location of time histories and element and node labels.
3. Interface element having friction angle of 17 degrees used between back of wall and soil.
4. Beam element used to represent lead sheet applying surface load behind wall.

FIGURE 6.14: Mesh Used in FLAC Analysis of Centrifuge Test of Submerged Gravity Block Wall with Surface Load on Medium Dense Sand Layer

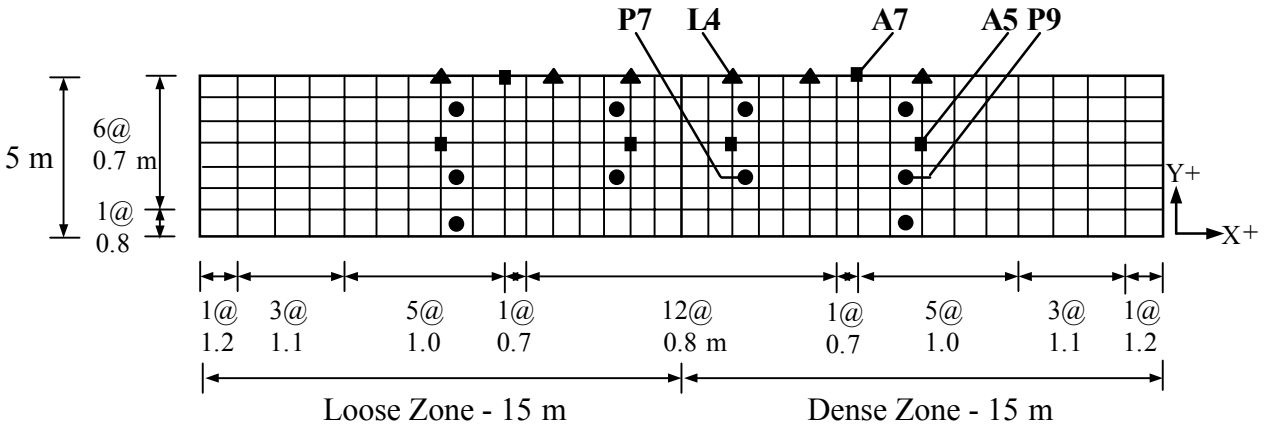

Time Histories Obtained:
- ● Pore pressure in element
- ■ X-acceleration at node
- ▲ Y-displacement at node

Notes:
1. Refer to Figure 6.11 for notes regarding side and bottom boundary conditions, location of time histories, and element and node labels.

FIGURE 6.15: Mesh Used in FLAC Analyses of Centrifuge Test on Adjacent Loose/Dense Sand Zones

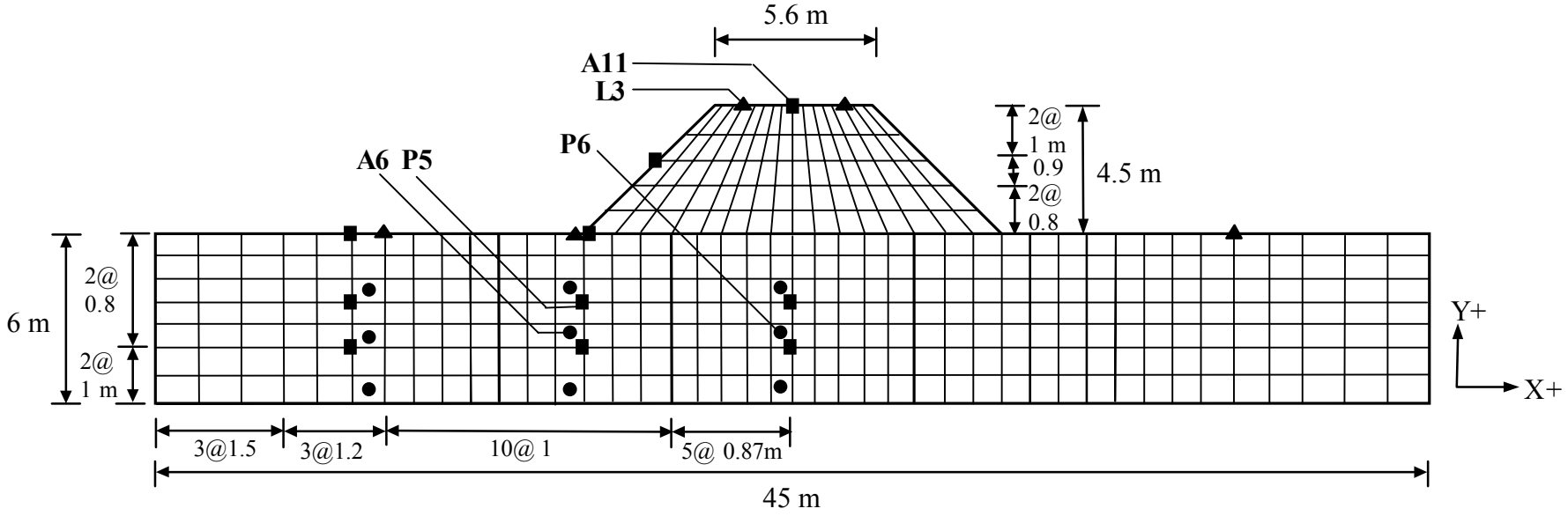

Time Histories Obtained:
- ● Pore pressure in element
- ■ X-acceleration at node
- ▲ Y-displacement at node

Notes:
1. Refer to Figure 6.11 for notes regarding side and bottom boundary conditions, locations of time histories, and element and node labels.
2. Model shown is for densified zone improvement. Other models tested by Adalier (1996) and simulated in FLAC included no improvement and gravel berms.

FIGURE 6.16: Mesh Used in FLAC Analysis of Centrifuge Test of Embankment on Loose Sand Layer with Densification Improvement

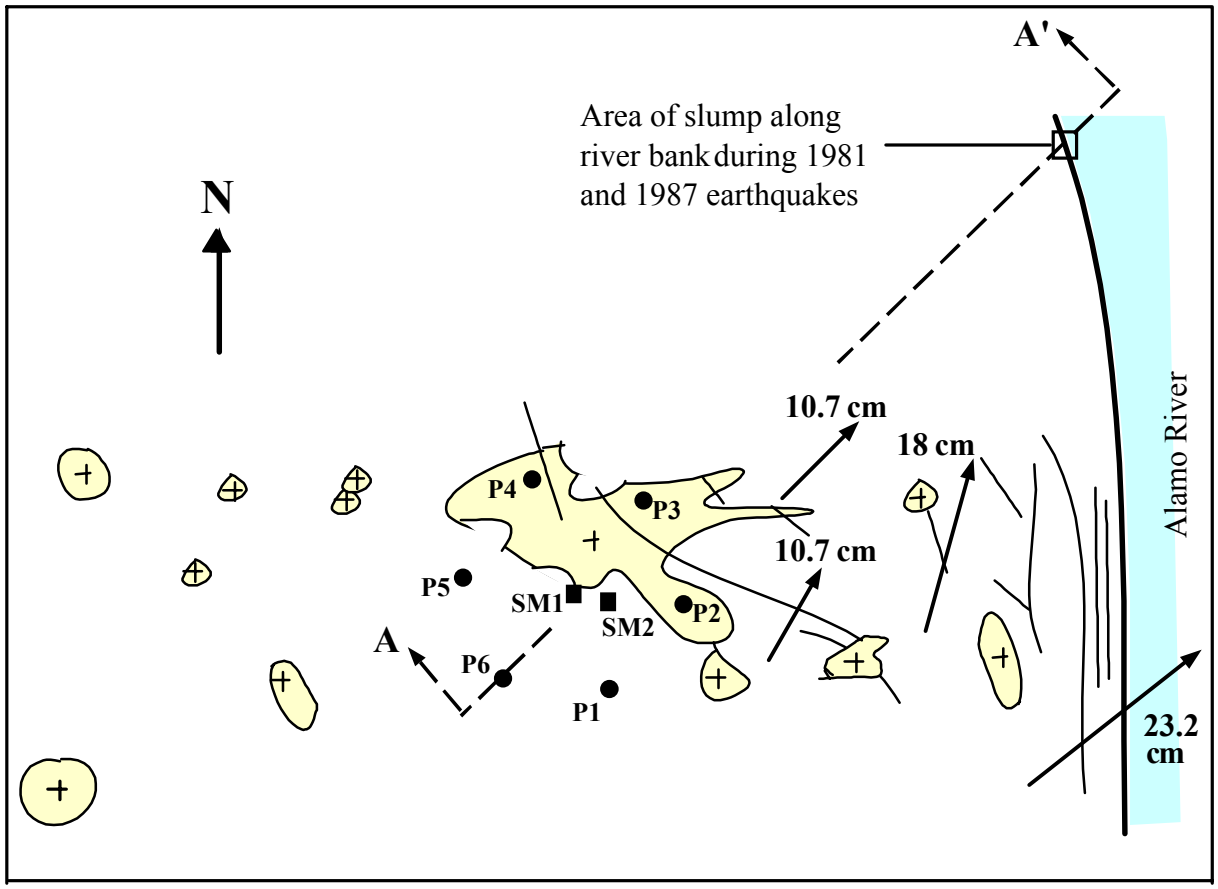

FIGURE 6.17: Plan of Sand Boils, Lateral Spreading, and Cracks at Wildlife Liquefaction Array After 1987 Superstition Hills Earthquake (after Bazier et al., 1992)

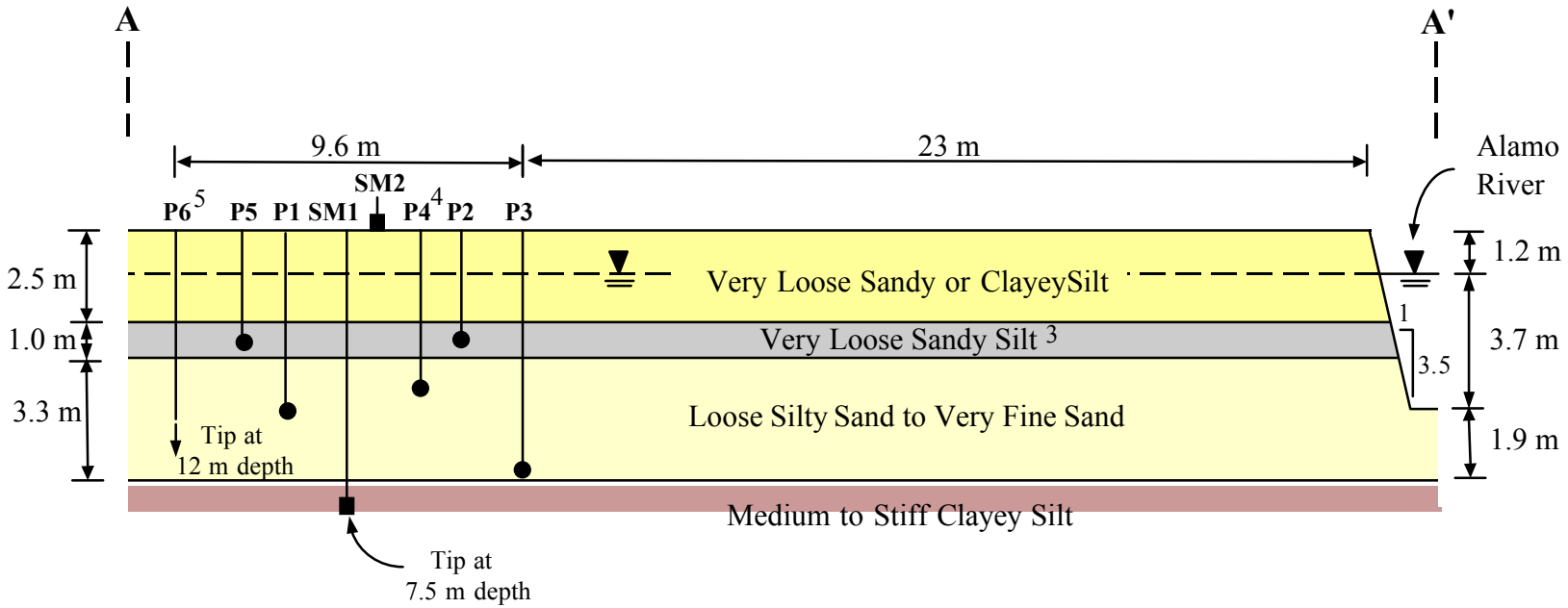

P2 Piezometer (Pore Pressure Transducer)

SM1 Accelerometers (horizontal and vertical)

Notes:

1. Instruments are offset perpendicular to section line A-A' as shown on Figure 6.17.
2. Profile based on information provided in Baziar et al. (1992) for vicinity of instrument array. Profile assumed to be same between instrument array and river.
3. Sandy silt layer also described as silty sand layer in Baziar et al.
4. No data provided in Baziar et al. for piezometer P4.
5. Tip of piezometer P6 located in silt layer at 12 m depth.

FIGURE 6.18: Section A-A' Showing Soil Profile and Instrumentation at Wildlife Liquefaction Array (after Baziar et al., 1992)

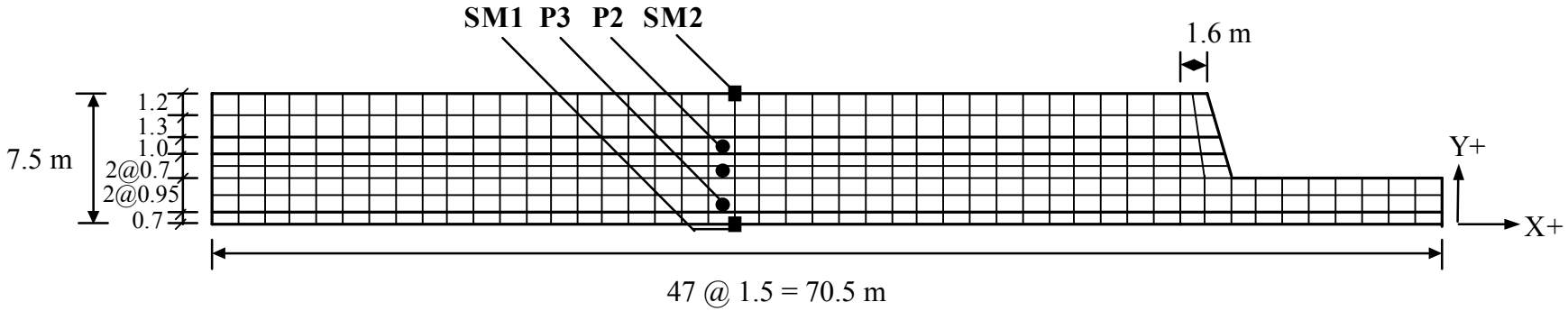

Time Histories Obtained:

- ● Pore pressure in element
- ■ X- and Y-acceleration at node

Notes:

1. Horizontal (x) velocity record applied to nodes along bottom and sides of grid. Vertical (y) velocity record applied to nodes along bottom of grid.
2. Label indicates predicted time history for a particular element or node is provided as a figure, along with measured response. Label is same as instrument identification used at monitored site. Depth of node or element relative to ground surface is approximately the same as in field.

FIGURE 6.19: Mesh Used in FLAC Analysis of Centrifuge Test of Wildlife Site During 1987 Superstition Hills Earthquake

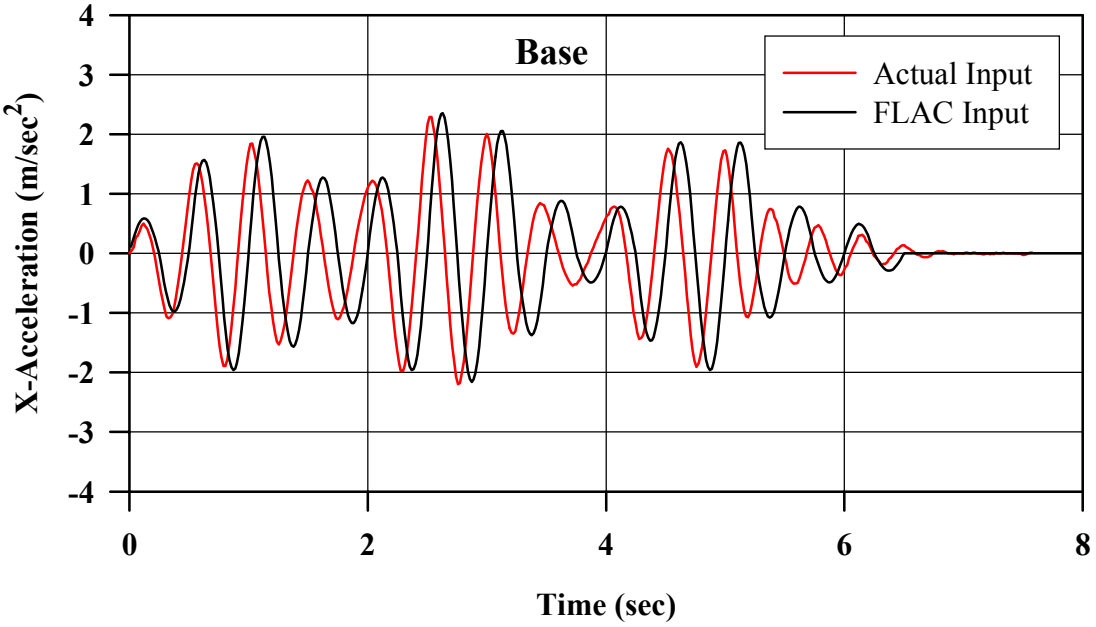

FIGURE 6.20: Actual and FLAC Input Base Acceleration Records for Uniform, Medium Dense Sand Layer in Centrifuge Test

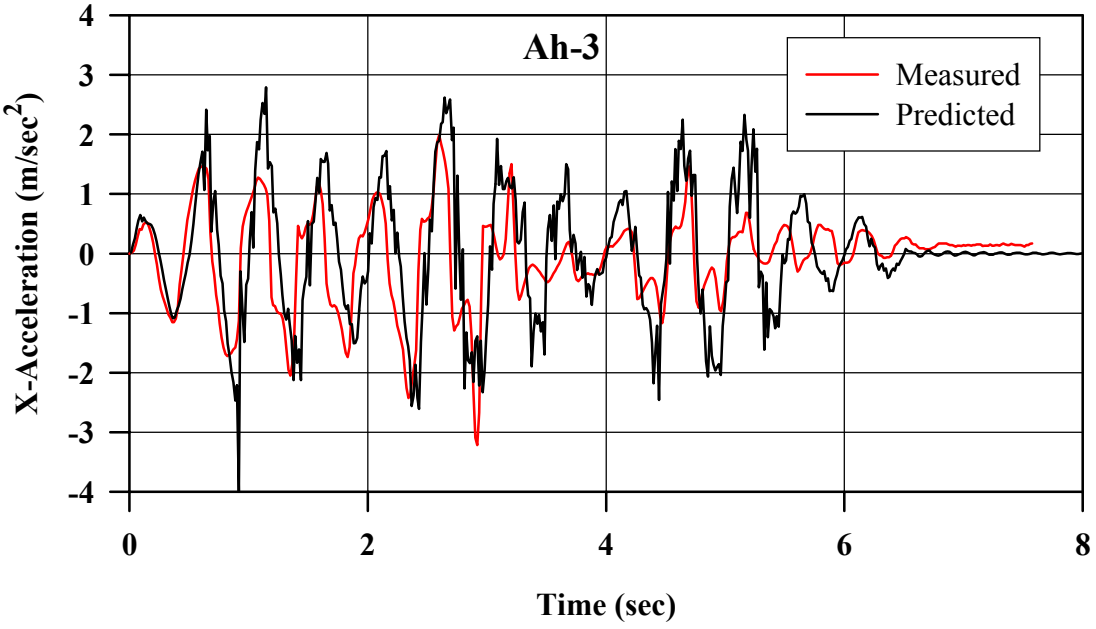

FIGURE 6.21: Measured vs. Predicted X-Acceleration at Ah-3 for Uniform, Medium Dense Sand Layer in Centrifuge Test

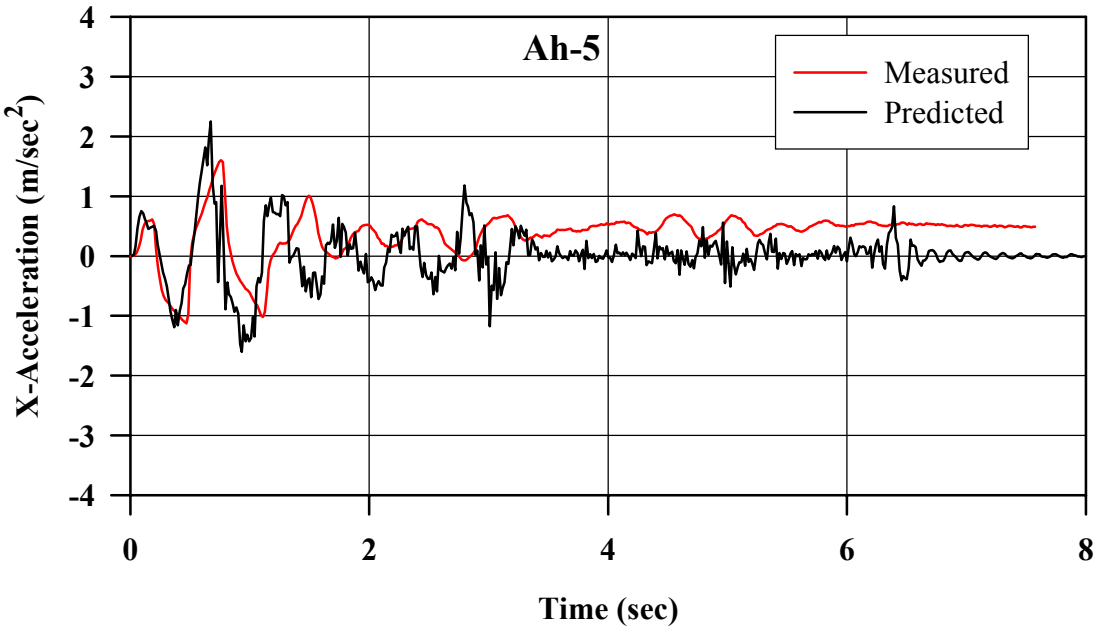

FIGURE 6.22: Predicted vs. Measured X-Acceleration at Ah-5 for Uniform Medium Dense Sand in Centrifuge Test

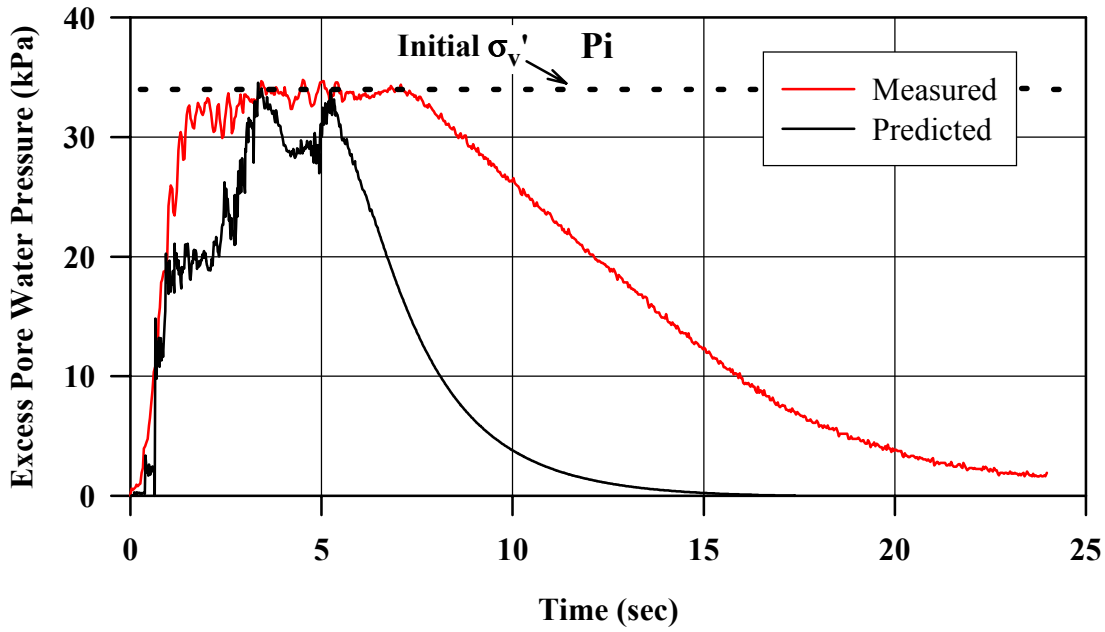

FIGURE 6.23: Predicted vs. Measured Excess Pore Pressure at Pi for Uniform, Medium Dense Sand in Centrifuge Test

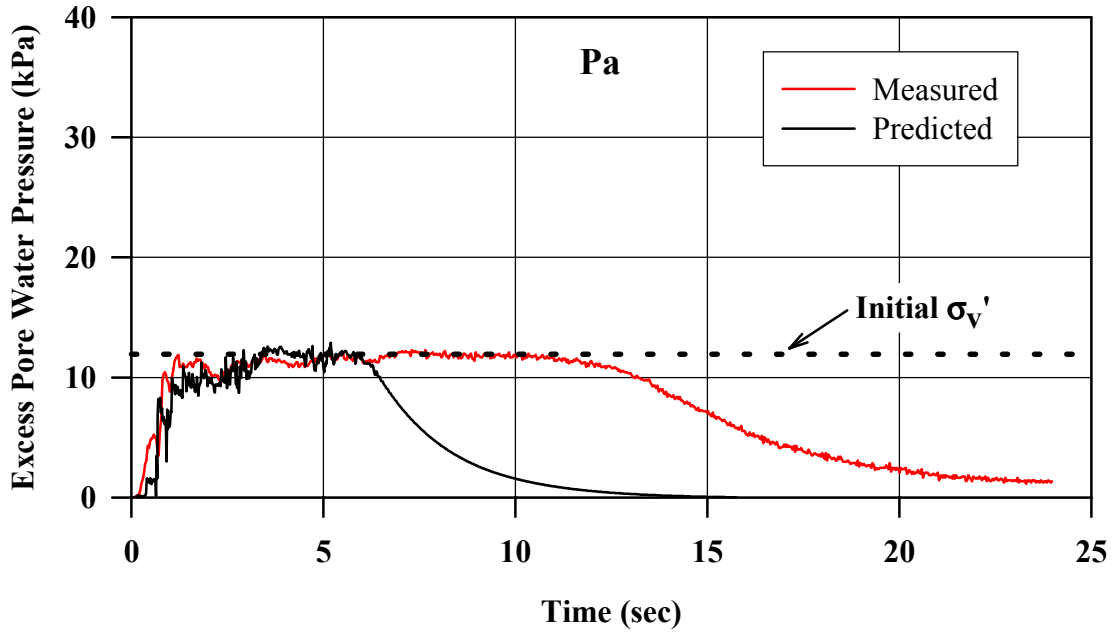

FIGURE 6.24: Predicted vs. Measured Excess Pore Pressure at Pa for Uniform, Medium Dense Sand in Centrifuge Test

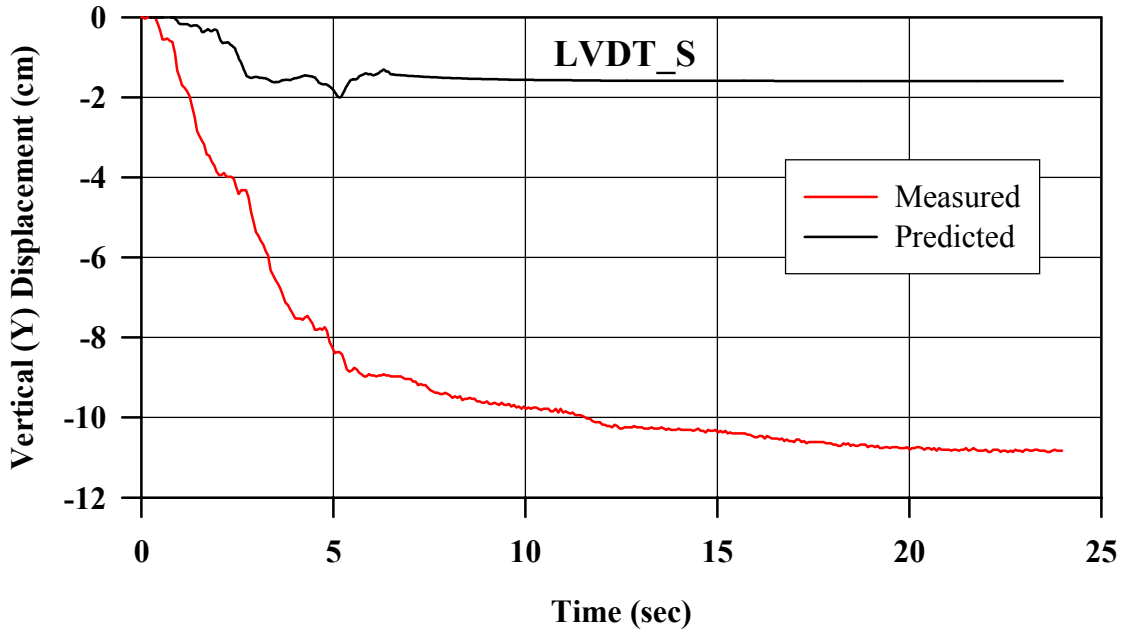

FIGURE 6.25: Predicted vs. Measured Vertical Displacement at LVDT_S for Uniform, Medium Dense Sand in Centrifuge Test

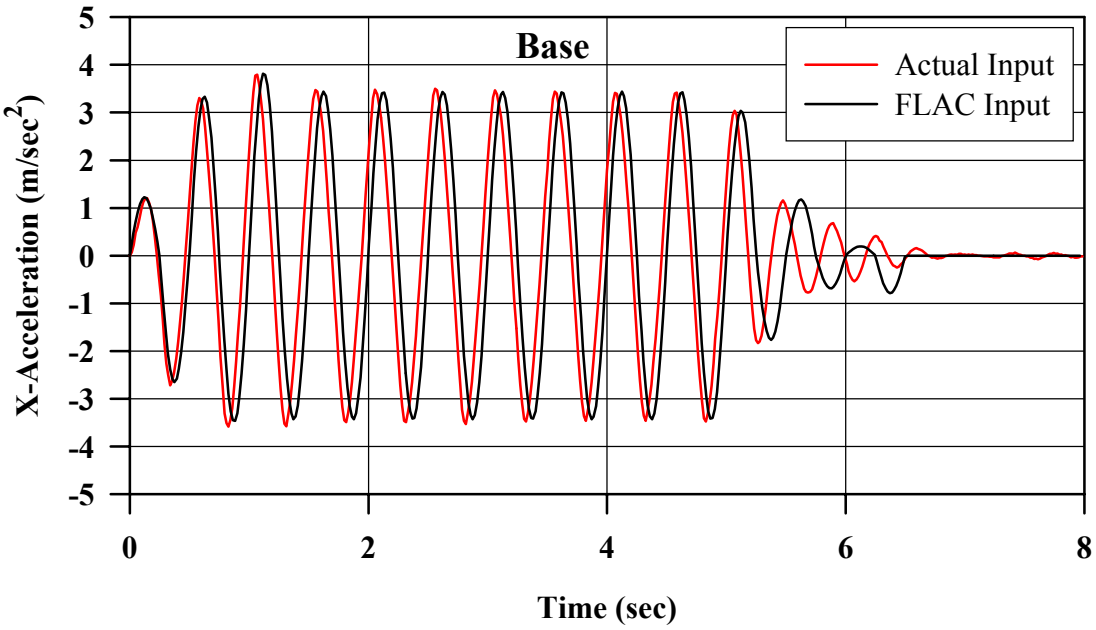

FIGURE 6.26: Actual and FLAC Input Base Acceleration Records for Footing on Medium Dense Sand Layer in Centrifuge Test

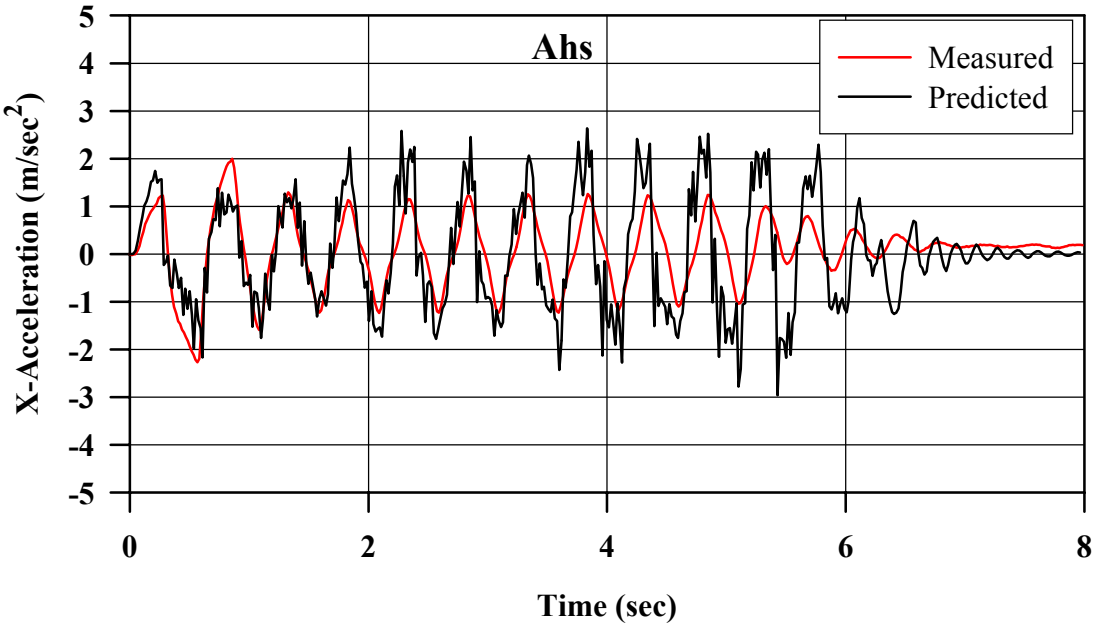

FIGURE 6.27: Predicted vs. Measured X-Acceleration at Ahs for Footing on Medium Dense Sand Layer in Centrifuge Test

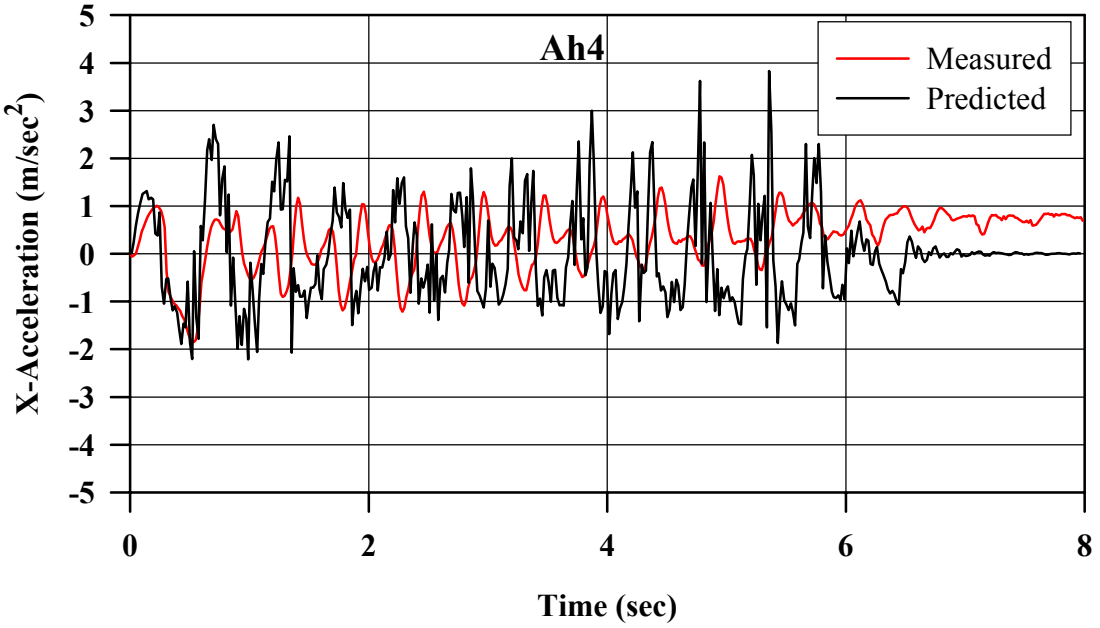

FIGURE 6.28: Predicted vs. Measured X-Acceleration at Ah4 for Footing on Medium Dense Sand Layer in Centrifuge Test

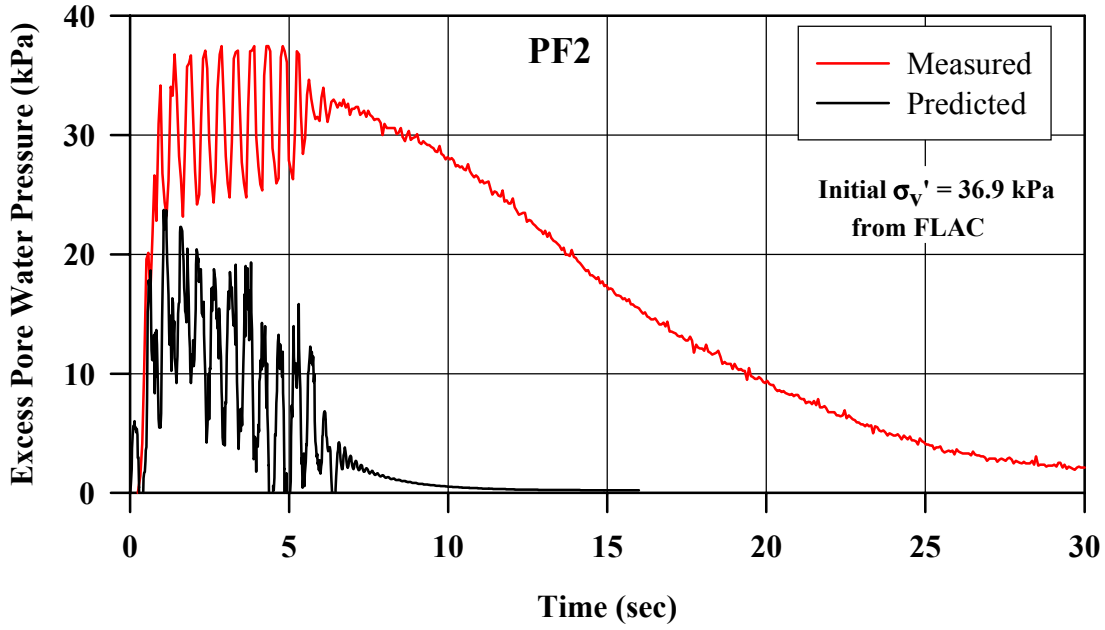

FIGURE 6.29: Predicted vs. Measured Excess Pore Pressure at PF2 for Footing on Medium Dense Sand Layer in Centrifuge Test

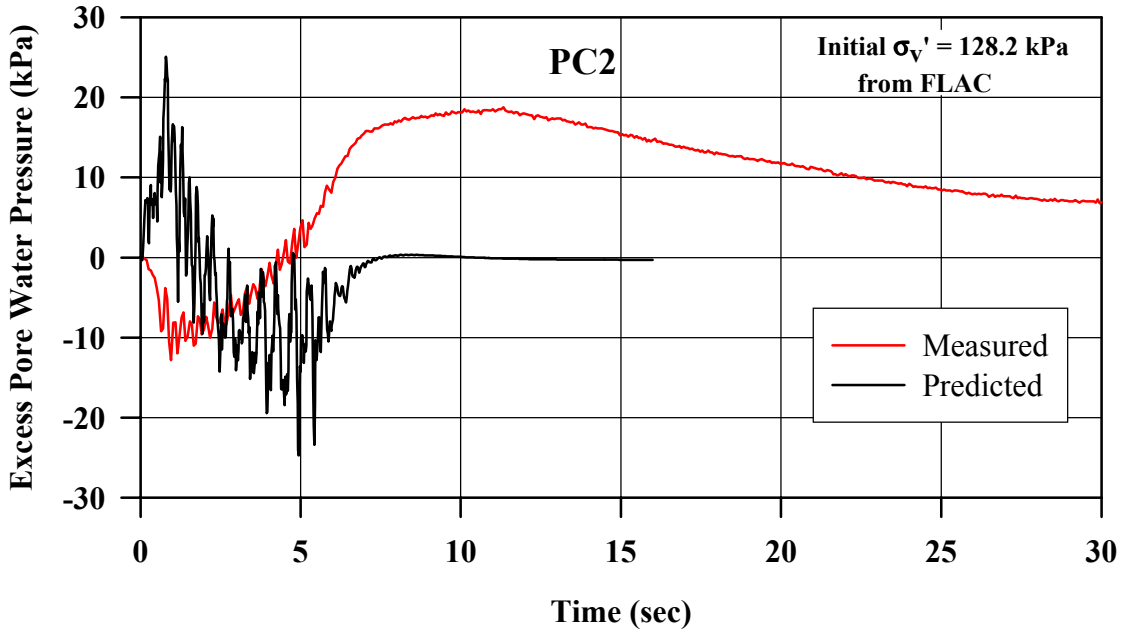

FIGURE 6.30: Predicted vs. Measured Excess Pore Pressure at PC2 for Footing on Medium Dense Sand Layer in Centrifuge Test

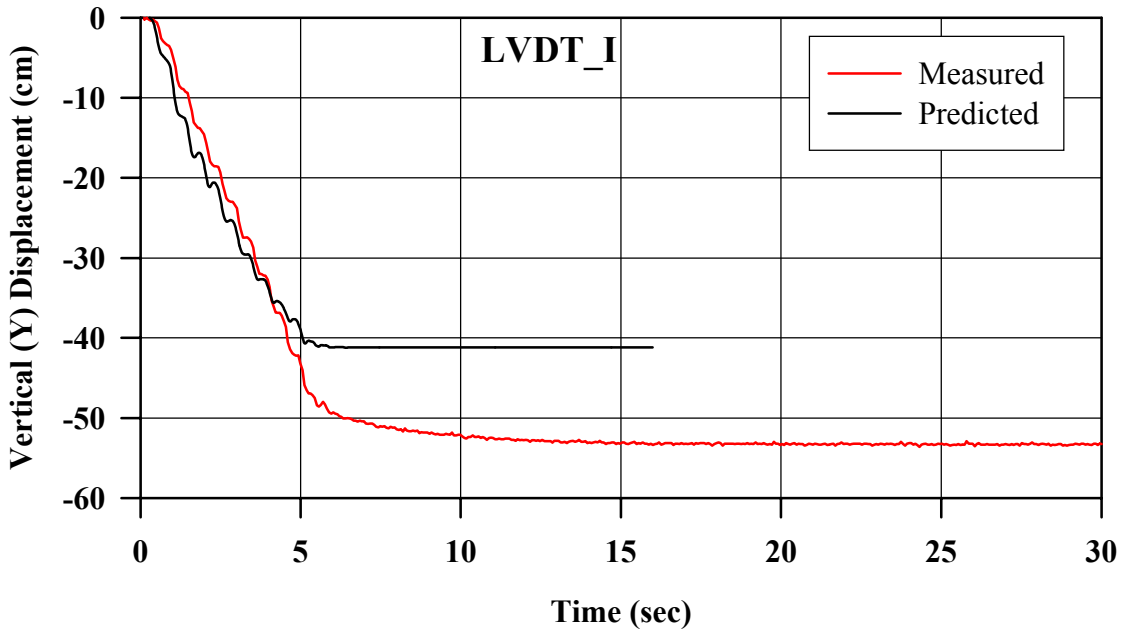

FIGURE 6.31: Predicted vs. Measured Vertical Displacement at LVDT_I for Footing on Medium Dense Sand Layer in Centrifuge Test

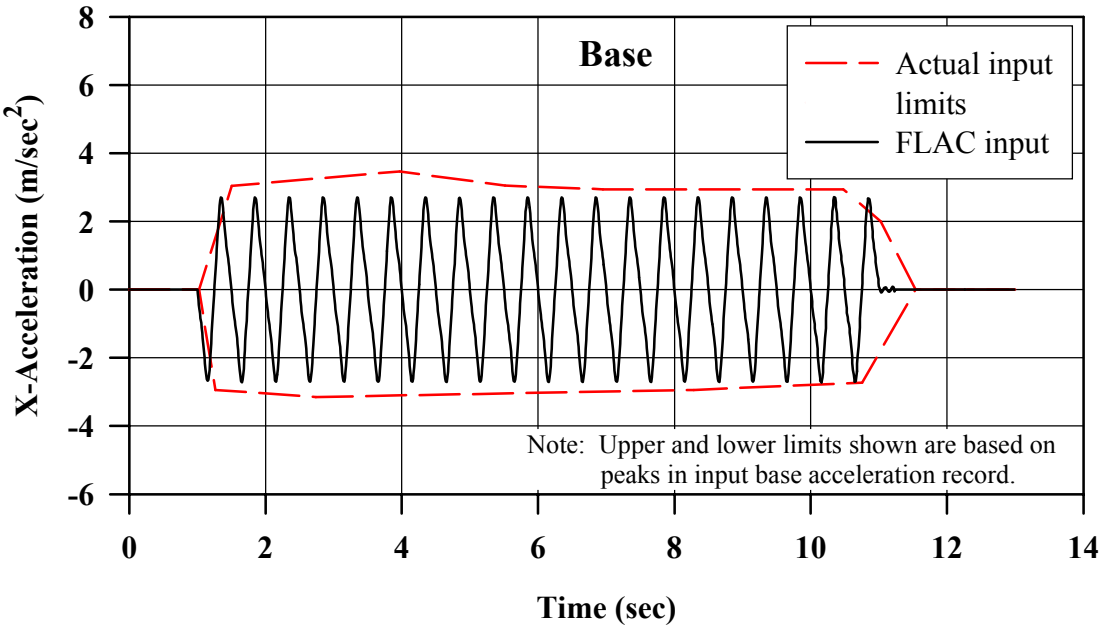

FIGURE 6.32: Actual and FLAC Input Base Acceleration Records for Dense Sand Embankment on Loose Sand Layer in Centrifuge Test

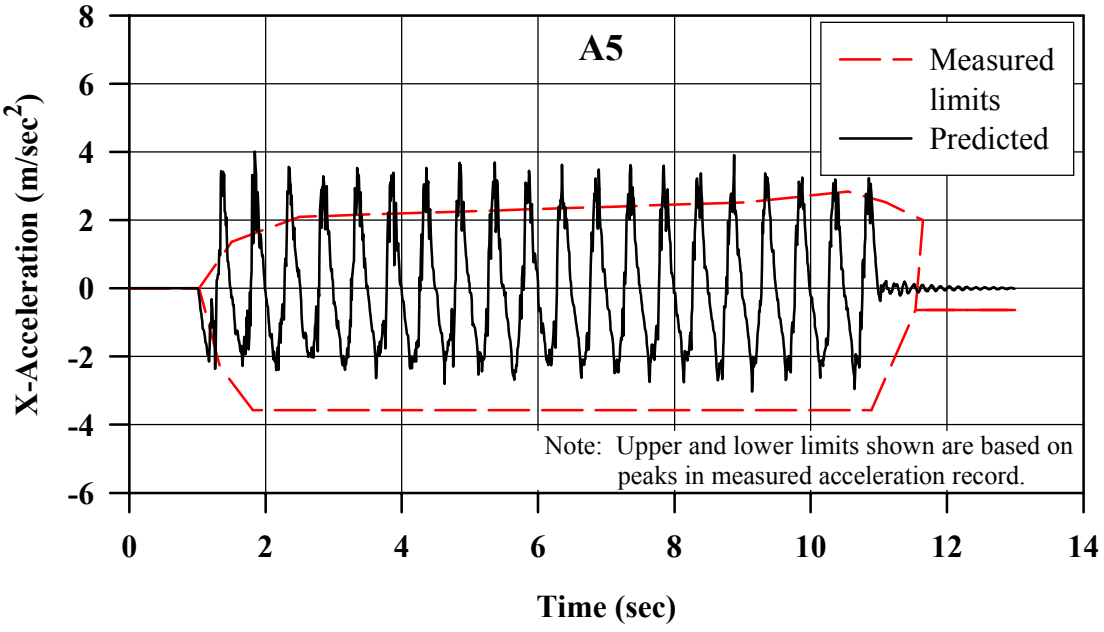

FIGURE 6.33: Predicted and Meaured X-Acceleration at A5 for Dense Sand Embankment on Loose Sand Layer in Centrifuge Test

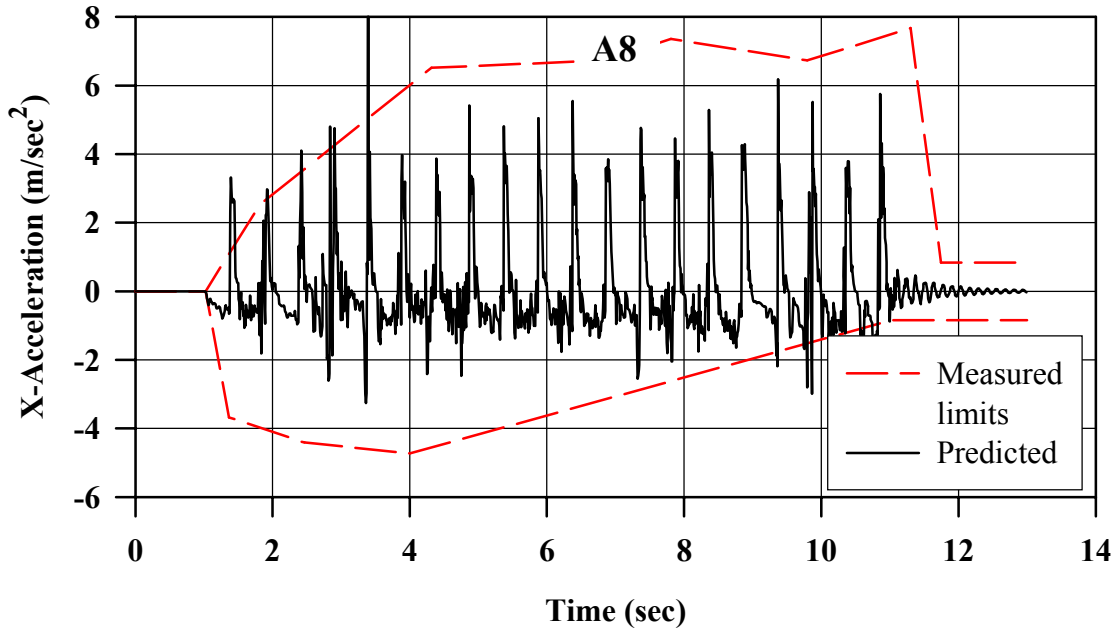

FIGURE 6.34: Predicted and Measured X-Acceleration at A8 for Dense Sand Embankment on Loose Sand Layer in Centrifuge Test

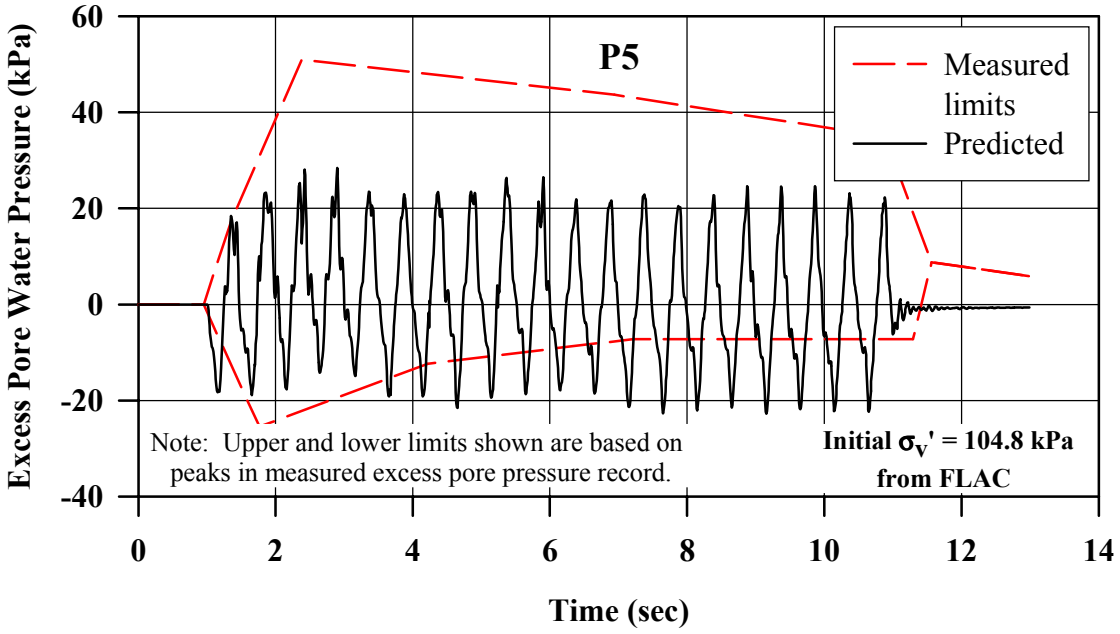

FIGURE 6.35: Predicted and Measured Excess Pore Pressure at P5 for Dense Sand Embankment on Loose Sand Layer in Centrifuge Test

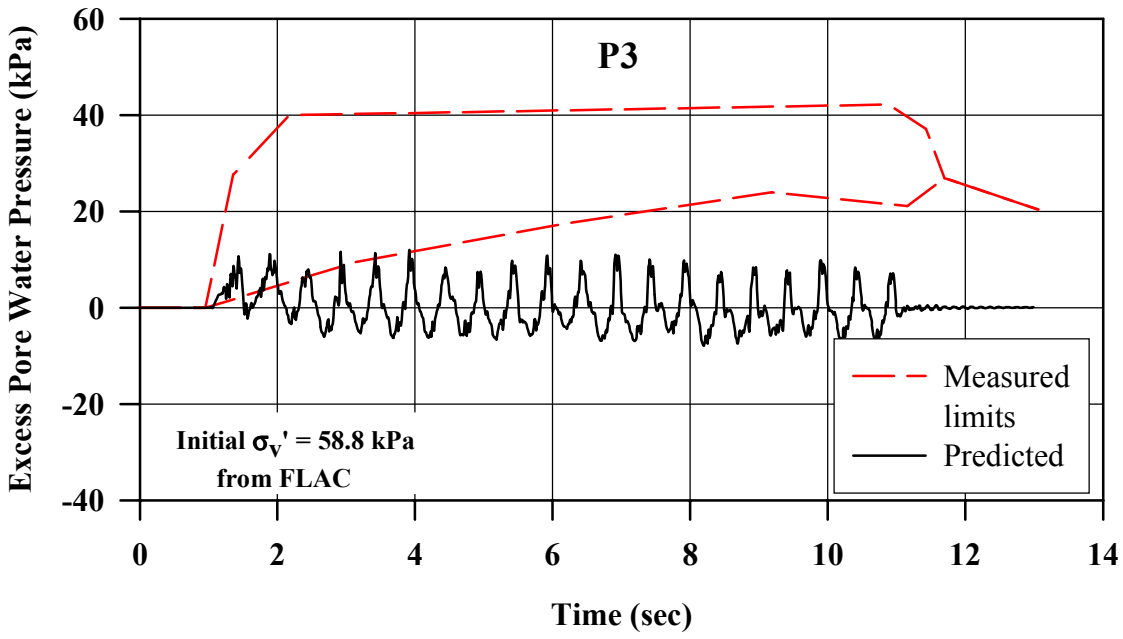

FIGURE 6.36: Predicted and Measured Excess Pore Pressure at P3 for Dense Sand Embankment on Loose Sand Layer in Centrifuge Test

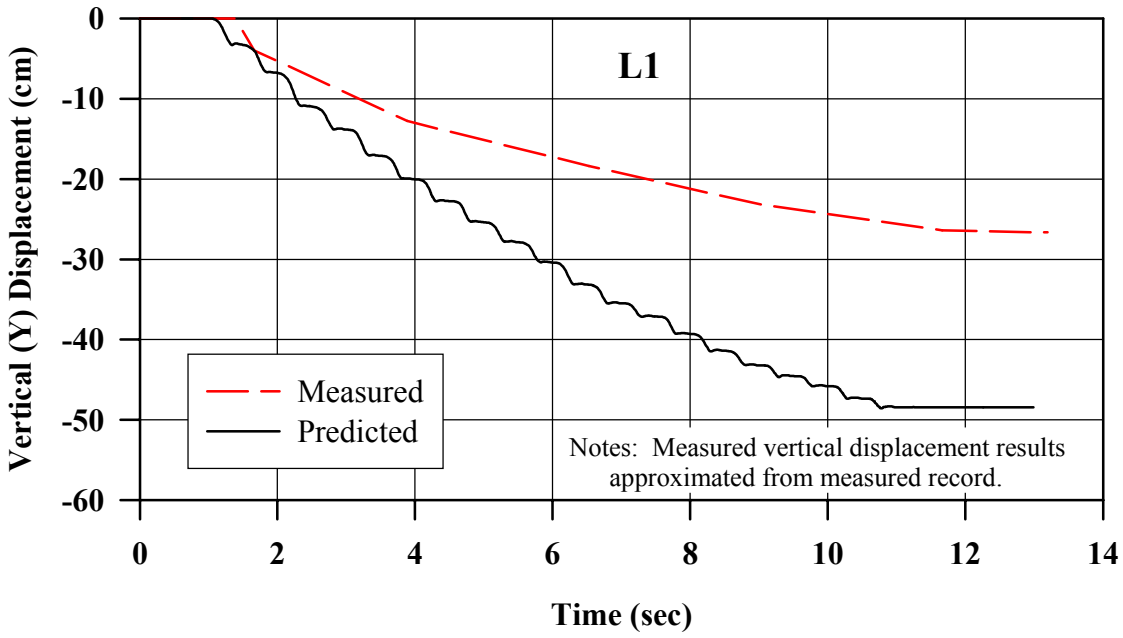

FIGURE 6.37: Predicted and Measured Vertical Displacement at L1 for Dense Embankment on Loose Sand Layer in Centrifuge Test

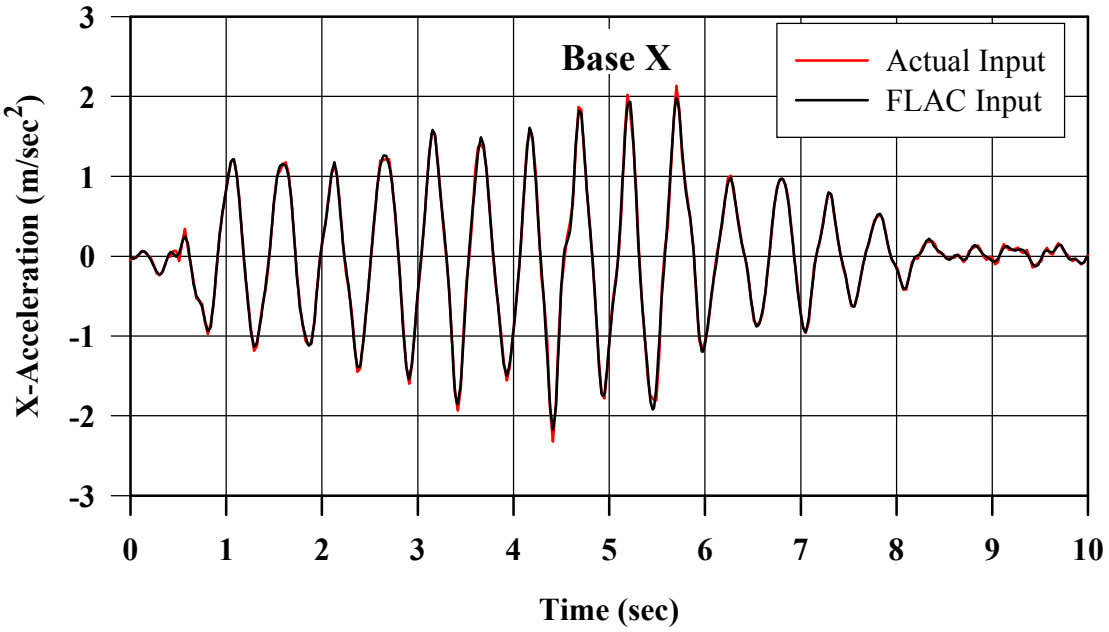

FIGURE 6.38: Actual and FLAC Input Base X-Acceleration Record for Submerged Gravity Retaining Wall on Medium Dense Sand Layer in Centrifuge Test

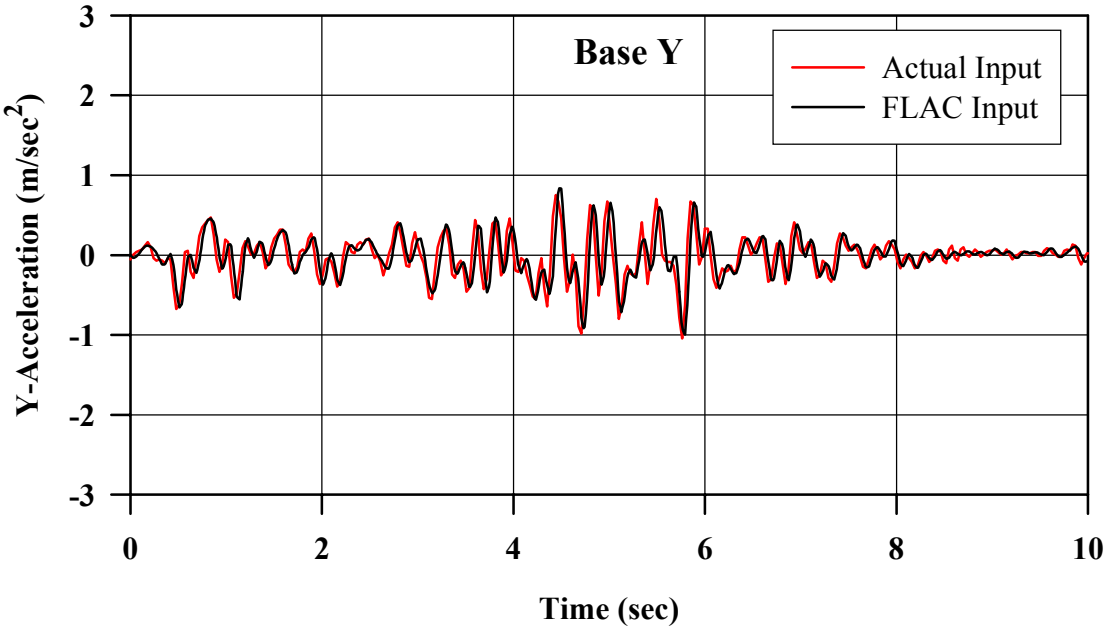

FIGURE 6.39: Actual and FLAC Input Base Y-Acceleration Record for Submerged Gravity Retaining Wall on Medium Dense Sand Layer in Centrifuge Test

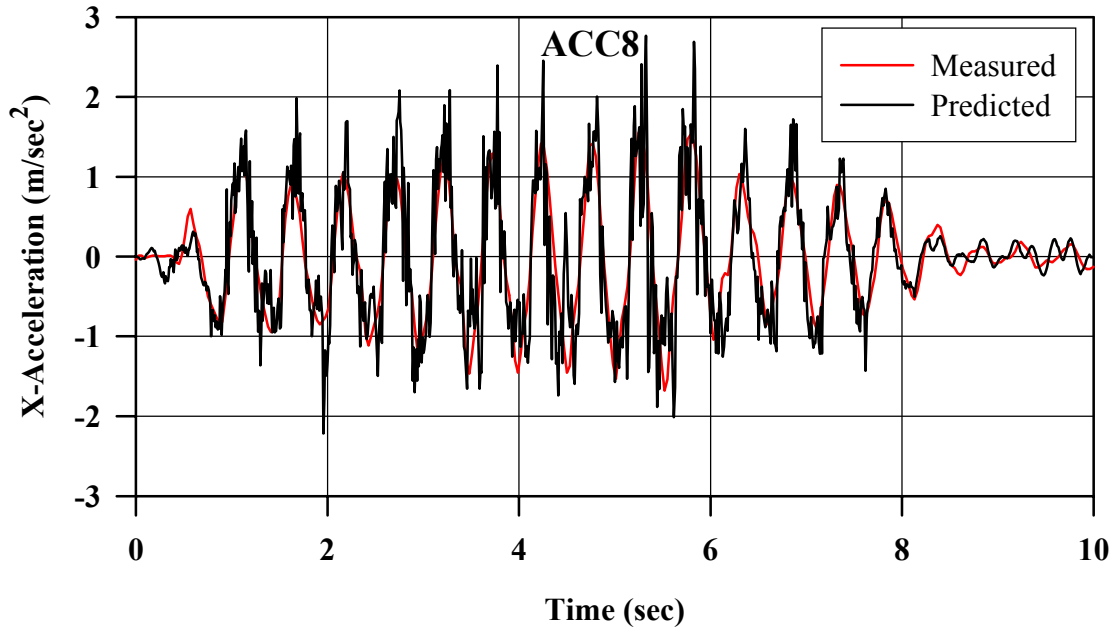

FIGURE 6.40: Predicted and Measured X-Acceleration at ACC8 for Submerged Gravity Retaining Wall on Medium Dense Sand Layer in Centrifuge Test

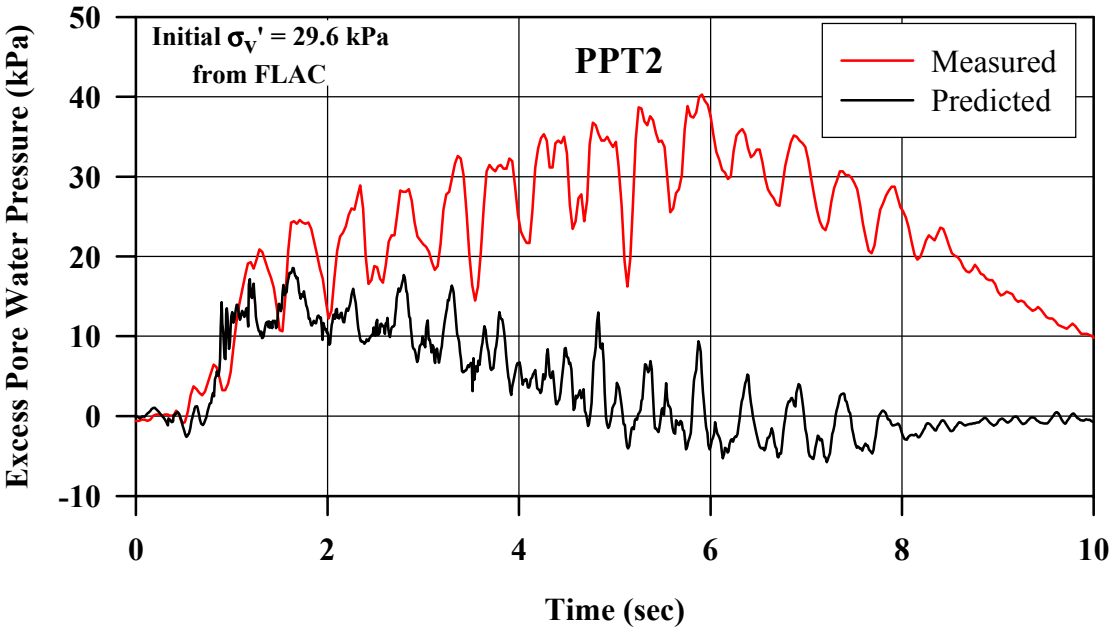

FIGURE 6.41: Predicted and Measured Excess Pore Pressure at PPT2 for Submerged Gravity Retaining Wall on Medium Dense Sand Layer in Centrifuge Test

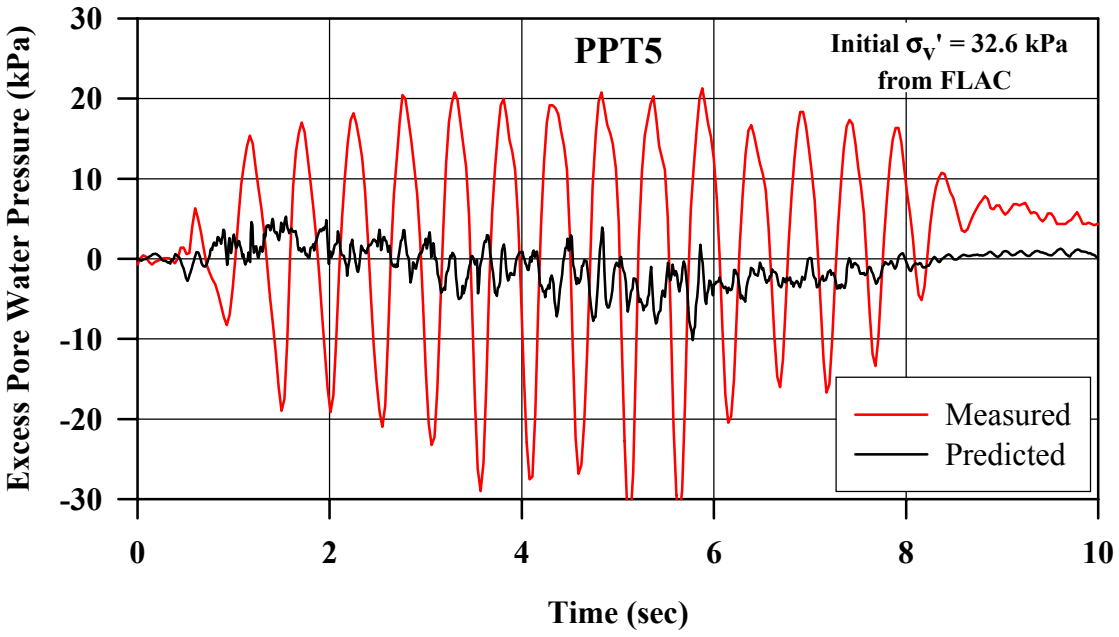

FIGURE 6.42: Predicted and Measured Excess Pore Pressure at PPT5 for Submerged Gravity Retaining Wall on Medium Dense Sand Layer

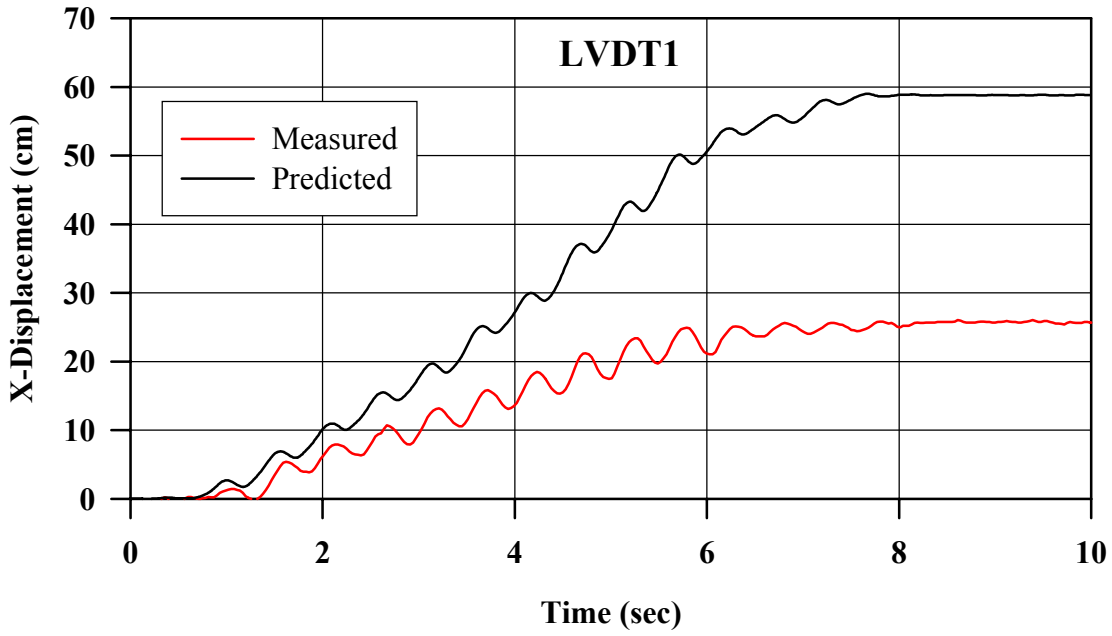

FIGURE 6.43: Predicted and Measured X-Displacement at LVDT1 for Submerged Gravity Retaining Wall on Medium Dense Sand Layer in Centrifuge Test

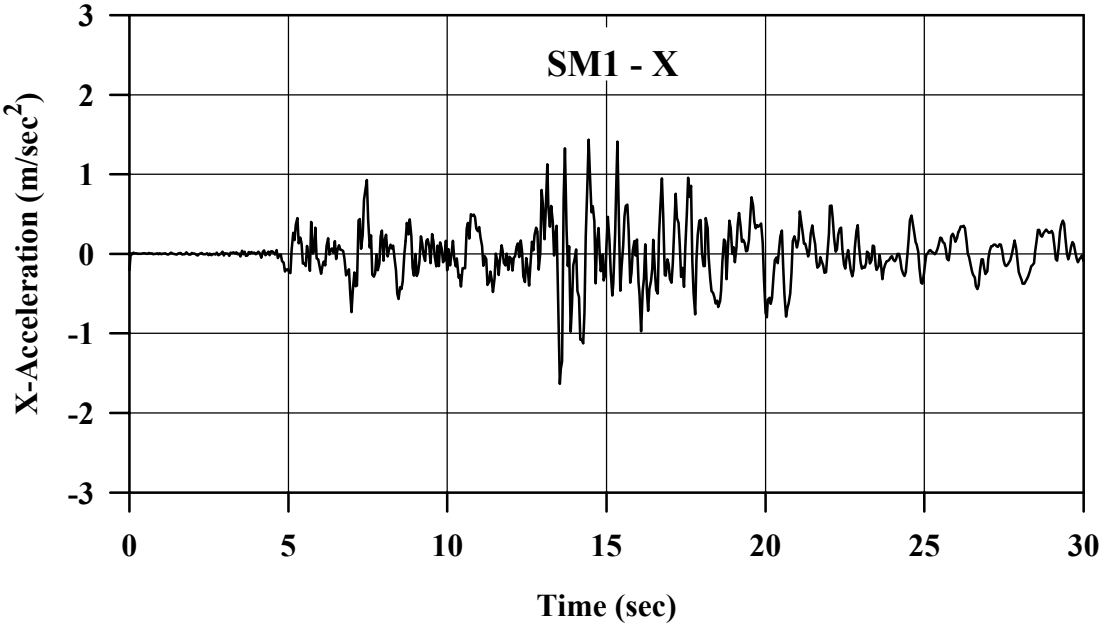

FIGURE 6.44: Horizontal (X) Acceleration Measured in North-South Direction at SM1 at Wildlife Site and Input in FLAC Analysis

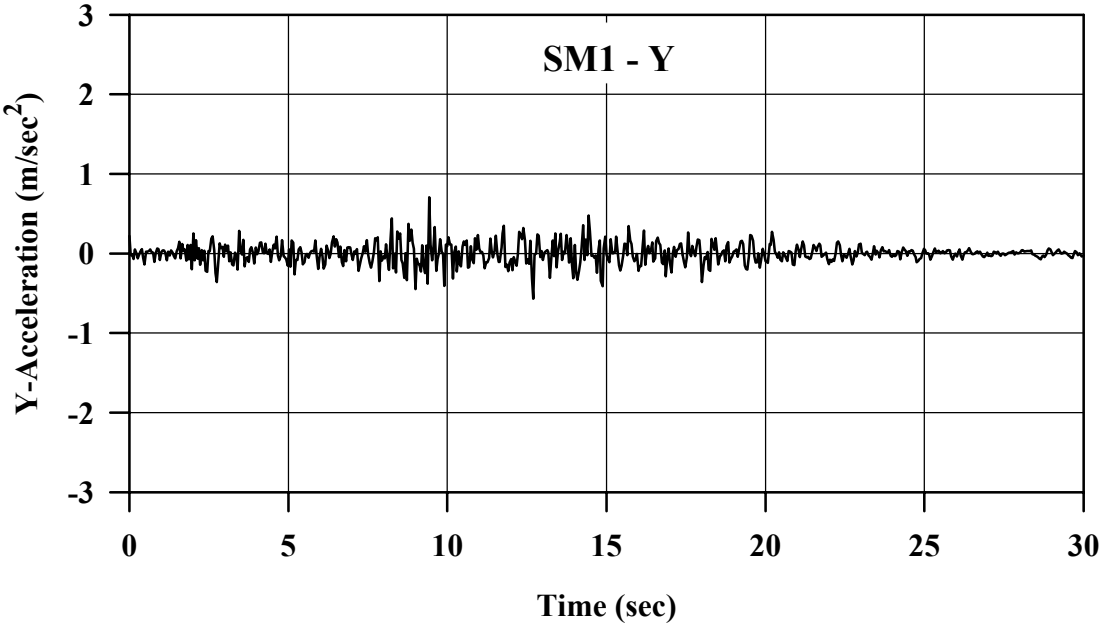

FIGURE 6.45: Vertical (Y) Acceleration Measured at SM-1 at Wildlife Site and Input in FLAC Analysis

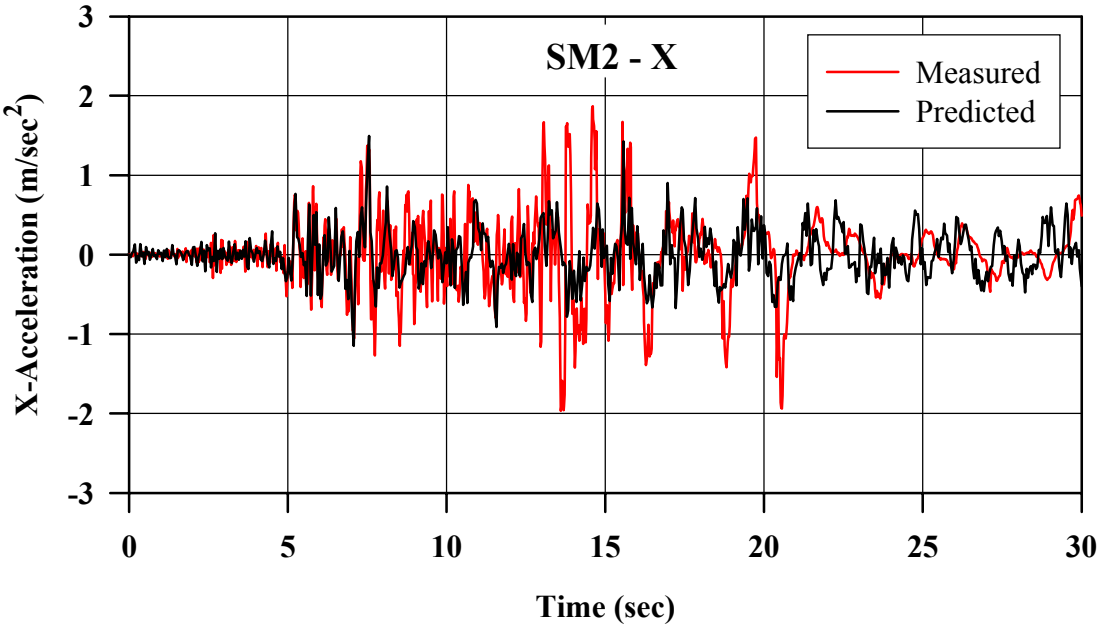

FIGURE 6.46: Predicted and Measured Horizontal (X) Acceleration in North-South Direction at SM2 at Wildlife Site

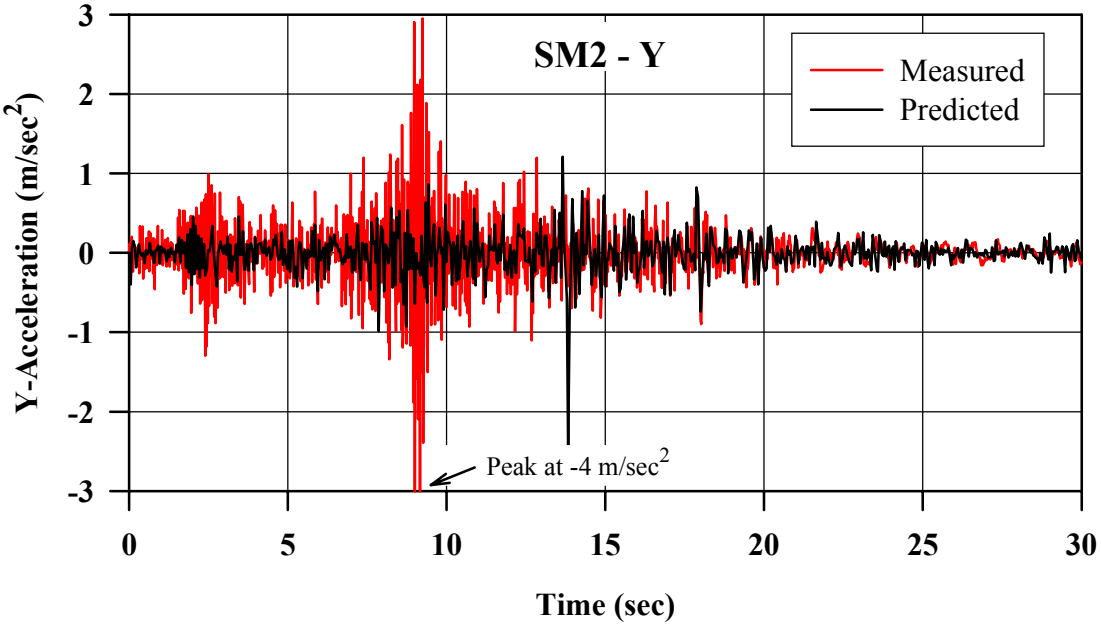

FIGURE 6.47: Predicted and Measured Vertical (Y) Acceleration at SM2 at Wildlife Site

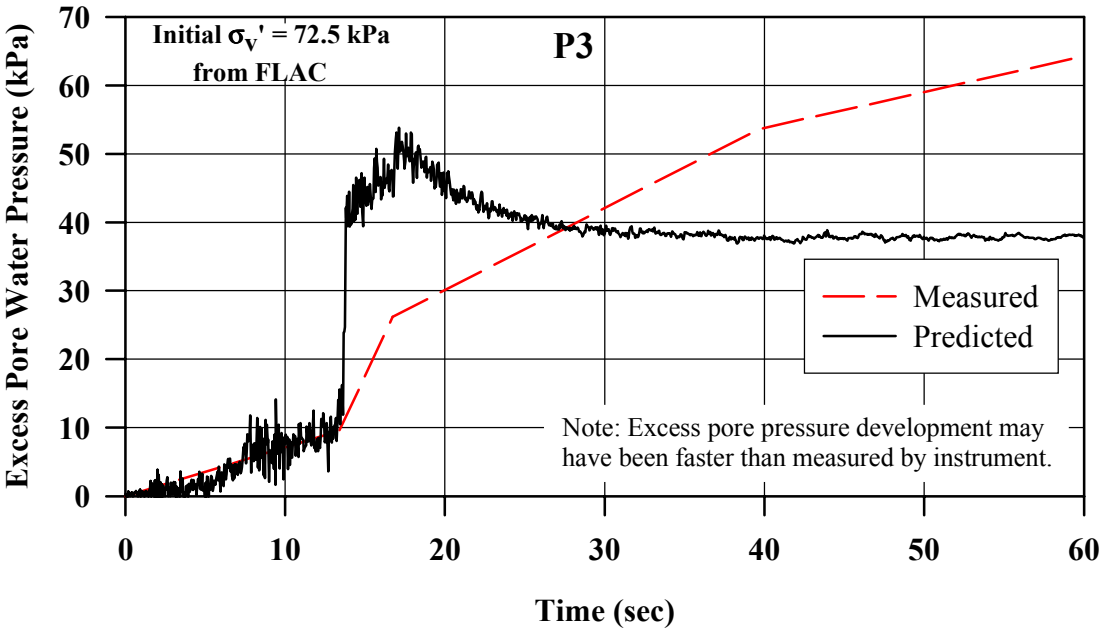

FIGURE 6.48: Predicted and Measured Excess Pore Pressure at P3 at Wildlife Site

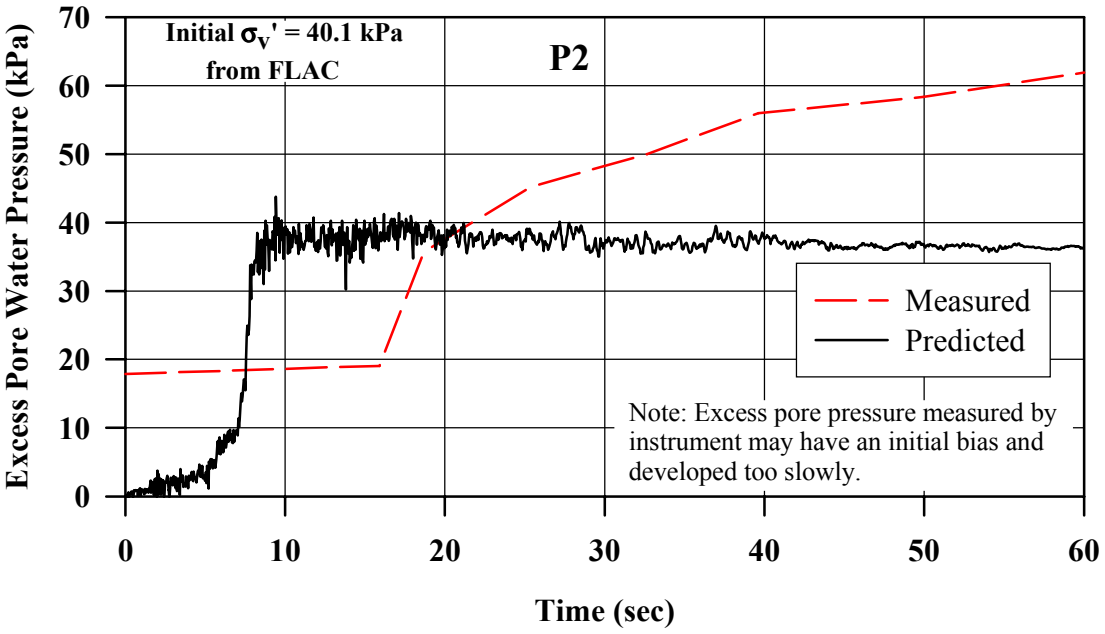

FIGURE 6.49: Predicted and Measured Excess Pore Pressure at P2 at Wildlife Site

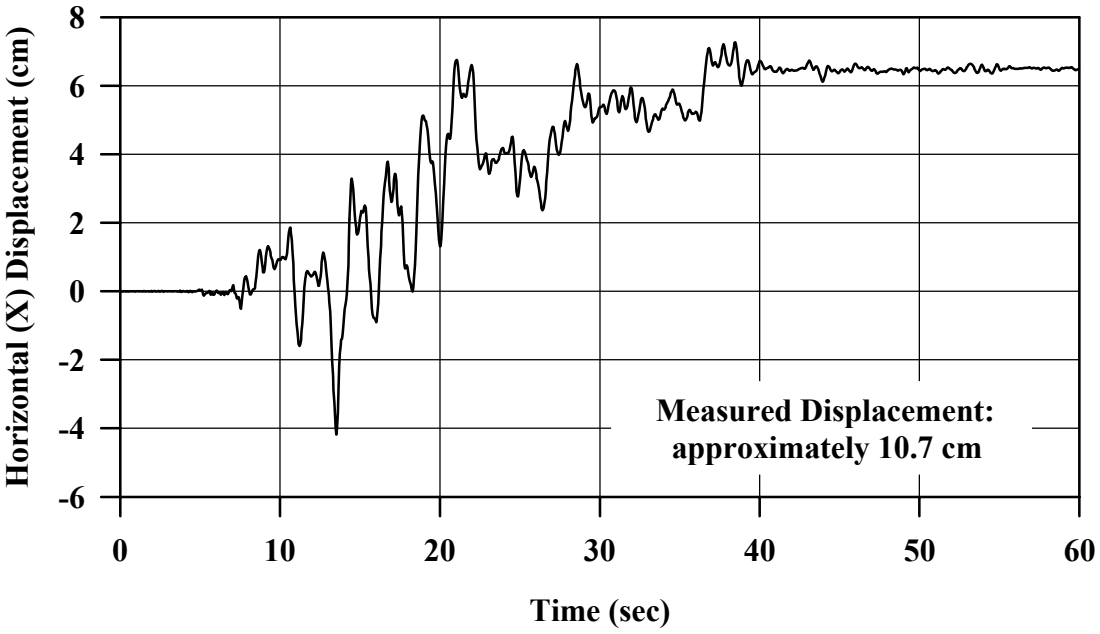

FIGURE 6.50: Predicted Horizontal (X) Displacement of Ground Surface at Instrument Array at Wildlife Site

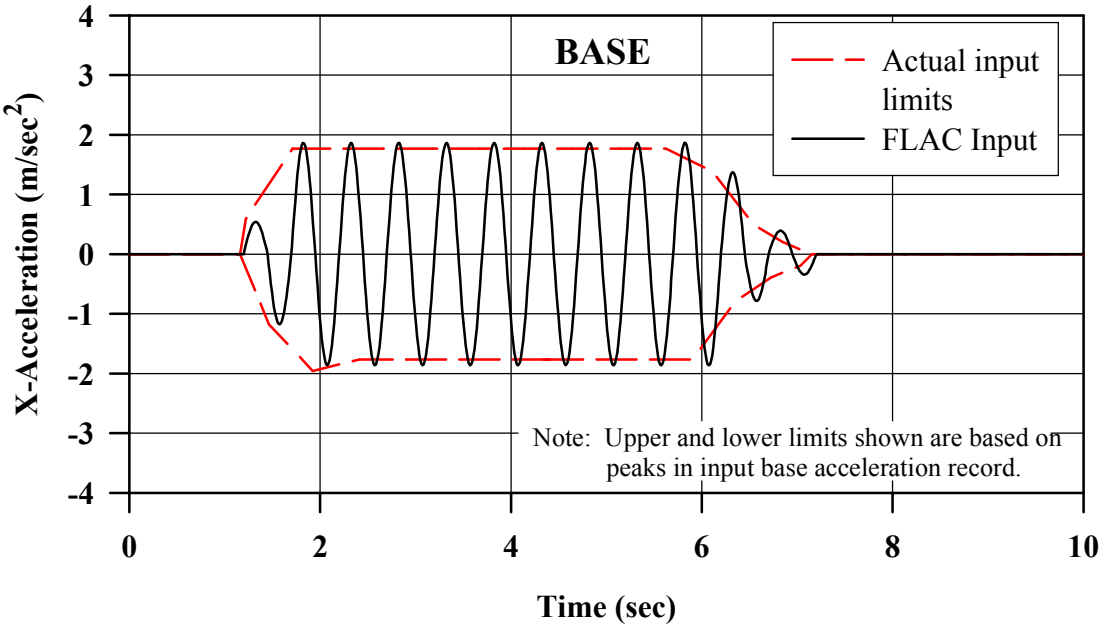

FIGURE 6.51: Actual and FLAC Input Base Acceleration Records for Adjacent Loose-Dense Sand Zones in Centrifuge Test

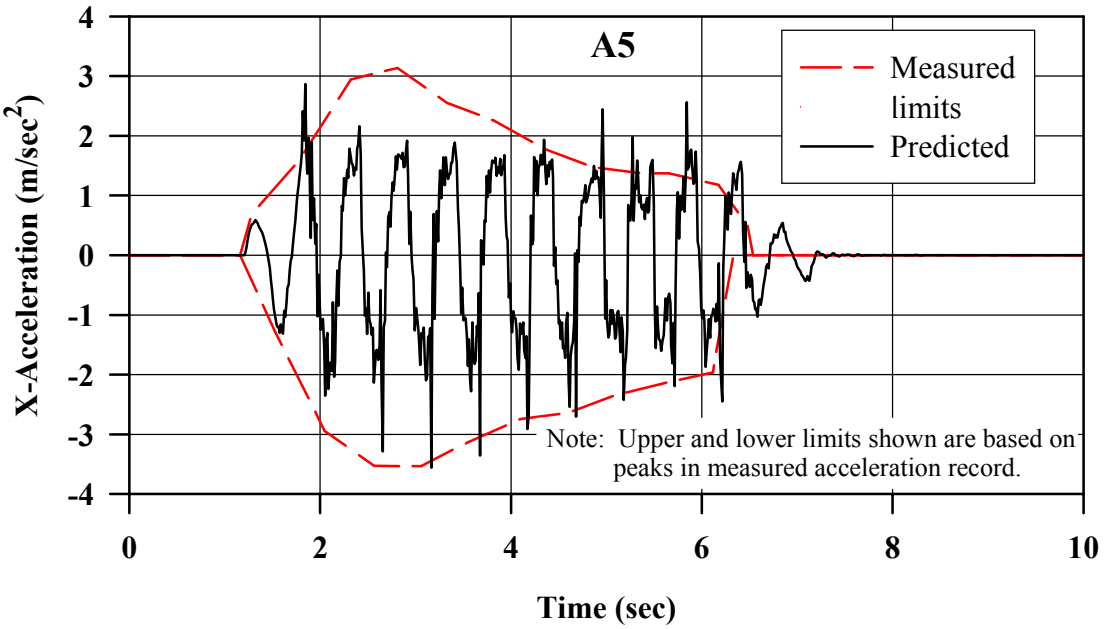

FIGURE 6.52: Predicted vs. Measured X-Acceleration at A5 for Adjacent Loose-Dense Sand Zones in Centrifuge Test

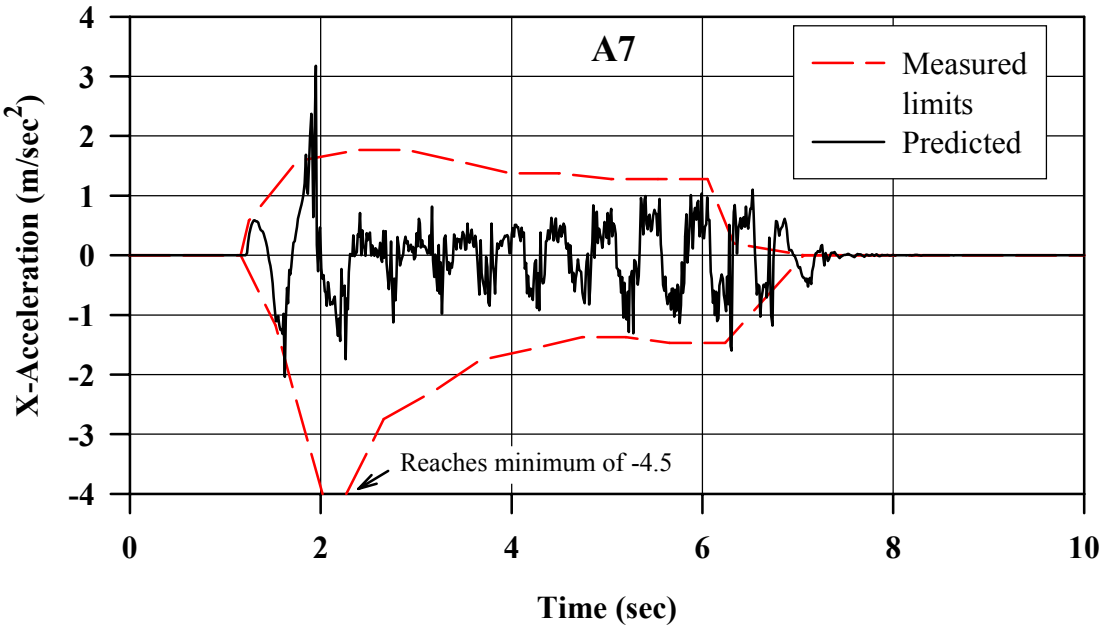

FIGURE 6.53: Predicted vs. Measured X-Acceleration at A7 for Adjacent Loose-Dense Sand Zones in Centrifuge Test

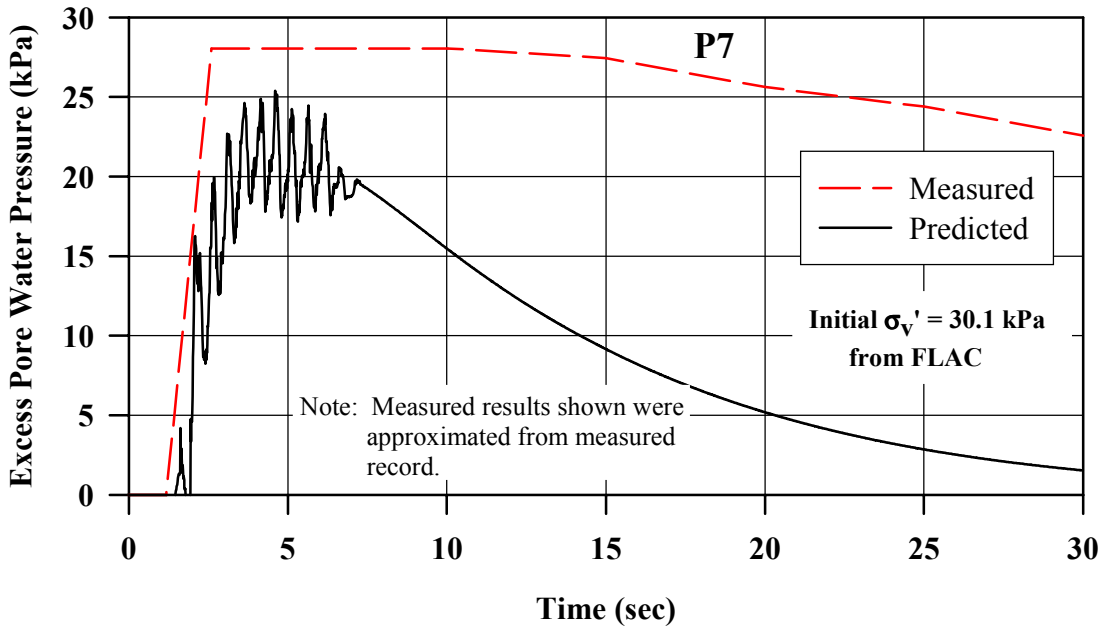

FIGURE 6.54: Predicted vs. Measured Excess Pore Pressure at P7 for Adjacent Loose-Dense Sand Zones in Centrifuge Test

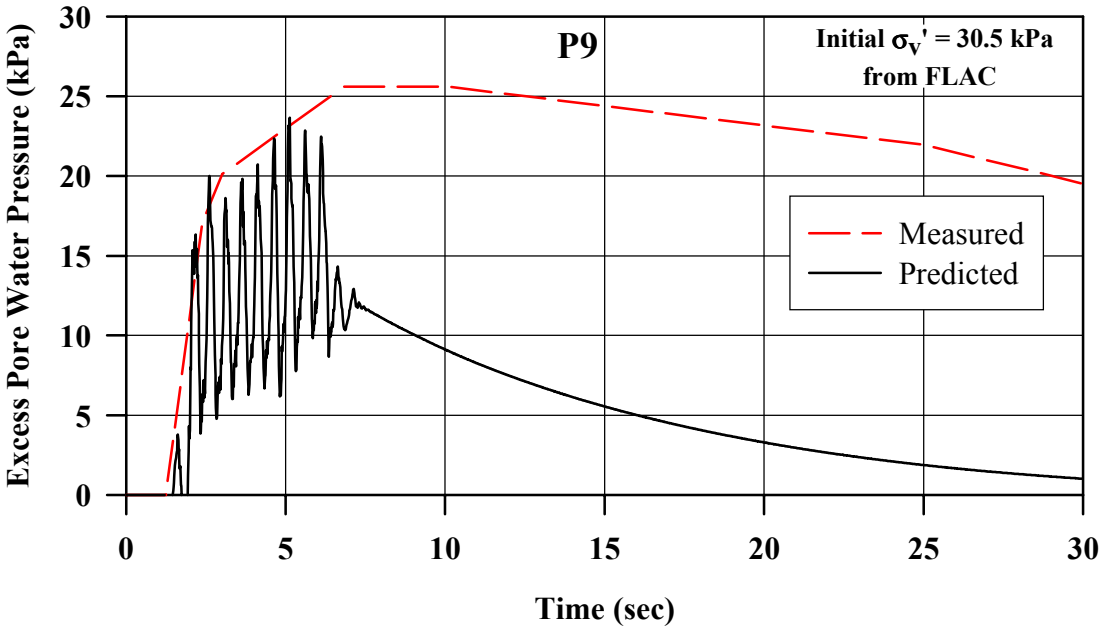

FIGURE 6.55: Predicted vs. Measured Excess Pore Pressure at P9 for Adjacent Loose-Dense Sand Zones in Centrifuge Test

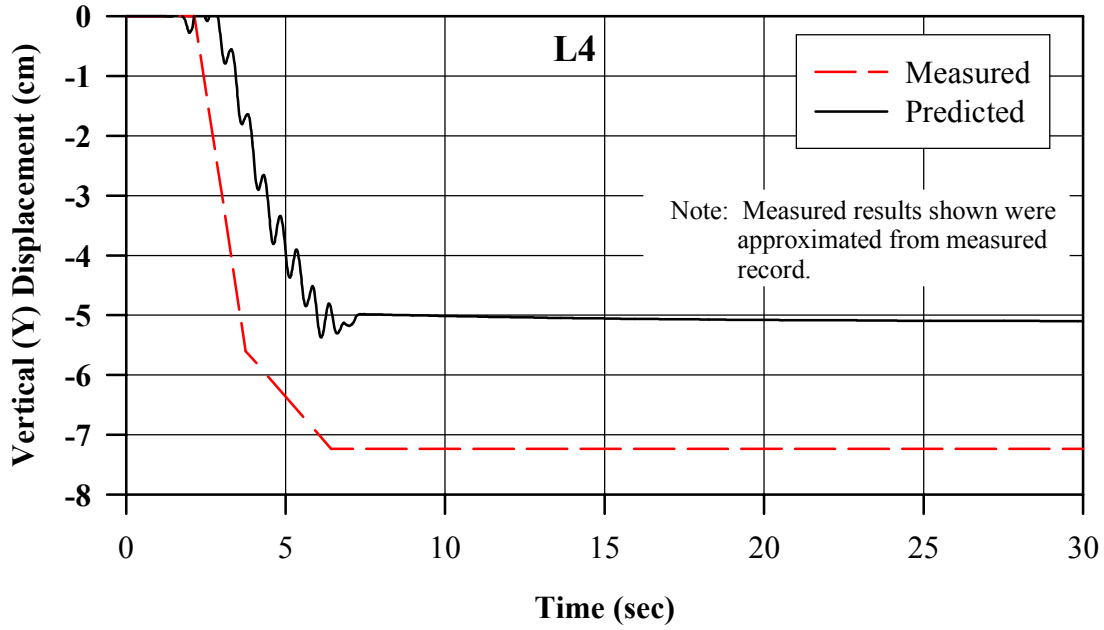

FIGURE 6.56: Predicted vs. Measured Vertical Displacement at L4 for Adjacent Loose-Dense Sand Zones in Centrifuge Test

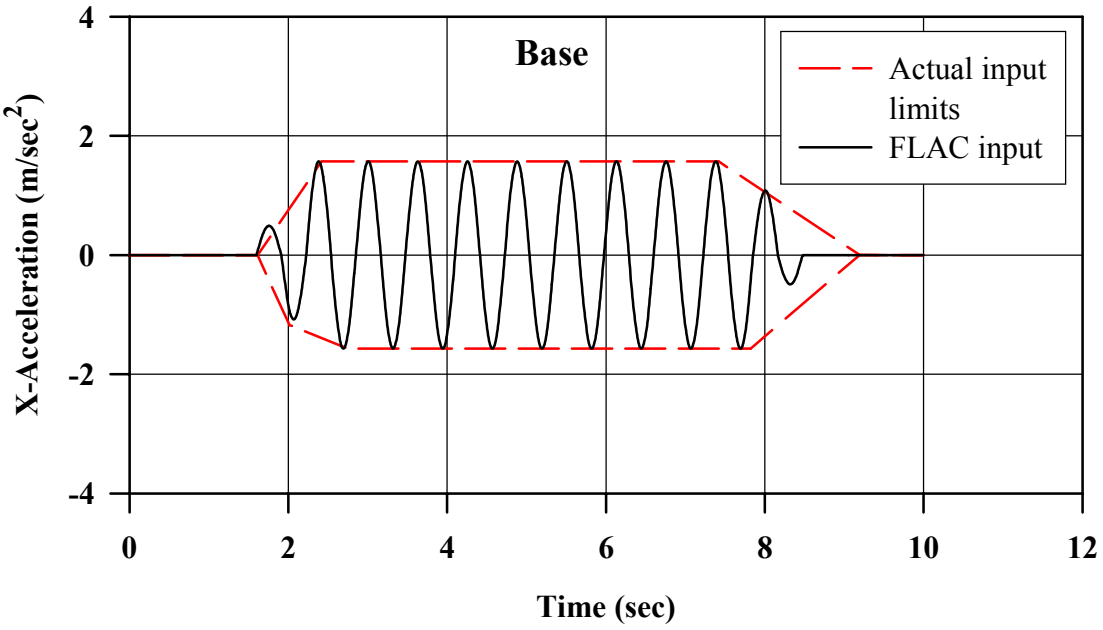

FIGURE 6.57: Actual and FLAC Input Base Acceleration Records for Embankment on Loose Sand Layer with Dense Zones in Centrifuge

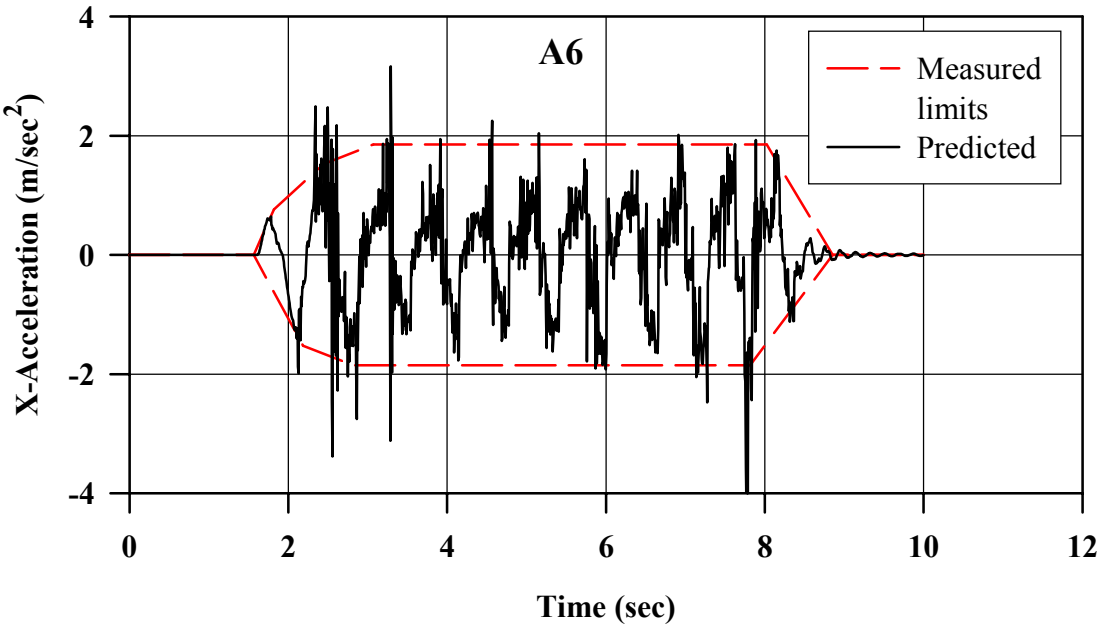

FIGURE 6.58: Predicted and Measured X-Acceleration at A6 for Embankment on Loose Sand Layer with Dense Zones in Centrifuge Test

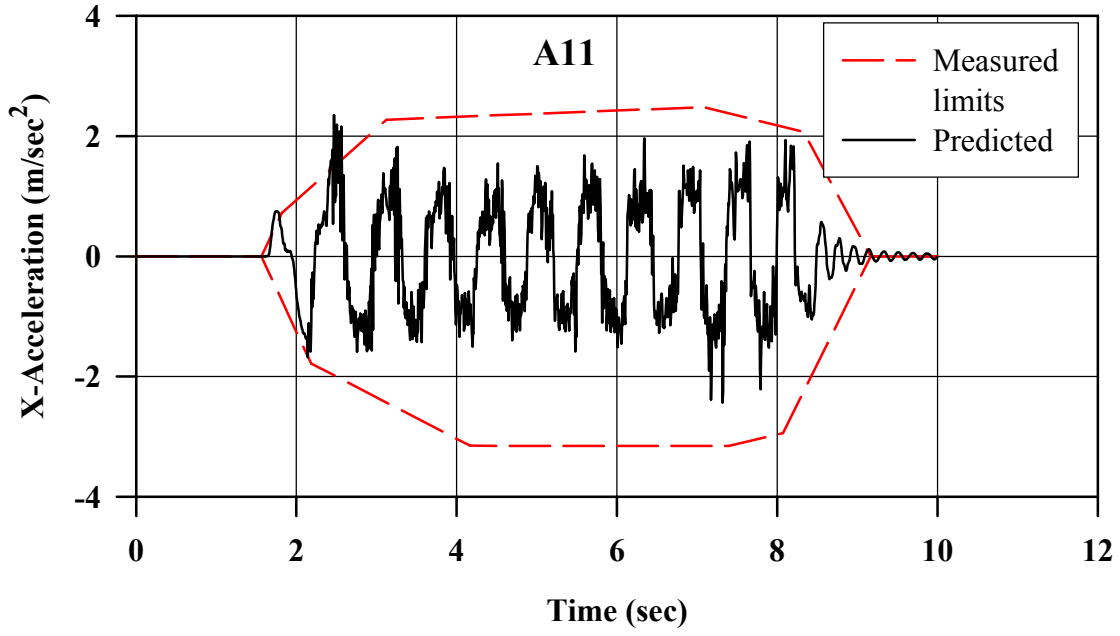

FIGURE 6.59: Predicted and Measured X-Acceleration at A11 for Embankment on Loose Sand Layer with Dense Zones in Centrifuge Test

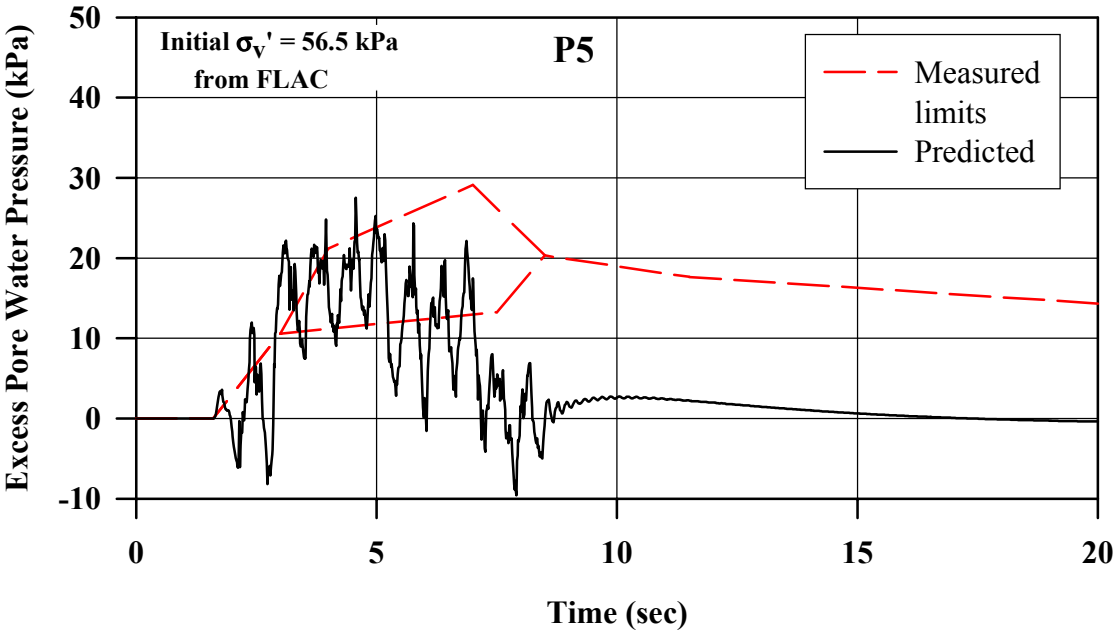

FIGURE 6.60: Predicted and Measured Excess Pore Pressure at P5 for Embankment on Loose Sand Layer with Dense Zones in Centrifuge Test

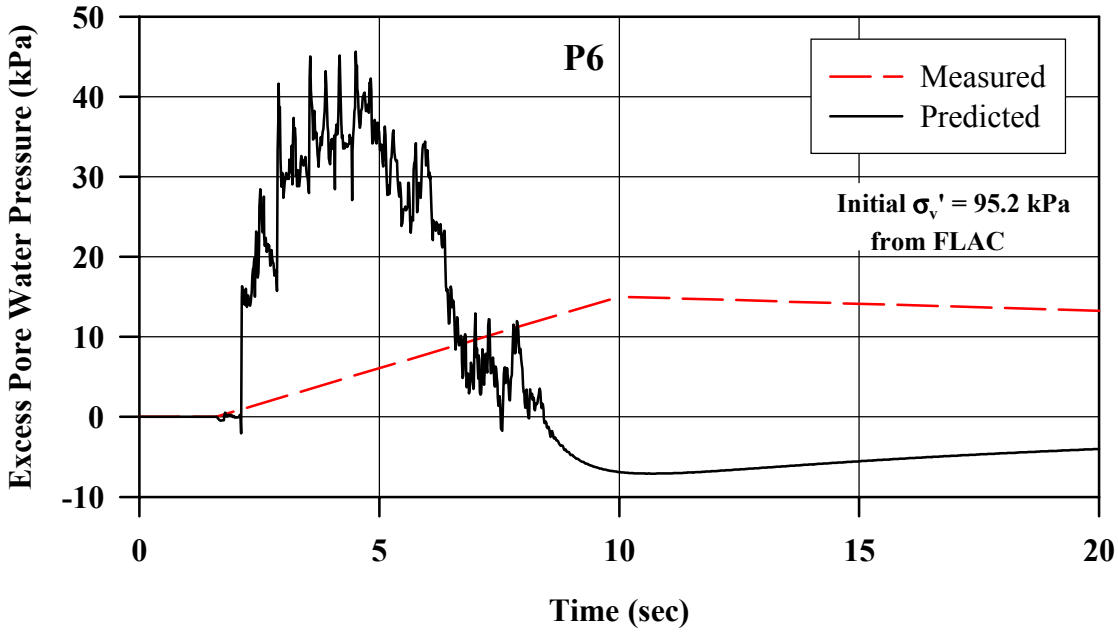

FIGURE 6.61: Predicted and Measured Excess Pore Pressures at P6 for Embankment on Loose Sand Layer with Dense Zones in Centrifuge Test

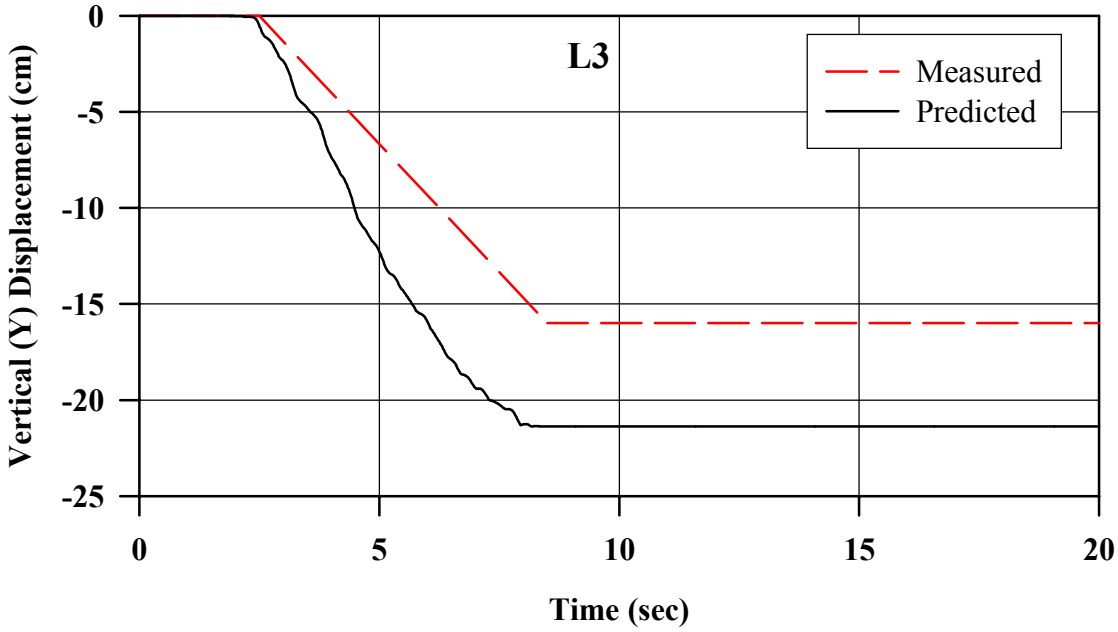

FIGURE 6.62: Predicted and Measured Vertical Displacement at L3 for Embankment on Loose Sand Layer with Dense Zone in Centrifuge Test

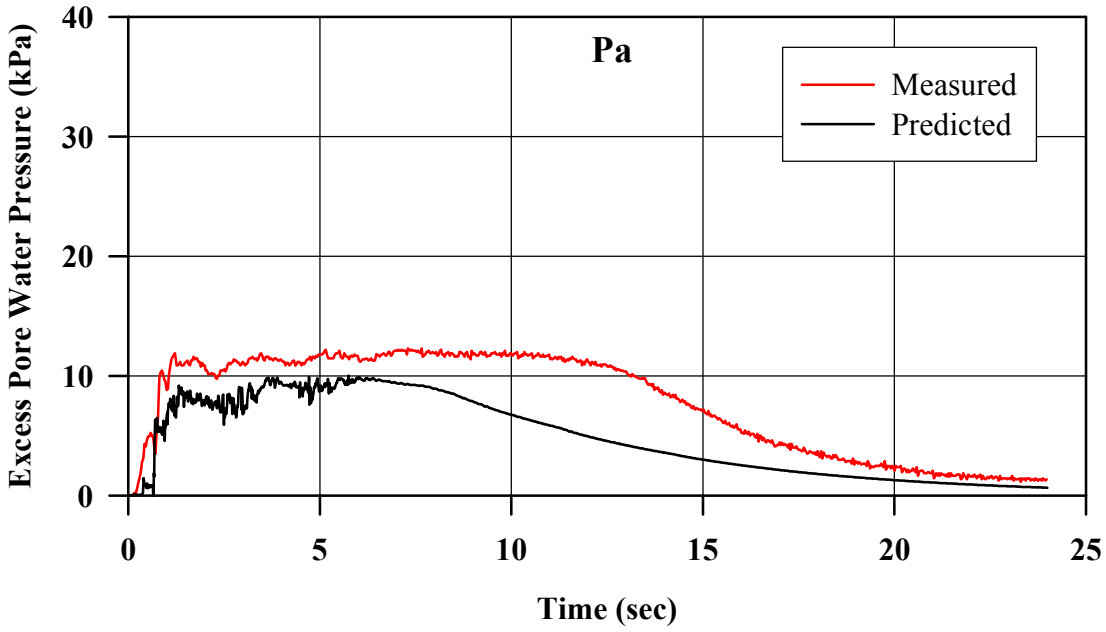

FIGURE 6.63: Predicted Excess Pore Pressure at Pa for Uniform Medium Dense Sand in Centrifuge Test Using Re-solidification Concept

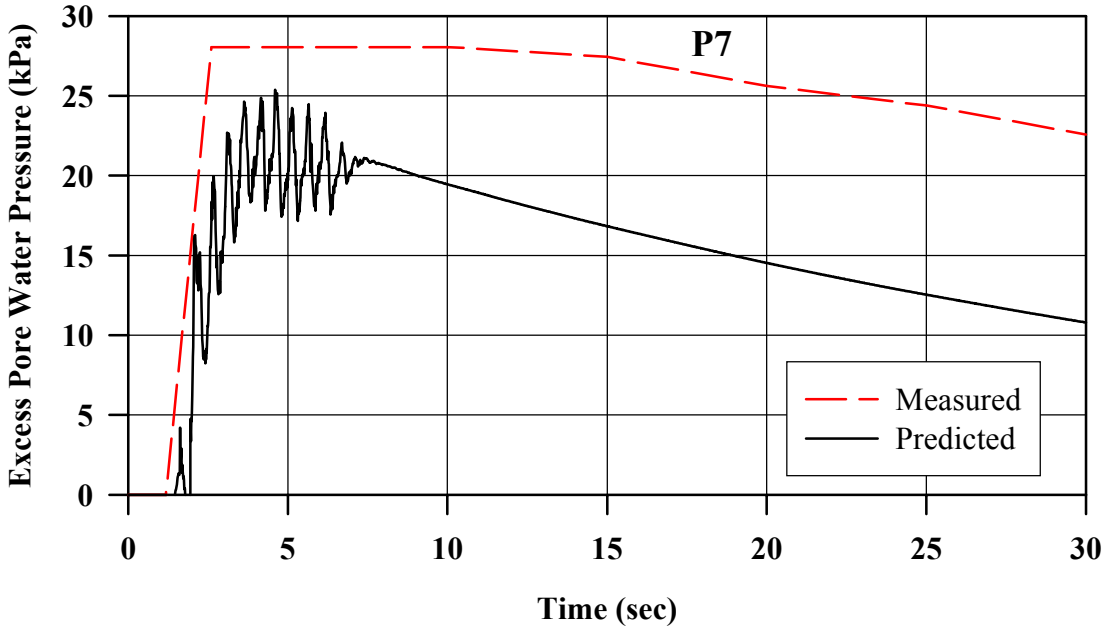

FIGURE 6.64: Predicted Excess Pore Pressure at P7 for Adjacent Loose-Dense Sand Zones in Centrifuge Test Using Re-Solidification Concept

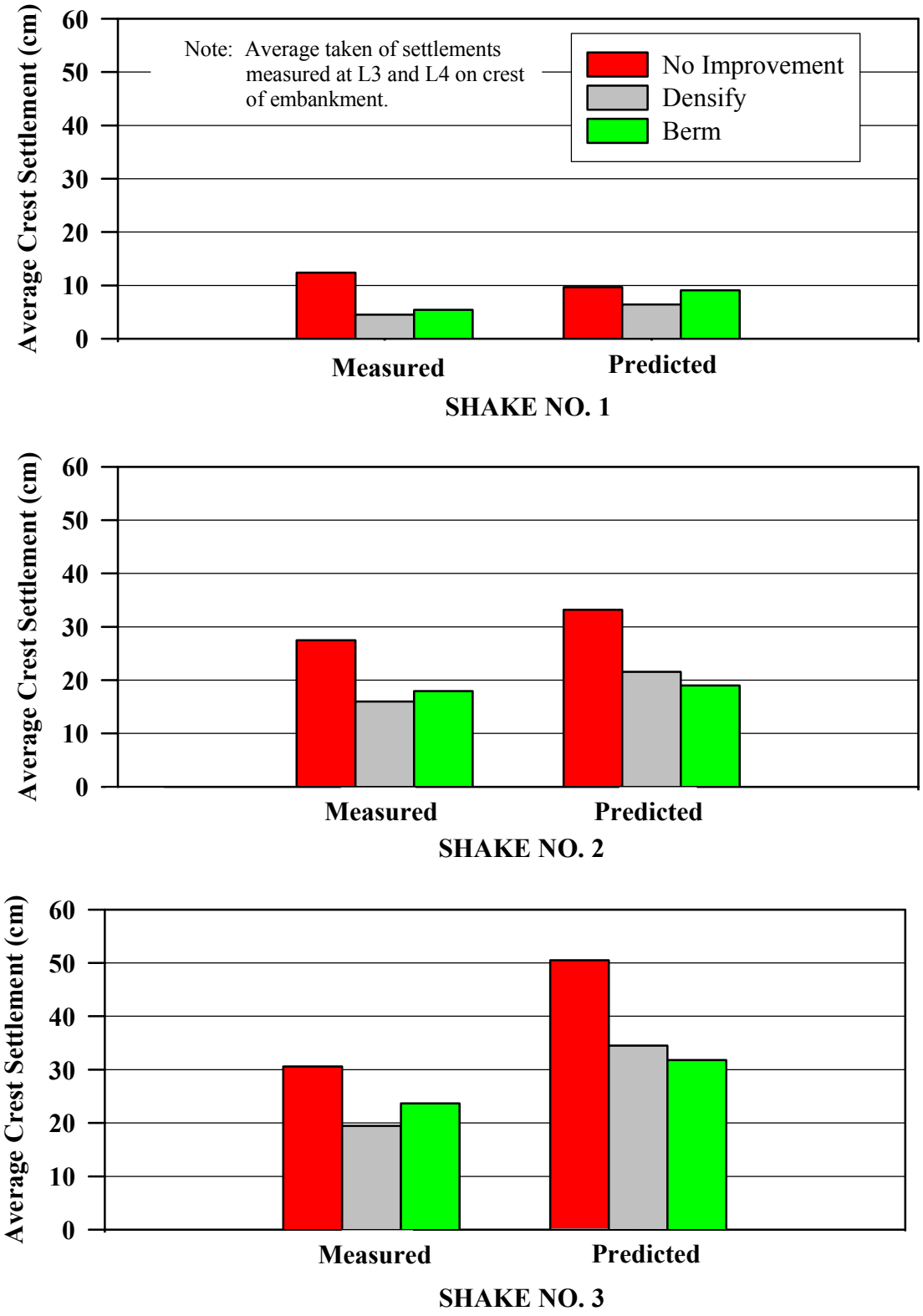

FIGURE 6.65: Predicted and Measured Crest Settlements for Embankment on Loose Sand with Different Improvements for Centrifuge Test by Adalier (1996)

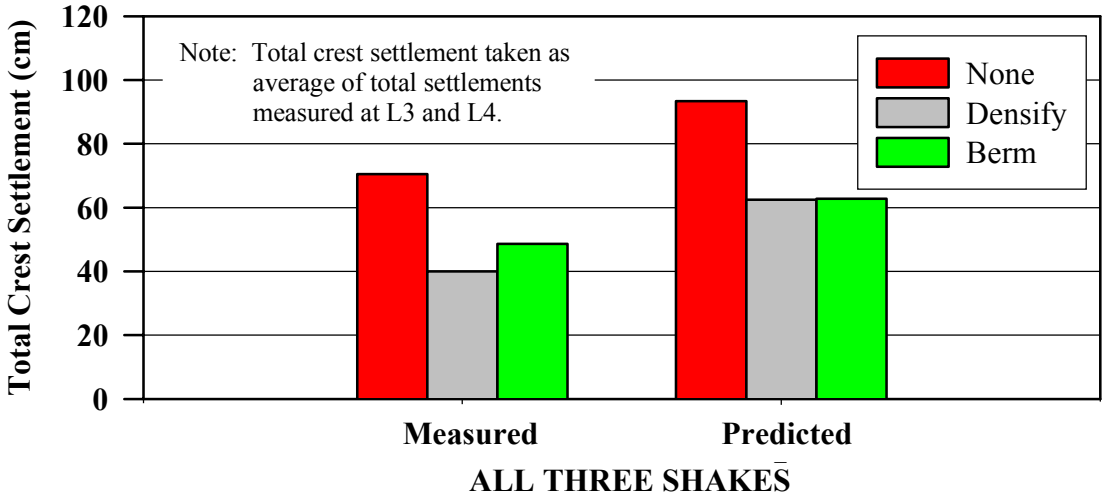

FIGURE 6.66: Predicted and Measured Total Settlements for Crest of Embankment Accumulated Over Three Shaking Events in Centrifuge Test by Adalier (1996)

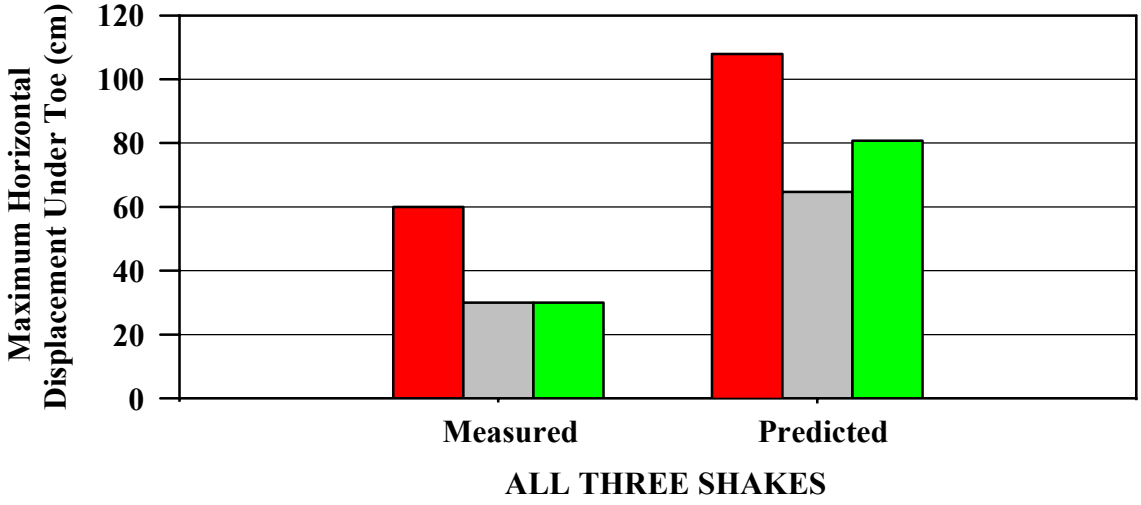

FIGURE 6.67: Predicted and Measured Maximum Horizontal Displacement Under Toe of Embankment Accumulated Over Three Shaking Events in Centrifuge by Adalier (1996)